Aarhus University

Master Thesis

Investigation of complex control landscapes of an evaporative cooling process

Author:
Poul A. Ejlertsen

Supervisor:
Jacob F. Sherson

A thesis submitted in fulfilment of the requirements for the degree of Master in physics

in the

Quantum Measurement and Manipulation group
IFA

12. December 2016

AARHUS UNIVERSITY

Abstract

Master

Investigation of complex control landscapes of an evaporative cooling processe

by Poul A. Ejlertsen

This thesis reports on transport experiments with ultra-cold atomic clouds and Bose-Einstein Condensates (BEC), and different means of optimally creating a BEC with evaporative cooling. The first part of the thesis presents an experiment with the movement of a thermal atom cloud and a BEC controlled by a moveable optical tweezer. The results indicate the validity of a 1D classical model to describe the center-of-mass oscillations in relation to the movement duration, in the case of the translation of a BEC.

The second part is an investigation of the optimal control landscape for the process of evaporative cooling of neutral atoms. This is realized by the usage of three different methods. The first by systematic scans based on our intuition of the physical problem. The second method is a search performed by an optimization algorithm. The third by using crowdsource, realized by gamifying the evaporation problem. New strategies for producing a high yield BEC atoms were found, with the last method of gamification resulting in the highest BEC yield ever obtained in our setup, being $2.76 \cdot 10^6$ BEC atoms.

Resumé

Denne afhandling beretter om et transport experiment med ultrakolde atomskyer og Bose-Einstein kondensater (BEC), og forskellige metoder til optimalt at danne en BEC med fordampningskøling. Den første del af denne afhandling præsenterer et eksperiment med translation af en termisk atomsky og en BEC controlleret med en bevægelig optisk pincet. Resultatet indikerer gyldigheden af en 1D klassisk model til at beskrive massemidtpunkts-svingningerne i relation til bevægelsens varighed, i tilfældet af translation af en BEC.

Den anden del er en undersøgelse af det optimale control landskab af fordampningskølingsprocessen af neutrale atomer. Dette er realiseret ved brugen af tre forskellige metoder. Den første metode bruger en systematisk skanning baseret på vores fysiske intuition vedrørende problemet. Den anden er en søgning lavet af en optimiseringsalgoritme. Den tredje ved at bruge gruppe-resurser, realiseret ved gamificering af fordampningsprocessen. Nye strategier til at danne mange-atom BEC'er var fundet, med resultatet fra gamificeringen værende det højeste udbytte nogenside opnået i vores opstilling, med $2.76 \cdot 10^6$ BEC atomer.

Acknowledgements

First of all I would like to thank my supervisor Jacob F. Sherson for his guidance and for always being inspiring and visionary. Then a great thanks to Aske for his help and counselling, always being ready to come with explanations, good perspectives and a new LabView trick. Also I will thank Robert a lot for reading through a large part of my thesis and to come with helping advices even when being at a Christmas party. A big thanks to Ottó and Jens for reading parts of my thesis. Of cause also thanks to Romain, and to Nicolai for being a great lab-DJ. Thanks to Kristbjörg and Jesper for giving a hand in the last moment and keeper the morale high. Then a thanks to the 700 players playing our ALICE-game and to Jonathan and Lærke for their help. Last a huge thanks to my parents and my dear sister for always being there.

Preface

During this master project I have been a part of a larger group and cooperated with different persons. The work I have done has been in a collaboration with others in the group, and for the sake of transparency I will outline here what part I have had in the different projects. In the following I will go trough each chapter and explain my part:

- Chapter 3: The Analysis server, the Camera module and the AOD module I developed and the remote part was in collaboration with a scientific employee.
- Chapter 4: I made the characterization of the AOD and was the lead on the translation of the atom cloud experiment. I was a part in the realization of the gamification of the translation of the atoms.
- Chapter 5.3: This section was brought for introductory reasons, and wasn't involved in implementation nor data-analysis.
- Chapter 5.4: I was not involved in the experimental part of the landscape-scans, but did all the data analysis presented.
- Chapter 5.5: A PhD student had the lead, and I was only a minor part of the implementation of the algorithm. I did all the data analysis presented.
- Chapter 5.6: I has a part in the technical realization of the ALICE-game, and I was involved in the design and realization of it. I did all the data analysis presented. The game was developed by CODER, and I was not involved in creating it.

Contents

Chapter 1

Introduction

The macroscopic quantum phenomenon, known as a *Bose-Einstein Condensate* (BEC), was first proposed in 1924 by Satyendra Nath Bose and Albert Einstein [1]. A BEC is a state of bosonic matter wherein all the particles occupy the energetically lowest state. It is created by cooling the atoms down to a temperature close to the absolute zero. The first experimental realization of an BEC was achieved in 1995 [2], and since has the interest for this exotic state of matter grown in the physics community. The development of still more sophisticated cooling and manipulation techniques has driven the field to an astonishing level of control over the quantum nature of atoms. This strong control has brought the field of BEC physics into a new exciting place, where ideas of new technologies, based on quantum mechanical phenomenons, are being realized in the laboratories. An example of new ideas in regard to quantum technology is *Atomtronics*[3, 4], which is a sub-field of ultracold atomic physics with the vision of making atom analogs of electronic materials, devices, and circuits. Another example is the highly desired quantum computer, in which many designs has been proposed [5, 6]. In the Quantum Measurement and Manipulation Group (QMMG) at Aarhus University, lead by Jacob Sherson, an experimental setup for creation and manipulation of ultracold atoms atoms has been realized, with the long term goal of creating a quantum computer. The experiment is controlled through a computer control system, going by the name ALICE. This system is able to create large BEC of ^{87}Rb atoms by evaporative cooling, manipulate the atoms with optical tweezers and take non-destructive images of the condensate by using off-resonant light.

In this thesis, the work I have done during the 11 months I have been in the group, is presented. I have been involved in two projects, one being the transport of a cloud of atoms and the other being evaporative cooling of atoms. The common ground of these

projects is the control of these experiments trough a newly designed remote control system. The structure of this thesis is therefore twofold:

- An investigation of the translation of a thermal atom cloud and the translation of a BEC, to better understand the relation between the center-of-mass oscillations induced by the movement, and the duration of the movement. This understanding can be used for designing optimal movement protocols for none-adiabatic transport of atoms. This is realized by using an Acousto Optical Deflector (AOD) for making a movable optical tweezer.
- An investigation of the optimal control landscape for the process of evaporative cooling of neutral atoms, for getting an impression of the landscape topology. This can give knowledge of the success of the performance of optimization algorithms in the control landscape. To explore as much of the control landscape as possible, three different methods ares used: The first is by making systematic scans based on our physical intuition of the problem. The second is a search performed by an optimization algorithm called dCRAB. The third is by gamifying the problem and opening for public access.

Contents

The thesis is structured as follows:

Chapter 2: Project background

An outline for the experimental setup, with its methods and techniques for cooling, trapping and manipulation of atoms.

Chapter 3: ALICE - An automated remote control system

An overview of the control system of the experiment (ALICE), together with a description of new added functionality.

Chapter 4: Arbitrary optical potential control

A new added module to ALICE will be introduced. This module is used to create and control an optical tweezer by using an Acousto Optical Deflector (AOD). The moveable

tweezer is used to make an experiment consisting of a translation of a thermal cloud and a BEC. A gamification[1] of the atom cloud movement will be presented.

Chapter 5: Optimal control landscape of the creation of BEC atoms

An investigation of the control landscape for the evaporative cooling process. Three different methods is used to map out this landscape.

- By making manual scans, where the scan parameters are from the an expression describing a evaporative cooling process.
- By using a state of the art optimization algorithm.
- By a gamification of the evaporative cooling process, letting people from outside the science community search the control landscape.

Chapter 6: Conclusion and Outlook

A summary of the content of the thesis is outlined together with an outlook of the next steps for the group to take.

[1] Apply game elements to problems without a direct game context.

Chapter 2

Project background

The experimental setup created in the Hires group at Aarhus University is able to produce and manipulate ultra-cold ^{87}Rb atoms. In this section a short overview of the Hires experiment is presented, together with a basic explanation of the techniques used in order to cool, manipulate and image atoms. For a full description of the experimental setup, see [7].

2.1 A typical experimental sequence

In order to produce ultra cold atoms, several cooling techniques need to be applied to the ^{87}Rb atoms, which are ordered in a sequence generated by our control system called ALICE. In the following a typical production sequence will be explained. Later the different individual phases and techniques will be elaborated. The experimental setup used is shown in figure 2.1.

Firstly the atoms are loaded from a dispenser into a 2D MOT chamber where the atoms are cooled by a magneto-optical trap in two dimensions. The pressure in this chamber is about 10^{-7} mbar. Due to the fact that the atoms are only confined in two dimensions they can propagate freely in the direction towards a 3D MOT chamber. A laser beam is used to push the atoms towards this chamber. The coupling between the two chambers is through a differential pressure tube, generating a difference in pressure of about two orders of magnitude. Two coils in an anti-Helmholtz configuration are located at the top and the bottom of the 3D MOT chamber respectively and deliverers an magnetic gradient field up to 150 G/cm. In this chamber the atoms are cooled down by the 3D MOT and by *Doppler cooling*, down to a temperature about $50\mu K$. The atoms are now cold enough to be confined only by the magnetic field. By having the two Helmholtz coils on a movable rail, the atoms are transported from the 3D MOT chamber to the cube

chamber by moving the coils. In the cube chamber the atoms temperature is further lowered by *microwave evaporation*, and lastly by evaporative cooling by lowering the trap potential, making the atoms crossing the transition to a Bose-Einstein condensate (BEC). It is also an option to transfer the atoms to the last chamber, called the science chamber. A laser is attach to a controllable translation stage, which can move the focus of the beam. By trapping the atom cloud by this beam, the cloud can be transported.

2.2 Bose-Einstein condensate

Bose particles, which are particles with integer spins, has the property that they can occupy the same quantum state. This allows a gas of Bosons to be in a phase called a BEC, were multiple of the particles are in their lowest energy state. When in this phase the description of the gas as a number of moving particles following classical thermodynamics breaks down, and the system is described by a single wave function instead. Figure 2.2 shows a series of pictures taking in our laboratory of the transition from a classical gas to a BEC. In the following comes a description of the transition to a BEC for the noninteractive case, following [8].

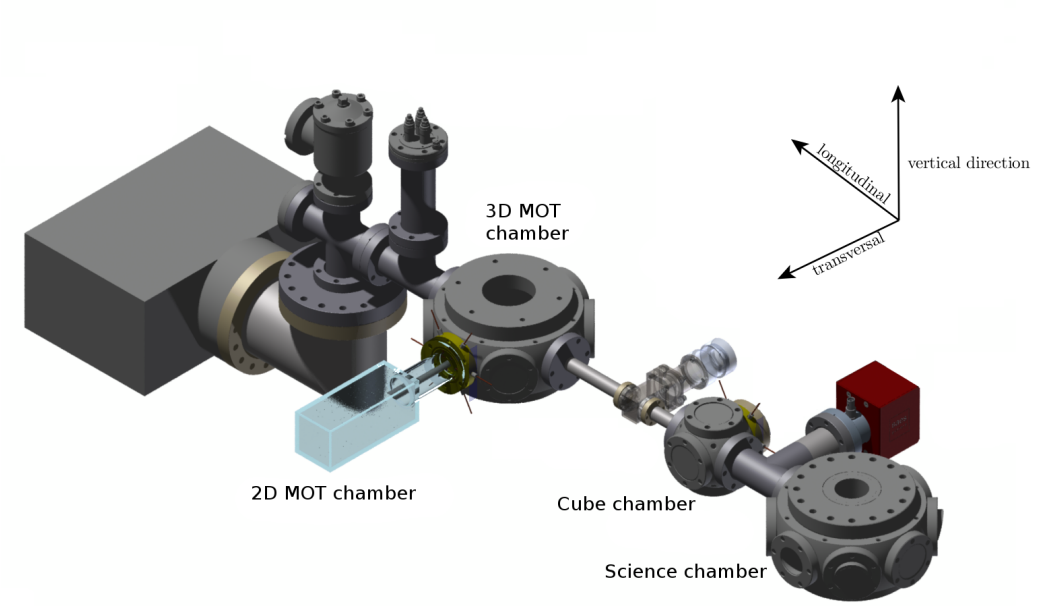

Figure 2.1: Illustration of the experimental setup. Adapted from [7]

2.2.1 Non interacting Bose gas

For a noninteracting ideal Bose gas in thermodynamic equilibrium, the average population of the state i is given by the Bose-distribution

$$N_i = \frac{1}{e^{(\epsilon_i - \mu)/k_\mathrm{B}T} - 1} \tag{2.1}$$

where ϵ_i denotes the energy of the state i, k_B is the Boltzmann constant, T is the temperature of the system and μ is the chemical potential. In a BEC a finite part of the particles are in the ground state with energy ϵ_0 and the rest in the exited state with energy $\epsilon_{i>0}$. When the Bose gas is cooled enough a transition to the BEC occurs. The temperature between these two phases is called the critical temperature T_C, and is defined as the highest temperature where a macroscopic occupation of the lowest energy state starts to appear. It is used as the criteria for when a BEC starts to occur. The number of particles in the exited state is giving by the integral over the average population weighted with the density of state

$$N_{excited} = \int_0^\infty d\epsilon\, g(\epsilon) N(\epsilon) \tag{2.2}$$

The critical temperature can be determined by the condition that all particles are populated in the exited states with $\mu = 0$

$$N = N_{excited}(T_c, \mu = 0) = \int_0^\infty d\epsilon\, g(\epsilon) \frac{1}{e^{\epsilon/k_\mathrm{B}T} - 1} \tag{2.3}$$

Assuming that the particles are trapped in a three dimensional harmonic potential, then solving the integral gives

$$k_\mathrm{B}T_c = 0.94\hbar\overline{\omega}\, N^{1/3} \tag{2.4}$$

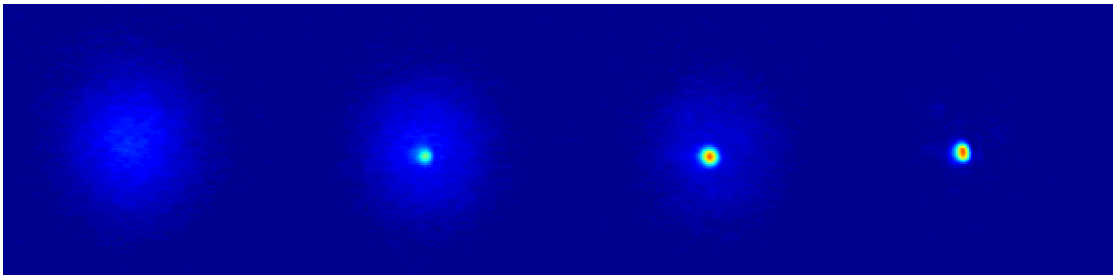

Figure 2.2: The transition from a thermal cloud to a BEC, depicted by images taken from our laboratory. The high intensity on the images to the right indicates a BEC cloud.

where $\overline{\omega} = (\omega_x\omega_y\omega_z)^{1/3}$ is the mean trap frequency with $\omega_{x,y,z}$ the three harmonic trap frequencies.
By using the expression for T_c, the number of particles in the BEC can be formulated as

$$N_0 = N\left[1 - \left(\frac{T}{T_c}\right)^3\right] \tag{2.5}$$

It is useful to introduce the phase-space density

$$\rho = n\lambda_{db}^3 \tag{2.6}$$

This is defined as the number of particles contained within a volume equal to the cube of the thermal de Broglie wavelength $\lambda_{db} = \sqrt{\frac{2\pi\hbar^2}{mk_BT}}$. When the phase-space density is above the value $\rho \simeq 2.6$ the BEC starts to appear. This can be interpreted as being that value where the wave functions for the particles starts to overlap.

2.3 Trapping and cooling neutral atoms

In order to make the phaseshift from a thermal cloud to a BEC, the phase-space needs to go below the critical value. This can be realized by cooling the atoms down below the critical temperature T_c which depends on the density of the cloud. In this section the techniques used in our experiment to archive this will be described.

2.3.1 Optical trapping

Neutral atoms can be trapped by a laser beam by exploiting the induced dipole moment of the atoms, emerging due to the oscillating electric field **E** of the laser light. The interaction between the induced dipole moment and the electric field leads to a shift in the energy, which creates an attractive or repulsive dipole force determined by the detuning of the laser.
From the description in [9] the dipole moment is related to the amplitude of the electric field by

$$\mathbf{P} = \alpha(\omega)\mathbf{E} \tag{2.7}$$

where α is the complex polarizability of the atoms, which depends on the driving frequency ω of the oscillating electric field. The interaction potential of the induced dipole moment is given by

$$U_{\text{dip}} = -\frac{1}{2}\langle \mathbf{p}\cdot\mathbf{E}\rangle = -\frac{1}{2\varepsilon_0 c}\text{Re}(\alpha)I \tag{2.8}$$

with c being the speed of light in vacuum, ϵ_0 the vacuum permeability and $I = 2\varepsilon_0 c|E|^2$ denoting the intensity of the light beam. Assuming that the detuning $\Delta \equiv \omega - \omega_0$ fulfils $|\Delta| \ll \omega_0$, where ω_0 is the resonance frequency. Then following [9] who are using a semi-classical approach to find an expression for the polarizability and inserting it into the above expression for the energy gives

$$U_{\text{dip}}(\mathbf{r}) = \frac{3\pi c^2}{2\hbar\omega_0^3}\frac{\Gamma}{\Delta}I(\mathbf{r}) \tag{2.9}$$

The parameter Γ in the expression is called the damping rate and corresponding to the spontaneous decay rate of the excited level. From the above equation it is apparent that a red detuning of the laser ($\Delta < 0$) will give a negative potential and thereby an interaction that attracts atoms into the light field, were a blue detuning ($\Delta > 0$) will make the atoms be repelled by the light field. The expression for the scattering rate Γ_{sc} can also be found from a semi classical approach and which for $|\Delta| \ll \omega_0$ is

$$\Gamma_{\text{sc}} = \frac{3\pi c^2}{2\hbar\omega_0^3}\left(\frac{\Gamma}{\Delta}\right)^2 I \tag{2.10}$$

The dipole potential scales with I/Δ and the scattering rate by I/Δ^2. To avoid heating by photon scattering, large detuning and high intensity is therefore favourable.

2.3.2 Magnetic Trapping

Another way of trapping neutral atoms is with a magnetic field which is due to the Zeeman effect. In analogy with a current loop, the angular motion of the electric charge induces a magnetic dipole moment

$$\hat{\boldsymbol{\mu}} = -\frac{\mu_B}{\hbar}g_{\text{F}}\hat{\mathbf{F}} \tag{2.11}$$

where g_F is the Landé g-factor and μ_{B} is the Bohr magneton and $\hat{\mathbf{F}}$ is the total angular momentum operator. The interaction with the magnetic field $-\hat{\boldsymbol{\mu}} \cdot \mathbf{B}$ removes the degeneracy of the hyperfine states $|F, m_{\text{F}}\rangle$ due to the Zeeman effect. The splitting of the energy levels is shown in figure 2.3. The potential the atoms experience due to the zeeman effect is given by

$$U(\mathbf{r}) = \mu_{\text{B}} g_{\text{F}} m_{\text{F}} |\mathbf{B}(\mathbf{r})| \tag{2.12}$$

In this experiment we prepare the ^{87}Rb in the F = 2 state, where $g_{\text{F}} = 1/2$. From this follows that the m_F quantum number determines the effect the field has on the atoms. If $m_{\text{F}} < 0$, the state has the property of being *high field seeking* as the energy decrease

with the strength of the magnetic field. The states with $m_{\mathrm{F}} > 0$ has the property of being *low field seeking*, as the energy increase with the strength of the magnetic field. As in the case of the optical trap, this linear chance in energy makes it possible to trap neutral atoms prepared in some specific states. Opposite to the optical trap it is not possible to trap atoms in high-field-seeking states because no local maximum can exist for a magnetic field. In this experiment, the magnetic quadrupole field is used, realized with two coils in an anti Helmholtz configuration. The magnetic field strength from this is approximately linear when close to the center of the trap. The expression for the magnetic for a quadrupole trap is given by

$$\mathbf{B}(x, y, z) = B'(x, -2y, z) \tag{2.13}$$

where B' is the magnetic gradient which in our experiment has the strength $B' = 1.54\mathrm{G/cm/A}$. As the atom cloud becomes colder, the density in the region with the magnetic field about zero increases. For these atoms there is a probability to make a transition to an untapped magnetic state, and thereby escape from the trap. This phenomenon is called *majorana losses*. Because the atoms that escapes is the coldest, this leads to an undesired warming of the cloud. This effect can be circumvented by using an additional magnetic field or by adding an optical dipole field which sets a "plug" in the potential hole of the trap.

2.3.3 Magneto Optical Trap

A magneto optical trap (MOT) is a technique used to trap and cool neutral atoms by using a combination of light beams and a magnetic field. The method is used in most

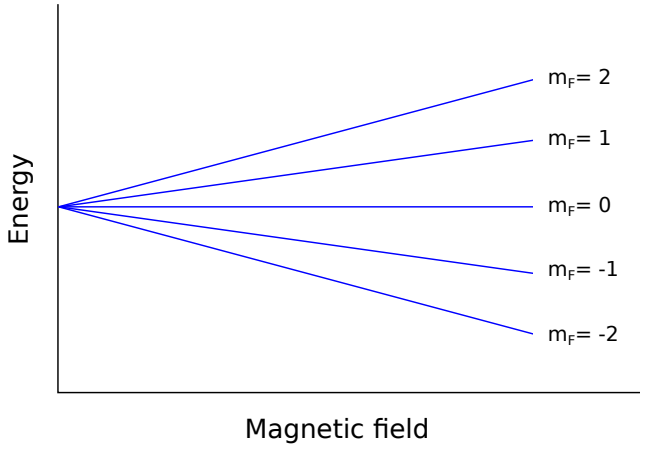

Figure 2.3: Illustration of the splitting in energy levels due to a magnetic field. The degenerate states are divided according to their M_{L} quantum number.

experiments making BEC in the initial cooling phase, cooling the atoms down to some hundreds of μK depended of the atoms [10].

Consider the situation of a light beam hitting a cloud of atoms. When an atom absorbs a photon from the beam it changes its momentum by $\hbar\mathbf{k}$, where $\mathbf{k}$ is the wave vector of the photon. A photon is emitted from the atom, making the momentum of the atom change by $\hbar\mathbf{k}$. The direction of the emitted photons are random, which on average sum out, leaving an extra momentum contribution in the propagation direction of the light, creating a *ligth force*. This force is proportional to the scattering rate of the photon which is dependent on the detuning of the light $\Delta = \omega_{\text{atom}} - \omega_{\text{laser}}$. By using two lasers in opposite directions, this scattering effect can be used to cool down neutral atoms. Due to the Doppler shift an atom moving with velocity v will see an photon with an effective detuning $\Delta_{eff} = \Delta + kv$, and the light force acting on the atom will depend on its velocity. This will slow down the atoms in the direction of the lights propagation, and lead to cooling of the atoms, called *Doppler cooling*.

Though the light beams has no spacial dependence in the propagation direction, and hence no trapping of the atoms is realized. To realize this, a quadrupole magnetic field is applied, making use of the Zeeman shift to confine the atoms. The atomic transitions becomes spacial dependent and with the right laser detuning and right magnetic field, the effective force can be designed so it points towards zero magnetic field. The lower limit of the cooling is bound by the recoil temperature, which is due to the heating of a single photon emission. For ^{87}Rb atoms, this temperature is $T_{\text{R}} = 0.4\,\mu\text{K}$. The technique described here can be used to create cooling and confinement in all three spacial dimensions by using two opposite pointing laser beams for each dimension.

2.4 Evaporative cooling

In order to cool a cloud of atoms enough to make the crossing to the BEC phase, a cooling technique know as *evaporative cooling* is necessary. This method is illustrated well by thinking of the cooling of a cup of coffee by blowing the steam emerging from the liquid away. The water molecules in the coffee transfers energy to each other by elastic collision and with some probability a particle receives enough to go to the gas phase and escape form the cup, cooled by evaporation. Blowing away the steam makes place for new particles to evaporate. In a thermal cloud the energy of the particles are Boltzmann distributed, and by lowering the potential confining the atoms with most energy escapes or in other words the tail of the Boltzmann distribution is cut of. After this the cloud needs to rethermalize by some amount of time to retain the Boltzmann distribution, before lowering the trap potential further. The evaporation process can be realized in different ways, where the main used will be elaborated here.

2.4.1 Microwave evaporation

Microwave evaporation exploit the energy shifts in ^{87}Rb due to the Zeeman effect, and can be made in a quadrupole trap as is done in our experiment. The main idea is to drive a transition from the trapped state $|F = 2, m_{\mathrm{F}} = 2\rangle$ to the untrapped state $|F = 1, m_{\mathrm{F}} = 1\rangle$ by microwave radiation. By choosing a detuning frequency corresponding to the transition of the hot atoms to an untrapped state, and by gradually lowering this frequency the cloud can be cooled down removing these hot atoms.

2.4.2 Crossed dipol trap

Making evaporative cooling by lowering the trap potential, can be realized by different forms of trap configuration. In the following two types of these configurations called a *crossed dipole trap* and a *hybrid trap* will be explained.
An optical trap with confinement in all three spacial dimensions can be created by a single focused Gaussian beam tuned far away from the atomic resonant frequency, thereby not heating the atoms. The intensity distribution for a Gaussian beam propagating in the z-direction is given by

$$I(r,z) = \frac{2P}{\pi w^2(z)} \exp\left(-2\frac{r^2}{w^2(z)} \right) \tag{2.14}$$

were r denotes the radial coordinate, P is the power of the beam and $w(z)$ is the radius of the beam given by

$$w(z) = w_0 \sqrt{1 + \left(\frac{z}{z_{\mathrm{R}}}\right)^2} \tag{2.15}$$

where w_0 is called the beam waist and $z_{\mathrm{R}} = \pi w_0^2/\lambda$ is the *Rayleigh length*. Figure 2.4 shows the intensity for a focused Gaussian beam. From the expression 2.9 the potential is seen to be proportional to the intensity as $U(r,z) \propto I(r,z)$. The Gaussian potential can be approximated with a Taylor expansion by a cylindrical symmetric harmonic potential

$$U_{GB} = -\hat{U}\left[1 - 2\left(\frac{r}{w_0}\right)^2 - \left(\frac{z}{z_R}\right)^2\right] \tag{2.16}$$

where $\hat{U}$ is the potential trap depth. From this we can associate a trap depth for the axial z-direction and the radial direction

$$\omega_r = \sqrt{\frac{4\hat{U}}{m w_0^2}}, \quad \omega_z = \sqrt{\frac{2\hat{U}}{m z_R^2}} \tag{2.17}$$

Because the Rayleigh length is larger than w_0 by $\pi w_0/\lambda$ the radial direction has steeper potential gradient and thereby a stronger confinement of the atoms than in the axial direction.
The trap can be nearly isotropic by instead applying two Gaussian beams with equal waist perpendicular to each other which will give a strong confinement in all dimensions. This setup is called a crossed dipole trap. The potential for this configuration can also be Taylor expanded which gives the following trap frequencies

$$\omega_{x,y} = \sqrt{\frac{2\hat{U}}{mw_0^2}}, \quad \omega_z = \sqrt{\frac{4\hat{U}}{mw_0^2}} \tag{2.18}$$

The crossed dipole trap has a combination of large sized trap volume and a tight confinement which makes it suitable for evaporative cooling. It enables it to trap a lot of atoms and still has a steep enough trap to make it dense enough for a high collision rate.

2.4.3 Hybrid trap

A hybrid trap is a dipole trap with an added magnetic field. The atoms are initially trapped in the quadrupole trap and pre-cooled by microwave evaporation. Then the cloud is loaded to a single Gaussian dipole beam by gradually lowering the magnetic field in till the the magnetic field is at the strength of the gravitational force. In our case with ^{87}Rb prepared in the state $\mid F = 2, m_F = 2\rangle$, it correspond to a gradient at $B' = 15.3G/cm$. Now the remaining magnetic field is responsible for the confinement in axial direction were the dipole beam makes the confinement in the radial direction. From here the power of the dipole beam is lowered in till the phase-space density is high enough for BEC atoms to emerge.

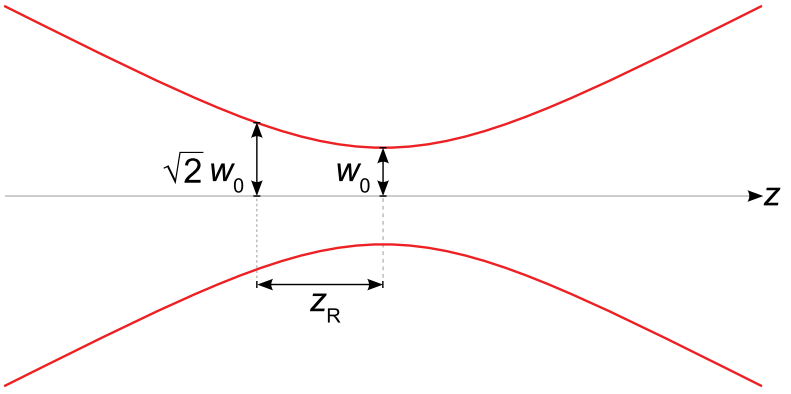

Figure 2.4: Illustration a Gaussian beam with the red curve indicate the width of the beam. z_R is the Rayleigh length and w_0 is called the beam waist.

2.5 Imaging

A typical probing method used to get information about ultra-cold atomic clouds and BECs is optical probing. Measuring of an atomic cloud by light can be performed in two ways. By off-resonant probing or resonant probing, where the resonance is when the transition frequency between the ground state and an excited state of the atoms is matched. In this section these two methods will be described.

2.5.1 Absorption

When shining resonant light on an atom cloud, the photons has a probability of exciting the state of the atoms, transferring their energy and thereby being absorbed. The light obtained by a camera will have a lower intensity in a region corresponding to the atom cloud due to this absorption. The optical density τ relates the intensity of the light before and after transmission by Beer-Lamber law as $I = I_0 \exp(-\tau)$. By taking three images τ can be obtained. The first is an image of the cloud taken with resonant light beam. The second is an image without the cloud, but with the light on. The last is a background image without the light used to cancel out noise and set an offset of the light intensity. From these images the optical depth can be found as

$$\tau = \ln\left(\frac{I_{light} - I_{background}}{I_{cloud} - I_{background}}\right) \tag{2.19}$$

The column density of the cloud is related to the optical density trough

$$\tau = \sigma \int n(z)dz \tag{2.20}$$

were z is the axial direction of the light, $n(z)$ is the column density and σ is the attenuation cross section. An disadvantages by this imaging technique is due to the heating of the cloud by the absorption of the photons, which leads to a destruction of the cloud. Therefore another technique has been implemented in our laboratory, called *Faraday imaging* explained in the next section.

2.5.2 Non destructive Faraday imaging

Nondestructive imaging, can give information about an atomic system without destroying it with heating effects. This due to the usage of off-resonant light. When a linear polarized light beam propagates trough an atom cloud, the plane of polarization of the light will be rotated, because of dispersive light-matter interactions. The underlying

mechanism of the interaction between light and matter can be described within the dipole approximation with the Hamiltonian

$$\hat{H} = -\mathbf{d} \cdot \mathbf{E} \tag{2.21}$$

where $\mathbf{d}$ is the induced dipole moment of the atoms and $\mathbf{E}$ is the electric field. As described in in [11], the effective interaction Hamilton can be written as two parts

$$\hat{H}_{\text{eff}} = \hat{H}_{\text{scal}} + \hat{H}_{\text{vec}} \tag{2.22}$$

where $\hat{H}_{\text{scal}}$ is the scalar part and $\hat{H}_{\text{vec}}$ the vectorial part. These are given by

$$\hat{H}_{\text{scal}} = \frac{1}{3} g \alpha^0 \hat{N}_{\text{at}} \hat{N}_{\text{ph}} \tag{2.23}$$

$$\hat{H}_{\text{vec}} = \frac{1}{2} g \alpha^1 \hat{F}_z (\hat{N}_+ - \hat{N}_-) \tag{2.24}$$

where g is the field factor $g = \omega / e\epsilon_0 V$ with V being the interaction volume. $\hat{N}_{\text{at}}$ and $\hat{N}_{\text{ph}}$ are the number operators for the atoms and photons, respectively and $\hat{N}_+$ and $\hat{N}_-$ are number operators for right and left polarized light, respectively. α^0 and α^1 are the polarizability, which depends on the detuning $\Delta_{f,f'} = \omega_f - \omega_{f'}$ between the two involved atomic transitions f, f'. Expressions for α^0 and α^1 can be found in [11]. $\hat{F}_{\text{z}}$ is the z component of the collective atomic angular momentum, where the z axis is the defined as the propagation direction of the light.

The eigenstates of the effective Hamiltonian $\hat{H}$, is given by the circularized polarization operators $\hat{N}_{+/-}$ with eigenenergies $E_{+/-}$. For the scalar part, a phase shift is induced, given by a superposition of the left and right polarized light, which is used in the imaging method *phase contrast imaging*. For the vectorial part, an phase shift θ_{F} dependent on the difference between the left and right polarized light is induced given by

$$\theta_{\text{F}} = \frac{1}{2\hbar} \int (E_+ - E_-) dt. \tag{2.25}$$

The effect of the vectorial part $\hat{H}_{\text{vec}}$ is rotation of the polarization plane of the light by an angle θ_{F}. For the case of atoms prepared in the $|F = 2, m_F = 2\rangle$ state, the angle can be expressed as

$$\theta_{\text{F}} = c(\Delta) \int n(\mathbf{r}) dz \tag{2.26}$$

where c is a coefficient dependent on the detuning, and $n(\mathbf{r})$ is the density of the atomic cloud. Thereby it is possible to map out the density distribution of the cloud by measuring the rotation of the polarization plan.

Chapter 3

ALICE - An automated remote control system

The complexity of many modern physic experiments sets high requirements on the experimental setup together with the requirement of computer control [12]. In the field of atom physics the preparation of the atoms in a given state, and the manipulation afterwards, makes the design of the experiment control system an important part of the setup. It can be beneficial having a design that is scalable, making it possible to extend or replace the setup with other functionalities. In our group, an experimental setup has been build in the form of a control system which goes by the name ALICE. This control system meets the versatility required for the complexity of our experiments and flexibility needed to realize them.

3.1 ALICE control system

The ALICE control system is created based on the idea of separating the technical challenges and the design of a specific experiment. This is handled by making an abstraction of the sub-processes involved in the possible experiments. For example is the creation of BEC atoms in our experiment realized by a sequence of multiple separable processes that need to be executed:

- Transport the atoms to the 3D MOT chamber.
- Cool the atoms in the 3D MOT.
- Transport the atoms to the cube chamber.
- Make evaporative cooling.

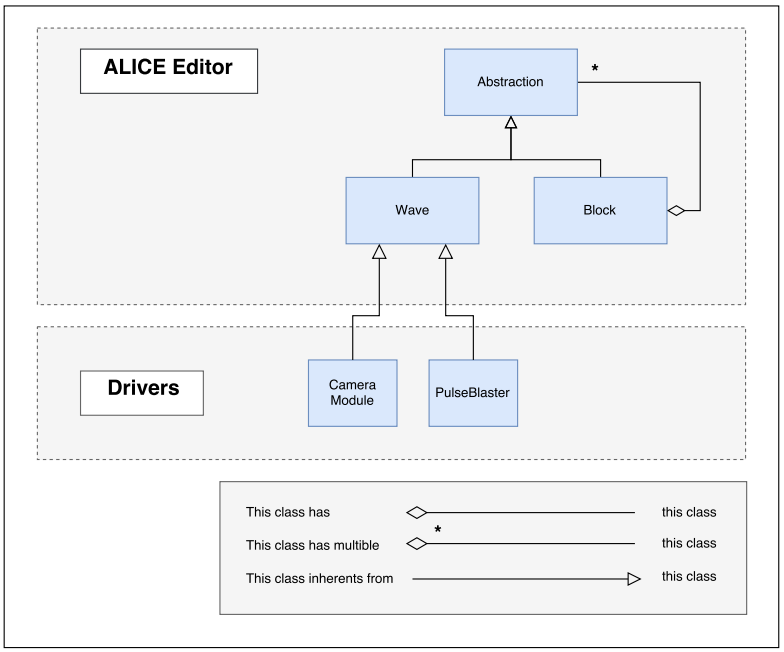

Figure 3.1: UML diagram showing the software architecture of the ALICE editor program. The terminology of an UML diagram is used, and is explained in [13].

Each of these processes are realized through multiple hardware equipments that need to be controlled in a sequential or parallel order. For instance in the case of evaporative cooling, two different laser beams and a magnetic field is controlled at the same time in parallel, and after the cooling a camera takes an image of the cloud.

A diagram of the control design is shown in figure 6.1. The abstraction of this sequence is made by atomize the experimental sequence into entities called *waves*. Each wave represent a given hardware functionality, which could be the time evolution of the magnetic field for a given experiment. For each wave some predefined parameters need to be sat, which are specific for each wave type. In the case of the magnetic field wave, parameters defining the time dependant magnetic field gradient is open for the user to choose. Multiple of predefined waves are accessible for the user. The waves can be put after each other in a sequential form or placed parallel beside each other. A sequence can be illustrated as an opposite tree, with time going down and each vertical line representing a wave. This gives the user the opportunity of creating the intended sequence necessary for a given experiment. A sequence created within this user interface can be saved as a *block*. The connection between the blocks and the waves is designed as a *composite pattern*, which is a programming design that in this case allows waves and blocks to be treated equally. This makes it possible to add a wave or a block into another block. Thereby larger parts of the experiment can be defined and kept in blocks, for example the evaporative cooling procedure, or even whole experiments.

With the design of ALICE it is relatively easy to add new functionality by adding new

hardware modules. The drivers for the modules has to be designed within the framework of ALICE to define a new wave for the new added functionality. To extend the control system for new requests I designed two modules that was added to ALICE. The first was for steering the dimple beam with an Acousto Optic Deflector (AOD), which is described in chapter 3. The second module was for controlling the cameras used in the experiment and for analysing the images taken, and is described in next section. For a detailed explanation of the ALICE control system see [14].

3.2 Closed loop system

The experimental system ALICE is build as a *closed looped* control system. A closed loop system is a system in which its control action is dependent on a feedback of the experimental output. It is used in our experiment to realize an automated optimization system. In the following the technical realization of the closed looped system is outlined in steps, following the schematic in figure 3.2.

1. For each step in the optimization, the ALICE editor starts by sending a request to the hardware system for an evaluation of an experiment with parameter values chosen by the optimization algorithm.

2. The experiment is executed.

3. After completion an image of the experiment is taken. Either by using absorption imaging with an uEye camera or by non-destructive Faraday imaging with an IXon camera.

4. The data acquisition are done by two stand alone programs programmed in LabView, which are located on computer 2.

5. For each of the two imaging methods, a stand alone program are used to analyse the images giving an output, which for example could be the BEC atom yield. Both of these programs are written in Matlab. The images is transferred to the analysis program through a so called *folder protocol*. This protocol works by the agreement that the image files are saving in a specific folder on the computer. The loading program constantly scans this folder for new files, which it loads and handles.

6. The result is send to the ALICE editor program also through a folder protocol.

7. The ALICE editor has the option of being in an optimization mode, that can either be local or remote. In both cases the connection to the optimization algorithm

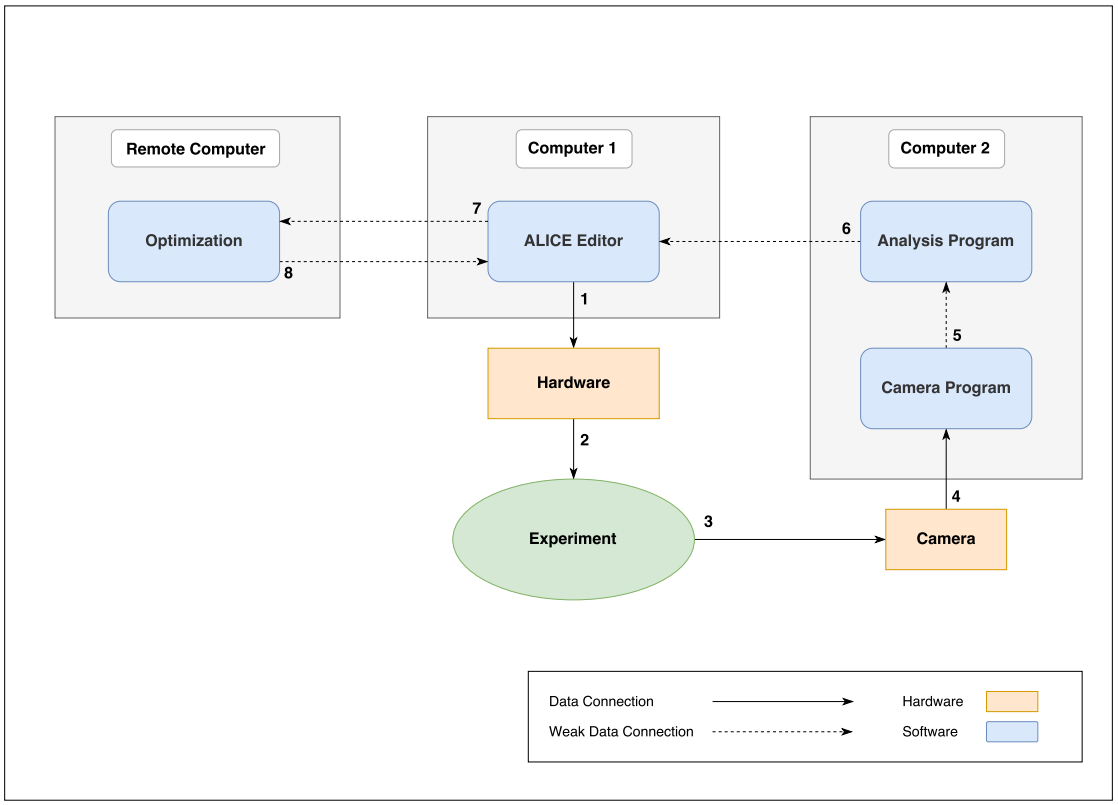

Figure 3.2: Block diagram showing the connections of the ALICE cloosed loop system.

happens trough a folder protocol. In the remote option a dropbox folder is used creating the remote functionality. A remote client can then gain access to the experiment through a ALICE-client LabView program that has the information about the address of the dropbox folder.

8. When the optimization algorithm has found new parameter values for evaluation, the information is send to the ALICE editor which completes the loop.

The communication trough the folder protocol can be problematic and is therefore referred to as a *weak connectivity*. The term of connectivity relates here to how well the data flow between entities is organized. It consist of the folder-scan agreement, which all depend on the name-string of the folder, which has to be set correctly in all separate programs. The connection can be vulnerable to errors when transferring the files and error handling is difficult to implement. Each program has to be started separately and set to a specific state to function, making a possibility for human mistakes.

In the next section a proposal of a new module for the ALICE system will be presented for solving some of the problems of the present design of the closed looped system.

3.2.1 Analysis Server module

For making a strong connectivity of the ALICE control system, the add-on module Analysis server is presented. This is a stand-alone program that includes handling of the cameras, the analysing of the images and a decision system. The foundation for the program has been made, but not all the parts have been realized. A block diagram shown in figure 3.3 present the concept of this new unit. The green blocks indicate the completed parts and the red indicate the not implemented, only conceptual, parts. In the following a description of the design is given:

1. The coupling to the ALICE editor is through a LabView network protocol. The ALICE editor need to give commands like which camera to use, which analysing method to perform and which decision tool to use. Furthermore specific settings need to be send for example exposure time for a specific camera.

2. The Analysis server has the responsibility to keep track of arbitrary many cameras of different types. Because of the different types of cameras, a programming design known as *strategy pattern* [13] is used. The idea of this is to make an abstraction of the camera object and let the abstraction be responsible for dealing with the general problem of taking an image, by calling the function *Take Image*. For each specific camera type it is mandatory to implement this function which will contain the specific needs of this camera type. This will make the program structure general, flexible and coherent.

3. A Graphical User Interface (GUI) can for each camera be opened by the Alice editor for manual handling.

4. Each camera has a analysis object which is also abstracted trough a strategy pattern. The analysis programs are made in Matlab making a it necessary for a function that can handle the communication between the two programming languages.

5. The Analysis server makes the handling of the return data through a messaging system, realized with the *Actor Framework* available in Labview [2].

6. The error handling unit makes checks for error massages or makes an independent analysis of the data given. If an error is present it bypass the optimization unit and makes a decision in relation to the next experimental sequence.

7. The Analysis server creates one optimization unit which handles the analysis results from all the camera units active. It can choose between local optimization

[2] http://ni.com/actorframework

methods or remote optimization. It makes a decision based on the data given and sends a new set of parameter values to the ALICE editor for the next experimental sequence.

3.3 Remote control system

An option for remote control of our experimental system has been added. A block diagram of the system i shown in figure 3.4. The remote connection is created with a folder protocol through dropbox. Multiple clients can have access to the control system, each with a specific experiment, due to a queue system implemented. When a client sends a request it is stored as a file in the a dropbox folder, denoted the queue, which works with the *first in, first out principle* (FIFO). When idle, the ALICE server scans the queue and loads a request file and sends it to the ALICE editor which executes the experiment. When complete a result is send to a result folder unique for each client. The client program is set to continuously scanning its result folder to retrieve the outcome of its request.

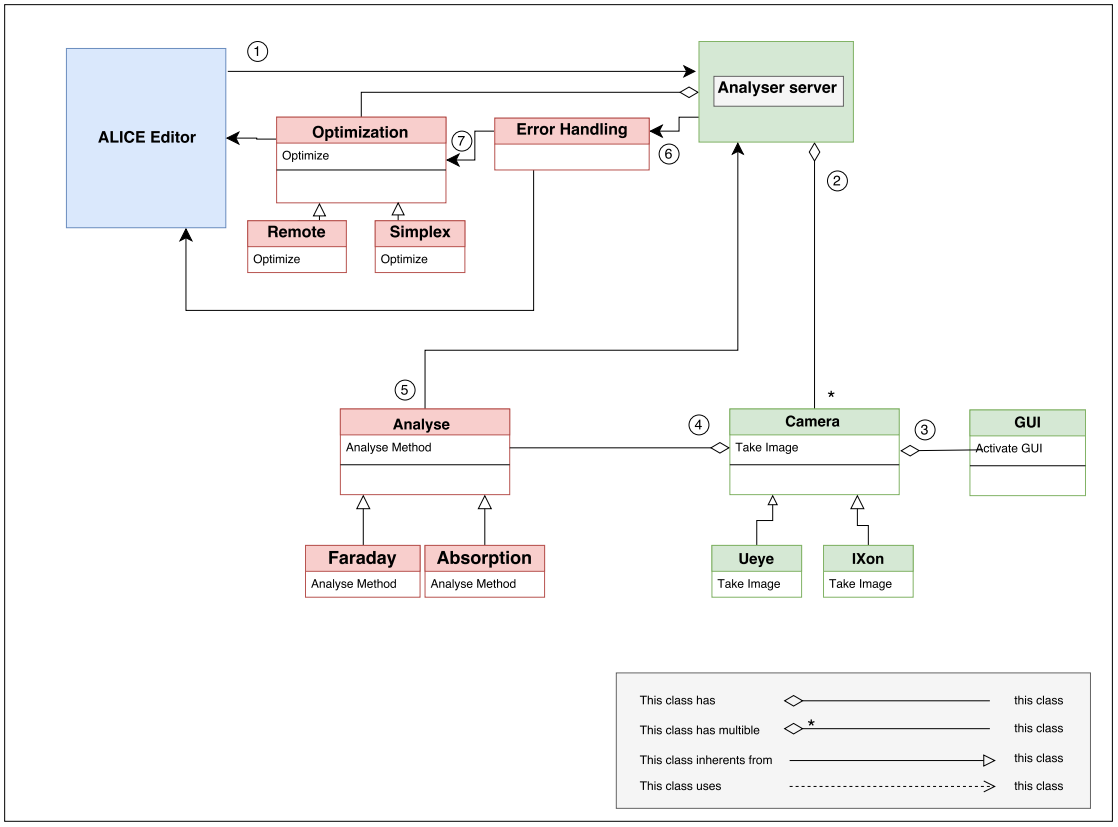

Figure 3.3: UML diagram for the conceptual design of the Analysing server. Green parts are implemented, and red parts are design ideas. The terminology of an UML diagram is used, and is explained in [13].

With our automated remote control system, we have been able to open our laboratory for physicist at universities around the world and to people that is not a part of the science community. In the next chapters the first results of this remote system will be presented and in chapter 4 it will be used to make a gamification of an experiment.

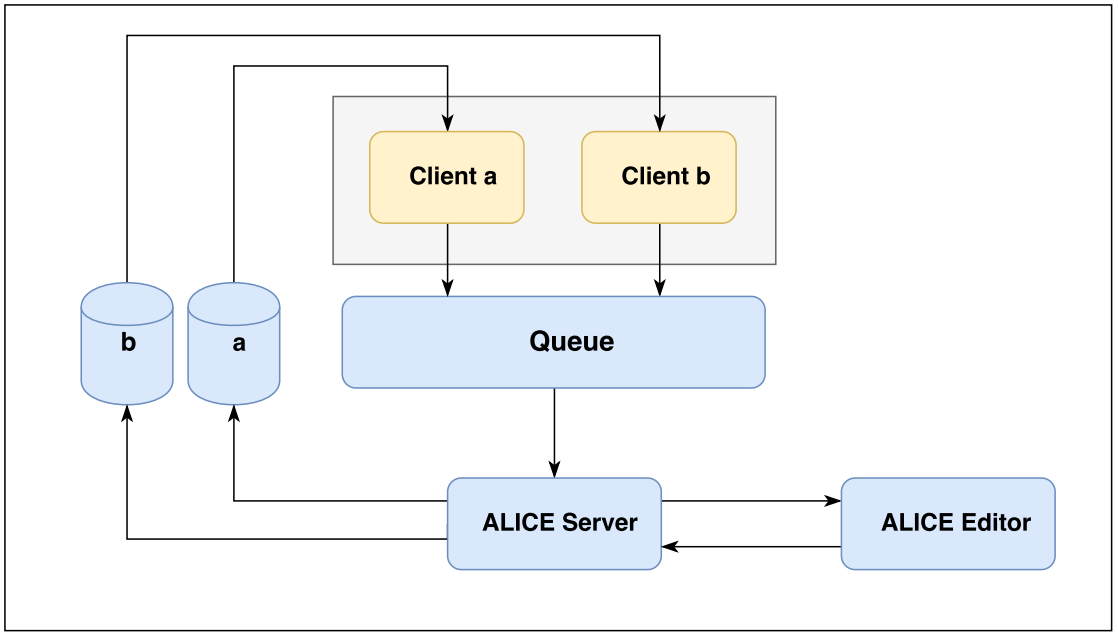

Figure 3.4: Block diagram of the implementation of the remote system.

Chapter 4

Arbitrary optical potential control

4.1 Introduction

The ability to gain complete control over the location of single atoms or atom clouds is growing still stronger, parallel with the aim of building quantum simulation systems or realizing a quantum computer. To obtain the control over neutral atoms a detuned light field can be used to make a confinement of the atoms as explained in 2.3.1. The light beam acts as a trapping potential which is called an *optical tweezer*. For steering the tweezer, different techniques can be used, where some prominent options are an *Acousto Optical Deflector* (AOD) or a *Digital Mirror Divice* (DMD).
An AOD is a crystal one can use to control the angle of a transmitted beam, thereby gaining control over the position of a laser beam. The DMD is a device consisting of a matrix of small mirrors, each with a size of tens of micrometers, which can be in two states, controllable with an electrical signal. With these devices an arbitrary light pattern can be realized, which can be used to form patterns of atoms, or perform steering of atoms by changing the configuration of the mirrors.
This chapter describes the use of a newly-designed module added to the ALICE control system, for controlling neutral atoms trough an AOD device. Firstly the functionality the AOD is explained, then the setup of the AOD system is described and a characterization of the performance of the AOD is made. The arbitrary control module is then used to investigate the translation of a thermal atom cloud or a BEC to understand the center-of-mass oscillations induces by the movement. Lastly two outreach projects are presented, using the ALICE remote control capability to enable people not being in the science community, to manipulate atoms in our experiment.

4.2 Acousto Optical Deflector

An Acousto Optical Deflector is a device which can realize an optical twezeer or a time averaged arbitrary optical potential. It is used widely in different kinds of experiments, for example to realize different topological constructions with ^{87}Rb atoms [15], using the AOD to control tweezer moving atoms [16], or making arbitrary patterns of a Fermi gas consisting of ^{6}Li atoms [17].

The AOD exploits the interaction between sound waves and light waves in a medium. It consist of a transparent crystal, that can be made of different kinds of materials. The presence of an acoustic wave in the crystal modifies the density of it leading to a periodic grating of compressed regions and uncompressed regions, determined by the wavelength of the sound. This alters the refraction index, making it to a periodic entity determined by the soundwave [18]. This grating emerges as a set of parallel optical planes separated by the wavelength of the soundwave Λ.

Consider a light beam propagating trough the medium. The planes will reflect the light if the angle of incident θ satisfied the Bragg condition for constructive interference $\sin(\theta) = n\,\lambda/2\Lambda$, where λ is the wavelength of the light in the medium and n is an integer determining the order of diffraction. As shown in figure 4.1 the Bragg diffraction leads to a transmitted 0th order and a diffracted 1st order beam. For small angles $\sin(\theta) \simeq \theta$ the Bragg condition angle becomes proportional to the frequency of the sound wave

$$\theta = \frac{\lambda}{2v} f \tag{4.1}$$

were v is the velocity of the sound wave and f is the frequency of the sound wave. By manipulating the frequency of the sound wave, the angle for the Bragg condition θ can thereby be controlled, changing the angle of the 1st order beam in one axis.

To generate the sound waves a piezoelectric element is connected to the crystal, which is transforming an electric frequency wave to a mechanical wave. The AOD used in our setup, consist of two piezo-electric elements that are connected to the AOD crystal to send acoustic waves into it from two direction and thereby being able to manipulate the angle of the 1st order beam in two axis. This can for example be used as an optical tweezer for moving neutral atoms around in a two dimensional plane. By changing the frequency of the sound wave fast, the AOD can realize a time averaged arbitrary optical potential by changing the position of the beam fast enough in relation to the time-scale of the particles under consideration.

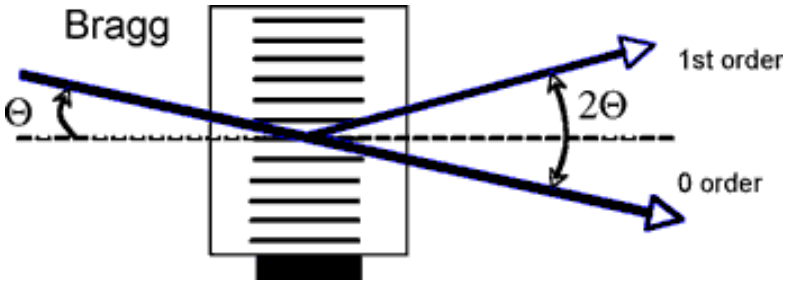

Figure 4.1: A light beam propagating trough an AOD crystal under the influence of acoustic waves. The beam is split in a transmitted beam (0th order) and a diffracted beam (1st order) due to Bragg diffraction on the sound induced planes. θ is the angle for which Bragg condition occur

4.3 Setup of the AOD control system

The ability of the AOD system to make arbitrary potentials with light is being used in our group for different tasks, and enables us to conduct a number of experiments. Especially, the ability to make a dimple beam for moving atoms is being exploited. The experiments involving the AOD is carried out in the science chamber. The setup is shown in figure 4.2. A full description of the setup can be found in [7].

To create the optical potential a 912 nm light beam is transferred through an optical fibre to the AOD board. The laser used is a Toptica DL Pro. Its output is amplified by a homebuilt TA leading to beam powers of up to 120 mW after the fibre and about 12 mW before the science chamber usable in the tweezer. A flipmirror is placed after the AOD to change between the science chamber and a CCD camera used for testing and characterisation of the AOD.

The AOD used in our experiment is of the model DTD-274HA6, from IntraAction Corporation and the crystal is made of TeO_2. The model consists of two crystals put

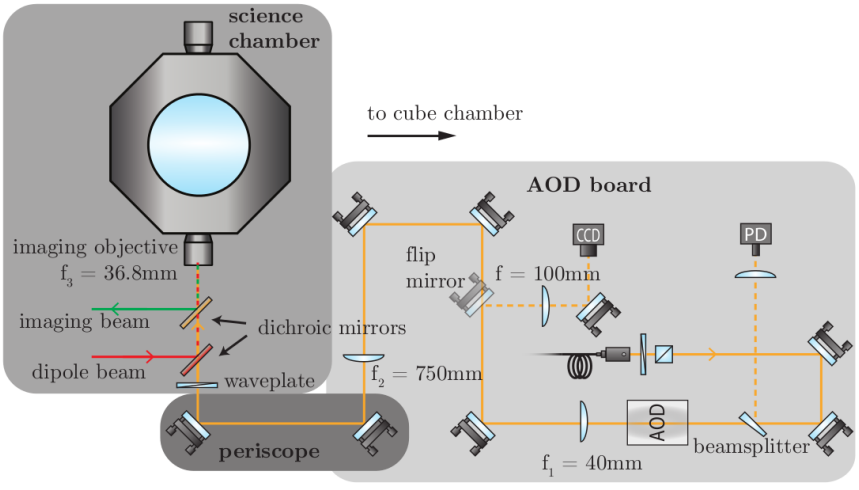

Figure 4.2: The experimental setup for the AOD. Adapted from [19]

together for deflecting the beam along two axes. It is specified to work in the center frequency at 27 MHz, and has a bandwidth of 16 MHz. Two homebuilt radio frequency (RF) amplifies deliver the waveform to the piezoelectric of the AOD with a maximum power of 1W,s limited by the AOD. For delivering the frequencies to the AOD crystal we use a waveform generator system of the serie PulseBlasterDDS-II^{TM} made by Spincore Technologies. It can deliver an output radio frequency in the range 5 kHz to 100 MHz for two analog channels, and has a pulse resolution of 13.3 ns with the shortest length of a pulse being 66.6 ns. The fast frequency shift can be exploited to make time-average arbitrary potentials with the AOD.
A program interface has been made in LabView to control the AOD trough the PulseBlaster. It has the following options:

- Creating a single constant beam with specified frequency and RF intensity
- Creating multiple constant beams with specified frequencies and RF intensities
- Movement of an custom defined pattern
- Movement of two beams
- Making a grid of points with user defined grid size and number of points
- Loading a gray scaled image file and translate it into a light pattern

This had been made in an object oriented programming style, with the strategy pattern mentioned in section 3.2.1, making it easy to add new functionality. Furthermore a LabView module has been made, which has been integrated into the Alice control system for the purpose of controlling the movement of a single beam through the block programming structure in the ALICE editor.
A DMD of the model DLP LightCrafter 6500 from Texas Instruments creates an arbitrary potential, used to make an imaging beam for non-destructive Faraday imaging. The image beam is projected onto an EMCCD camera of type Andor iXon Ultra 897, which is a CCD camera with an extra sensitive Electron Multiplying feature (EM).

4.4 Characteristics of the AOD performance

The intensity of the diffracted laser beam is dependent on two things. The angle of the diffracted beam in relation to the incoming beam and the power of the RF frequency

applied to the AOD crystal [20],

$$I_{\text{out}} = I_{\text{in}}\ g(f_x, f_y, I_{\text{RF}}) \tag{4.2}$$

where, I_{out} is the intensity for the diffracted beam, I_{in} is the intensity of the incoming beam, f_x, f_y are the frequencies of the RF signal, I_{RF} is the intensity of the RF signals and g is some function to be determined. To make a complete map for the output intensity a three dimensional scan over the parameters f_x, f_y, I_{RF} is needed to find $g(f_x, f_y, I_{RF})$.
A complete map is not necessary to perform the experiment of a translations of an atom cloud which is done in section 4.5. A scan was therefore made only for a constant value of the RF intensity $I_{\text{RF}} = 1W$. To make this scan, I made a LabView program that could make the PulseBlaster iterate trough 100 frequency grid points, in the range $f_{x,y} = [20\text{MHz}, 40\text{MHz}]$. For each iteration a frequency configuration is set, making a deflection of the beam with a specific angle, realizing a single of these grid points. Then a TTL signal is send from the PulseBlaster to a CCD camera, triggering it to take an image. This continues for all the 100 grid points, repeated five times. The images are then each integrated to find the total intensity for each frequency configuration, which for an average over five runs is shown in 4.3(b). The red points denotes the measured intensity values. Clearly a strong frequency dependence of the intensity is present. An image taken with the CCD camera of the a corresponding grid is shown in 4.3(a). The dependency of the intensity of the 1th order deflected beam in relation to the RF power was measured for the frequency configuration $f_x = 35\,\text{kHz}$, $f_y = 35\,\text{kHz}$ 4.4. The result of this is shown in figure 4.4. The plot shows a non-linear dependency, which was expected from [20].

When working with time averaged potentials, it is valuable to know how fast sampling can be done. This limit can be due to the delay of pulses from the frequency generator or due to the physical limitations of the AOD. By measuring the change in intensity of a photo diode connected to a fast oscilloscope, the risetime for a switch in frequency from 1 MHz to 29 MHz was measured to be $(8.0 \pm 0.1)\,\mu$s. The limitation on the switching speed of the AOD is due to the time taken for the sound wave to travel across the diameter of the light beam.
This limitation is important to know when estimating the number of spot that can be realized, still being able to trap an atom cloud. As an estimate for the time scale of an atom cloud, the trap frequency can be used, which gives the time period for an oscillation of the cloud. Lets make the approximation that an atom cloud will not evolve in a timespan less than 0.1 times the oscillation period. Saying that a dimple beam creates a trap with the highest trap frequency being 1 kHz. Then the time average potential will have a limit 12 spots.

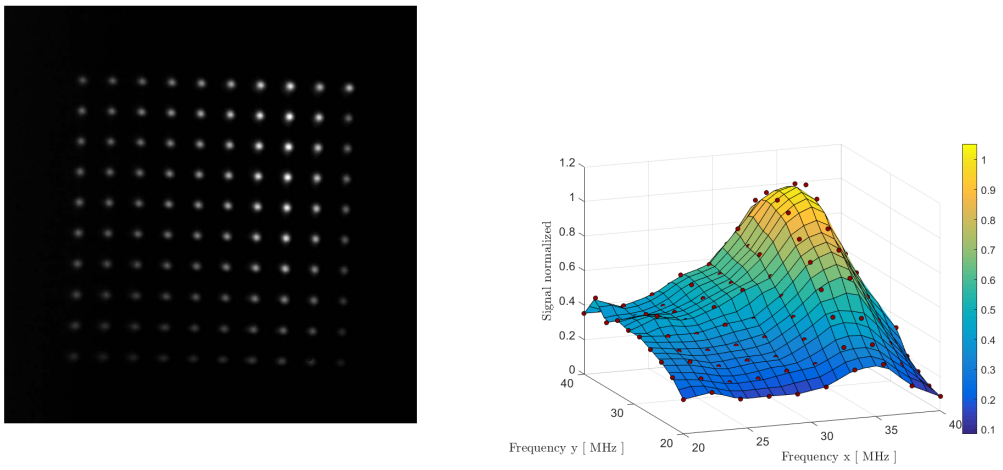

(a) (b)

Figure 4.3: a) Image of the grid formed by the time averaged laser light controlled by the AOD, taking by a CCD camera. b) Same intensity distribution as in a, but showed as each grid points normalized intensity values in relation to its frequency setting. The red dots indicates the grid points.

4.5 Translation of ultra cold atom clouds

In this section, I discuss the translation of an ultra cold atom cloud and the translation of a BEC cloud in a non-adiabatic manner. The control of the movement of the cloud is important in various experiments in atomic physics. For instance in our experiment, the cloud is moved from the cube-chamber to the science chamber with the longitudinal

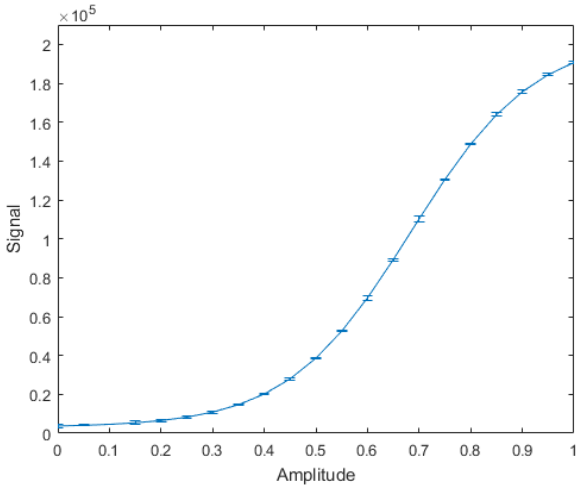

Figure 4.4: Plot showing the normalized intensity of the 1th order deflected beam in relation to the RF power. The frequency configuration was $f_x = 35\,\text{kHz}$, $f_y = 35\,\text{kHz}$.

dipole beam, which is a process that could be valuable to optimize and important to understand. A problem of interest is to move the cloud to a new location without any excitations of the clouds energy levels. This can easily be done in a adiabatic way, by moving the cloud slowly. The main task is to optimize this translation process in a non-adiabatic way, making it as short in duration as possible. In [21] they show that a simple model can describe the movement of the ultra cold cloud of ^{87}Rb atoms and in [22] they purpose theoretically founded movement protocols, giving optimal movement with no excitations for a chosen frequency of a harmonic trap potential. This investigation of the transport of atom clouds in this section will be based on those papers.

4.5.1 Translation model

To describe the behaviour of the ultra cold atom cloud under translation, a simple model of a one dimensional center-of-mass motion will be used to compare with the experimental data. This model has before successfully been used to describe the transport of a atom cloud [21]. The assumption for using a 1D model for our 3D problem, is that the center-of-mass movement is decoupled from the other degrees of freedom. In other words, the excitation will only occur in states involved with the direction of the center-of-mass movement.

Consider an atomic cloud in a harmonic trap initially at rest with the angular frequency ω_0. The position of the trap is given by the position of its center $x_c(t)$. To simplify, the cloud will be treated as a single particle. The movement of the trap will correspond to an extra force $-m\ddot{x}_c(t)$ being imposed on a particle of mass m, in regard to the inertial frame of the trap. We are are interested in finding an expression for the time dependent displacement of the particle in relation to the center of the trap. This can be done by considering the Lagrangian of the system

$$\mathcal{L} = T - U = \frac{1}{2}m\dot{x}^2 - \frac{1}{2}m\omega_0^2 x^2 \tag{4.3}$$

where $\mathcal{L}$ is the Lagrangian of the system, T its kinetic energy and U its potential energy and x is the displacement from the center of the trap. Solving the Euler-Lagrange equation

$$\frac{\partial \mathcal{L}}{\partial x} - \frac{d}{dt}\frac{\partial \mathcal{L}}{\partial \dot{x}} = -m\ddot{x}_c \tag{4.4}$$

the following expression for the amplitude A, with the conditions $x(0) = 0$ and $\dot{x}(0) = 0$, is given by

$$A(t) = \frac{1}{\omega_0} \int_0^t dt' \sin(\omega_0(t' - t))\ddot{x}_c(t') \tag{4.5}$$

It can further be shown the above expression can be rewritten on a complex form by the Fourier transform of the velocity profile from the movement of x_c

$$A(t) = |\mathcal{F}[\dot{x}_c](\omega_0)| \tag{4.6}$$

were $\mathcal{F}(f) = \int_{-\infty}^{\infty} f(t)e^{-i\omega t}dt$ is the Fourier transform.
Two different velocity profiles are under consideration. The first is a direct movement from location A to B with acceleration in the first half of the movement and deceleration in the later half 4.5(*a*). The second is a back-turning movement going from location A to B to A 4.5(*b*). The distance between A and B are in both cases given by d. Using 4.6 on these, the final oscillation amplitude can be calculated to be

$$A_{\mathrm{AB}}(T) = d\,\mathrm{sinc}^2(\omega_0 T/4) \tag{4.7}$$

$$A_{\mathrm{ABA}}(T) = 2d\,\mathrm{sinc}^2(\omega_0 T/8)|\sin(\omega_0 T/4)| \tag{4.8}$$

were $\mathrm{sinc(x)} = \sin(x)/x$ and T is the duration time of the movement. In the case of the direct movement an optimal duration time of zero amplitude is given when $T_n = 2nT_0$, where $T_0 = 2\pi/\omega_0$ is the period of oscillation of the trap, and n is a non-zero integer. The two expressions describes the oscillation amplitude of a single particle after a movement of duration T of the harmonic potential it is trapped in. In the next section these will be used to describe the center-of-mass oscillation of an atom cloud after a translation.

4.5.2 Experiment of the translation of an atom cloud

In the following the experiment of the movement of an atom cloud is outlined. The movement of the atom cloud were performed in the science chamber. The experimental sequence for a single experiment evaluation, starts with transporting the cloud from the cube chamber to the science chamber by the longitudinal dipole beam, that is placed on a movable translation stage. When the atoms have been transferred to the chamber, the dimple beam propagating in the transverse direction is turned on. The two beams will form a crossed dipole trap and cool the atoms with evaporative cooling. After the atoms are cooled, the longitudinal beam can either stay on and function as a reservoir, or be turned off leaving the atoms only in the dimple. The so called *dimple trick* can be

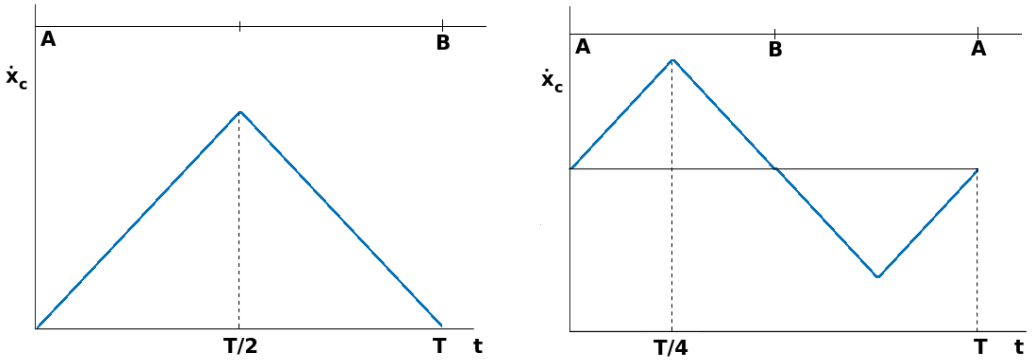

(a) (b)

Figure 4.5: The velocity profile for the two atom cloud movements under consideration. a) The movement from A to B. b) The movement from A to B to A.

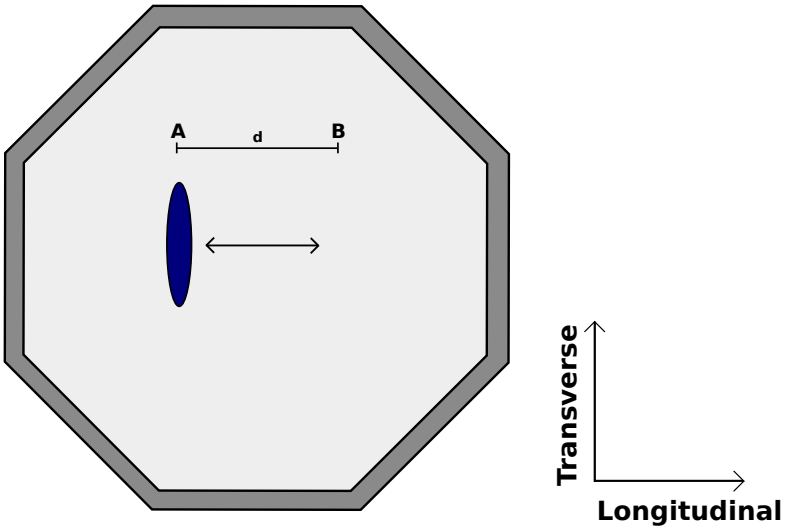

Figure 4.6: Illustration of the experimental situation for the translation of the atom cloud. The blue eclipse indicate the elongated cloud, and A and B are reference points for the movement. The distance between A and B is given by d.

used by the dimple beam, which function by locally enhance the phase space density to make the atoms cross the transition to the BEC state.

By using the beam-control module in Alice, the cloud was moved by the dimple beam on a predefined path, which was either the AB path or the ABA path, moved in the chamber in the longitudinal direction. In figure 4.6 an illustration of the path of the movement is given. When the dimple beam has accomplished its translation of the cloud, the centre-of-mass oscillations were measured by taking 21 images separated in time by 32-100 μs, with a non-destructive Faraday imaging system, using an Andor Ixon ultra

camera in fast kinetic mode. This mode gives the opportunity of high speed imaging by storage of multiple images locally before the relatively slow readout. The camera consists of two CCD chips of the size 512 x 512 pixels, put in serial, where the top one is the imaging chip and the lower is masked and used for storage. The top of the unmasked chip, consisting of 48 x 512 pixels, is being exposed by the imaging beam controlled by the DMD. An image is taken by letting the CCD chip being expose to the light for the duration of the exposure time. The charge of the top censors defining the image is then being propagated down the chip, and a new image is taken. This iteration continues in till all 21 images is taken. As soon as the charge reached the bottom of the last chip that data is transferred from the camera.
Using two Gaussian fit to the cloud, the position of the center of the cloud in the x,y plane can be calculated for each image. The expression for a damped oscillator is fitted to this position data to extract the amplitude of the center-of-mass oscillation in these two dimensions. One of the fits are shown in figure 4.8(*b*). At the end a destructive absorption TOF image is taking to get knowledge about the state of the cloud.

First the dimple beam waist was found. The expressions in 2.17 is relating the trap frequency of the dimple beam in the radial direction ω_r, which correspond to $\omega_{\text{longitudinal}}$ in our setup, to the trap depth $\hat{U}$ made by the dimple. This expression can be reformed by inserting the trap depth to get a relation between the trap frequency and the power of the beam P given by

$$\omega_r = f_r 2\pi = \frac{1}{w_0^2}\sqrt{\frac{2U_0}{m\pi^3}}\sqrt{P} \tag{4.9}$$

were w_0 is the beam waist, U_0 is a constant of the potential and m the mass of the trapped atoms.
In order to get the waist of the dimple beam, the cloud is being confined only by the dimple beam. The cloud is then being moved in order to observe the center-of-mass oscillation to extract the trap frequency for a given dimple power. Then the trap frequency in relation to the dimple beam power was measured, shown in figure 4.7. By using 4.9 as a fitting function, the beam waist was found to be $w_0 = (4.1 \pm 0.2)\mu$m, which is of the expected size.

The experiments involving the translation of a thermal atom cloud or a BEC by moving a dimple beam, is being described in the following. This will be done for the cases of a ABA movement of an thermal cloud, an ABA movement for a BEC and a AB movement for a BEC. In all cases the distance between A and B is $d = (5.2 \pm 0.2)\mu$m. The results will be analysis by comparing the data from the movements with the expressions in

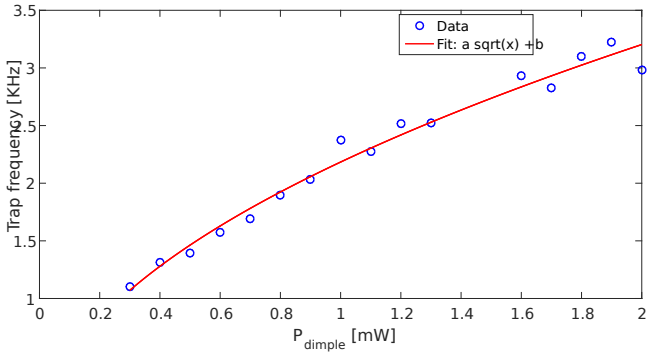

Figure 4.7: Trap frequency in relation to the power of the dimple beam. Blue dots are measured points and the red line is a fit to 4.9.

4.8, which describes the relation of center-off-mass motion of the cloud in relation to the duration of the translation procedure. A fit of the expression to the data with the variable parameters being ω_0 and a front factor multiplied to the expression denoted a.

The first experiment was by translating a thermal cloud along the path ABA. This was done 1500 times as a scan over the duration time T of the movement, in the time interval $T = [0.014, 4]$ms. The power of the dimple was set to $P_{\text{dimple}} = (1.5 \pm 0.1)$mW. The dimple power wasn't high enough to form a BEC, which could be concluded from the absorption image taking in the end. Because of bad fits of the oscillation, some data points was sorted out. First by a frequency threshold of $\omega_{\text{threshold}} = (16 \pm 4)\,\text{kHz}$ chosen as the mean of the frequencies from the experiment evaluations with a high bound. After this, every remaining image was manual decided whether they were usable or not. Figure 4.8(a) shows a scatter plot from the experiment showing the amplitude of the selected data in relation to the movements duration. The red curve is a fit of the translation model for the ABA movement in equation 4.8. The fit parameters was found to be $a = (0.31 \pm 0.02)$ and $\omega_0 = (15 \pm 2)$kHz. The mean frequency, of the data used, is $\omega_{\text{mean}} = (15 \pm 1.9)\,\text{kHz}$, which overlap with the frequency found by the fit within the bounds of one sigma. The model doesn't describe the data well, except the frequency and some of the structure of the data are captured by the model fit.

Making the same experiment for a BEC cloud can be realized using the dimple trick. For this a higher dimple beam power is needed, which was sat to $P_{\text{dimple}} = (4 \pm 0.1)\,\text{mW}$. A scan over the duration time in the range $T = [0.35, 1]$ms consisting of 800 experiment evaluations for the movement ABA was performed. The absorption images taken after the movement of the cloud confirmed that the cloud consisted of BEC atoms.
A lot of the measured data resulted in bad fits, especially when the amplitude was low. Therefore the data was filtered to only considering data within a fixed bound showed in figure 4.9(a) indicated by the black dotted lines. The threshold frequency

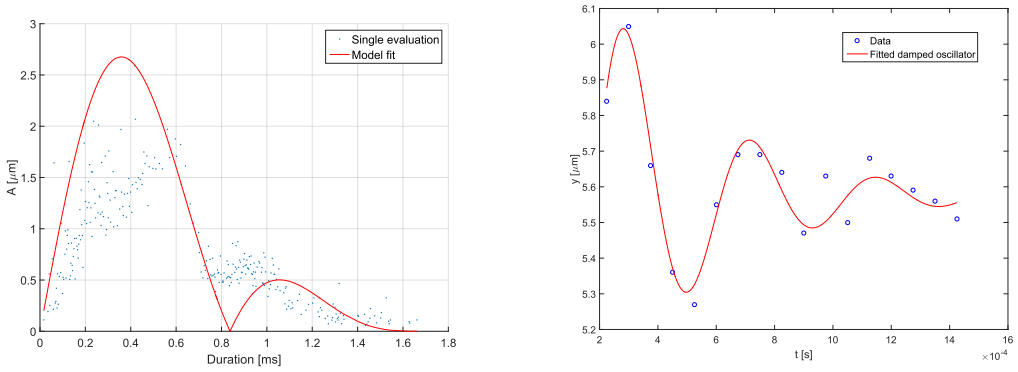

(a) (b)

Figure 4.8: a) Translation of a thermal atom cloud from location A to B to A. The blue data points is each from a single evaluation of a movement. The red curve is a fit to the transport model expression in 4.8. b) Data from a single atom cloud movement execution. The red curve is a fit to a damped oscillator.

$\omega_{\text{threshold}} = (33.3 \pm 1.9)$kHz was calculated by taking the mean of the trustworthy data within the red dotted lines. That data was considered trustworthy because of a high amplitude, resulting in good fits to the damped oscillator. The filtered data gives the data points shown in figure 4.9(*b*). A fit to the expression from 4.8 is shown as the red curve and gave the following fit parameter values. $a = (0.46 \pm 0.04)$ and $\omega_0 = (37 \pm 1)$kHz. In this case there is some difference between the measured trap frequency ω_{mean} and the one obtained from the fit. Notice that the frequency within the red punctuated area seems to drift, which could be explained by a failure of the harmonic approximation when the amplitude is large, which is discussed more later. This gives a calculated ω_{mean} that is estimated to low and could course the deviation from the value obtained by the fit. Because of noise in the measurements, the fitted amplitude cannot be lower than about 0.2 μm, so the dip showed in the model can't be confirmed.

Making the same experiment with an AB movement of a BEC cloud with a dimple power $P_{\text{dimple}} = (4 \pm 0.1)\,\text{mW}$ was realized. Here the mean trap frequency was $\omega_{\text{threshold}} = \omega_{\text{mean}} = (33.2 \pm 2.6)$kHz was found by taking the mean of the first 80 points. Because of bad fits, the amplitude was in this case calculated from maximum and minimum position values. A fit to the expression from 4.8 is shown as the red curve and gave the following fit parameters values. $a = (0.52 \pm 0.02)$ and $\omega_0 = (33 \pm 2)$kHz. Again the the amplitude for $A < 0.2\mu$m can't be measured so the low amplitude structure of the curve can't be confirmed. In this case the frequency obtained from the fit matched the measure ω_{mean} within the bounds of one sigma.

In both of the cases of the movement with the BEC, the 1D model for a classical particle in a moving harmonic potential, described the data with good agreement, except for a

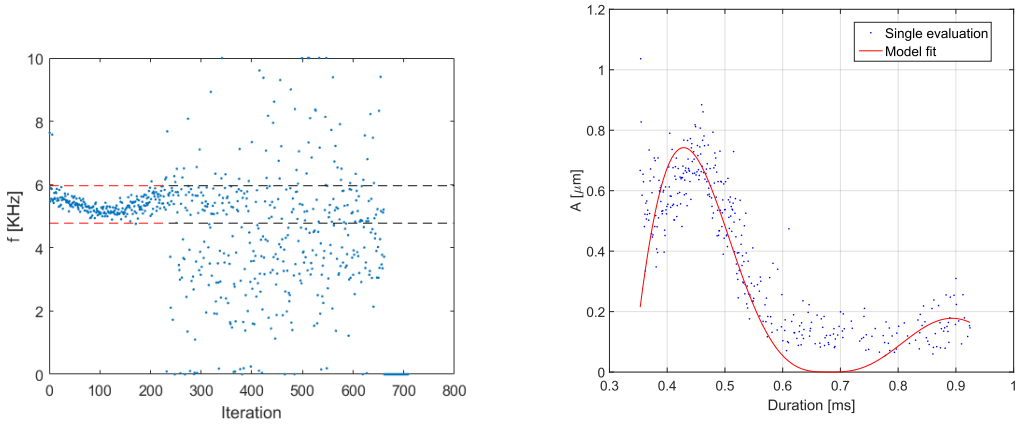

(a) (b)

Figure 4.9: Translation of a BEC atom cloud from location A to B to A. The blue data points is each from a single evaluation of a movement. a) The trap frequency in relation to duration time of the movement. The red punctuated defines the area used to calculate the mean trap frequency. The black punctuated lines is making a threshold for data to use for the plot in b). b) The amplitude of the center-off-mass oscillation in relation to duration time of the movement. The red curve is a fit to the transport model expression given by 4.8.

factor of $a = 0.5 \pm 0.08$. The lower amplitude of the measured data in relation to the model, can be because of the dampening effect which is visual in the plot showing the center-of-mass oscillation for a single translation, see figure 4.8(*b*). This dampening effect can be explained by that the fact that the dimple trap potential only can be approximated as a harmonic potential for small energies, dependent on the power of the dimple beam. When particles explores a potential away from the harmonic potential they will have a different period of oscillation dependent on there energy. The observed damping of the center-of-mass oscillation is due to the average of all these particles oscillation frequencies. To avoid this damping effect the depth of the trap in relation to the energy of the atoms need to be maximized. This will make the atoms be in the bottom of the trap where the harmonic oscillator approximation is more adequate. This can be realized by increasing the power of the dimple beam, and would explain the lower scaling factor needed for the cases with $P_{\text{dimple}} = (4 \pm 0.1)\,\text{mW}$. In the paper [21] a scaling factor of $a = 0.6$ has been used as well to match the experimental data with the model expression.

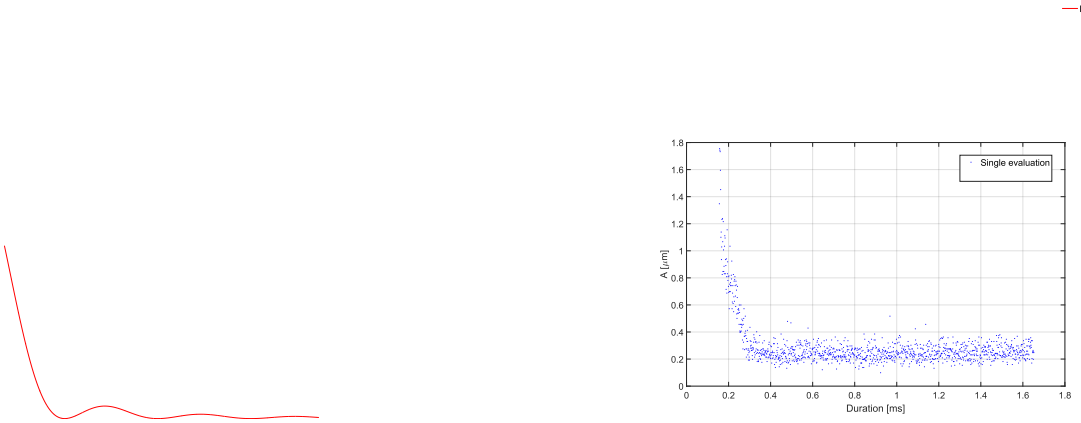

Figure 4.10: Translation of a BEC atom cloud from location A to B. The blue data points is each from a single evaluation of a movement. The red curve is a fit to the transport model expression given by 4.8

4.6 Outreach with remote control

Being able to control our system remotely has opened new opportunities. This gives us the possibility to open up the experiment for people outside our group, and even outside of the field of physics. In this section two projects will be outlined that focus on reaching out, based on the idea of involving the non-science community in scientific problems, known as *citizen science*. These two projects are both involving the ability of making arbitrary potentials with an AOD.

User-designed laser patterns In the LabView program I made for controlling the AOD, a functionality is included for transforming an user selected gray-color scaled picture file, to an arbitrary time averaged laser potential made by the AOD. A resolution of 1000 points, each point defined by a specific frequency set, is the upper bound for defining the time averaged laser potential. This can be used to give users outside the laboratory a possibility to make their own laser-pattern.
The idea is to give users access to the experiment through an user interface where they can upload there own custom defined pattern. The experiment will run and capture ultra cold atoms in the potentials defined by the users. The imaging system will then take a picture and send it back to the user as a "postcard". Then you can have your own personal unique picture made of atoms. As a first step of this idea I made an arbitrary potential of each letter in the alphabet, and took an image of each of them. It is only an image of the light beam with no atoms captured. A Matlab program was made to concatenate each picture to a sentence of choice. An example of this is shown in figure 4.11. An disadvantage by using a AOD system for this, as described in section 4.4, that we only can confine the atoms in a few number of potential trap, due to the relative

Figure 4.11: Example of a text writing by an time averaged laser beam controlled by an AOD.

slow change of beam position. Instead a DMD will could realize these "postcards" by making an arbitrary potential without time averaging.

User-controlled movement of atoms The controllability of the dimple beam, together with the possibility of remote control of our experiments, has inspired us to make a proof of concept of a gamification of the movement of an atom cloud.
The game called Bring Home Water (BHW), made by ScienceAtHome [3], is a gamification of an atom movement problem. The problem is about moving a potential to collect an atom in the ground state, to bring it back to the start location, also ending up in the ground state. The game is built on a simulated physical system, that describes the problem [23]. A game interface made in the programming platform *Unity* makes the player able to control the amplitude and the position of the potential with the mouse, thereby enable them to solve the problem as a gamified problem. The BHW gamification is describe in more detail in section 5.3
Instead of simulating the system, our remote control system makes it possible for game players actually to control the real atoms in the experiment through the game interface. This coupling between the game and the actual experimental system has been realized in our group. We are not able yet to realize a single atom in an optical tweezer, so instead of moving one atom, an ultra cold atom cloud is being translated. When a player is solving the movement problem in the game, the coordinates and amplitude for the potential defined by the player are transferred to the ALICE control system in the laboratory, which rescaled it to physical parameters and through its AOD-module reprogram the PulseBlaster to a new path and amplitude for the dimple beam. Then ALICE control system executes an experiential sequence leading to the movement of the cloud defined by the game player. In the end, the path can be recorded by our non-destructive Faraday imaging system to see the physical realization. To get a figure of merit in relation to the success of the given player solution, the amplitude of the center-of-mass oscillation emerging in the end of the atom cloud motion is chosen, which measure the residual energy of the cloud. For a given gameplay we record nine images

[3] www.scienceathome.org

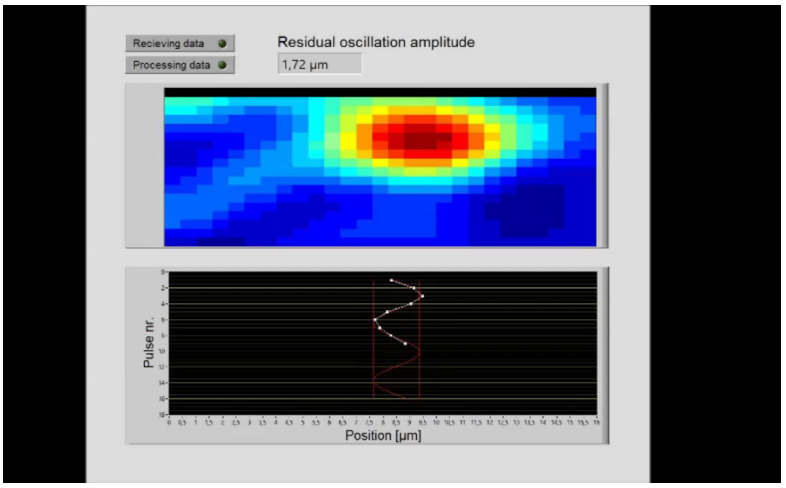

Figure 4.12: Screen-shot from a video feedback on the performance of a player, playing BHW connected to the real experiment. The top picture shows the cloud, and the bottom picture the measured center-of-mass oscillation of the cloud after the movement.

of the center-of-mass oscillation and make a fit to find the amplitude. A video of the oscillation and the score in form of the center-of-mass oscillation amplitude is then send to the player. This is not being implemented fully automated, in the extend that the execution of the atom movement based on the player data has to be done manually.
This version of the BHW game, coupled directly to the experiment, has not been open to regular players, but only tried at a conference organized by National Instruments in Texas. In figure 4.12 is a screen-shot of a center-of-mass oscillation result video, where the vice president of National Instruments is trying the game, succeeding in a "score" with an amplitude of $1.7 \pm 0.3\mu$m [4].

These two projects should be seen as the first minor steps in involving non-scientist in activities going on in our laboratory, with the aim of making a functional citizen science platform. A the next step a gamification of the process of evaporative cooling is described and analysed in detail in section 5.5,.

[4] A video from the presentation of this gamification at the National Instrument conference can be found by the link, at start time 43.30. : http://livestream.com/ni/events/5828512.

Chapter 5

Optimal control landscape of the creation of BEC atoms

5.1 Introduction

By having an automated closed loop experimental control system, opportunities arises for utilize sophisticated optimization of the experiment. The ability to control many parameters of physical entities creates a huge control landscape which quickly becomes too large to fully search through. This enables an interest in trying to somehow mapping out the topology of the landscape, in hope to find patterns or representations that can be used to get information about this vast space of possible solutions. In this chapter, the focus is on the task of optimizing the creation of BEC atoms by evaporative cooling. The goal of this chapter is not to optimize the process of the evaporation in order to obtain a large BEC cloud for a future experiment, but an analysis of this optimization landscape that forms, in the context of this problem. The discussion about the landscape will be about the formation of novel strategies for solving the problem, and the connection between these strategies.

In section 5.2 the concepts discussed in the chapter are introduced. In section 5.3 a short description of a problem that was a source of inspiration for this landscape analysis is presented. In section 5.4 a mapping out of the control landscape by using a theoretical model to define the controls, is performed. Furthermore an optimization algorithm is performed on our problem, obtaining a new novel strategy for evaporation. In section 5.5 an untraditional approach is taken by a gamification of the evaporation problem, involving people with minor knowledge of the physical problem, making a crowd sourced optimization.

5.2 Theoretical background

5.2.1 Optimal evaporative cooling

The cooling of an atom cloud by evaporative cooling, happens, by letting atoms with energy above the average escape from the trap, thereby lowering the mean energy of the cloud, cooling the atoms. Consider a cloud of thermal atoms confined in a potential, energy-distributed according to a Maxwell-Boltzmann distribution. The trap depth of the potential $\hat{U}$ is a measure for the lowest potential barrier that the atoms need to overcome to escape from the confinement of the trap potential. Keeping the same trap depth, the evaporation rate Γ_{evap} will decrease with a decreasing temperatures. To overcome stagnation, the strength of the potential trap is lowered over time. An efficient evaporative process is realized by only truncating the tail of the distribution, thereby only loosing the atoms in the cloud with the highest energy. The term $\eta = \hat{U}/k_B T$ called the truncation parameter is the ratio between the trap depth and the average thermal energy of the atomic cloud $k_B T$. It describes how large a part of the distribution is able to escape from the trap. For a large η only the end the tail has enough energy to break the confinement. When the atoms with highest energy has escaped from the trap an amount of time for rethermalization is needed. This time depends on the elastic collision rate

$$\Gamma_{\text{el}} = n\sigma\bar{v} \tag{5.1}$$

where n is the density of the atoms, σ is the elastic collision cross section and $\bar{v} = \sqrt{16k_B T/\pi m}$ is the mean velocity of the atoms determined by the temperature T of the cloud, with m being the mass of an ^{87}Rb atom.

In principle the evaporative cooling can be arbitrary efficient having enough time for the process. Going to the extreme, the truncation parameter can be set to such a high value that only an atom with the total energy of the cloud can escape the trap, in which case it would cool the rest of the atoms to the degenerate ground state. It would though take an infinite amount of time for an atom to randomly come to this high energetic state just by elastic collision. In practice other obstacles beside the waiting time arises. Those being inelastic three body collision and one body background collisions which both heat the cloud. The cross section for three body inelastic collisions grows with the cloud density, where background collisions is due to contaminated environments in the experimental vacuum system. Due to the background collisions, η has in practise an upper value where higher values will lead to a lower efficiency. Therefore a part of the optimization of the evaporation process is to find the right value of η for the experimental system in question.

Letting the objective being to create as large a possible fraction of BEC atoms in relation to the initial amount of atoms, the following parameter is a good figure of merit to explain the success

$$\gamma = \frac{\ln(\rho/\rho_0)}{\ln(N/N_0)} \tag{5.2}$$

where, ρ, ρ_0 is the final and initial phase space density, described in section 2.2.1, and N, N_0 is the final and initial atom number of the cloud. The scaling between the two parameters are exponential, therefore the logarithmic relation. In [24] a kinetic model for the evaporation cooling in a crossed dipole trap with experimental conditions, is used to optimize the process by controlling η and the average trap frequency. Using the theoretically obtained strategy they are able to reach a high value of $\gamma = 4.0$ during evaporation.
In the paper [25] a expression describing how the trap $\hat{U}$ need to be changed if η is to be remained constant, thereby controlling the collision rate of the particles through the whole evaporation sequence. An derivation of the expression will be outlined in the following.

Simplifying the notation the trap depth is denoted as U in the following. Taking the zero of energy to be at the trap bottom, atoms escaping the trap will have an average energy of $U + \alpha k_B T$, where it has been shown that $0 \leq \alpha \leq 1$ [26]. The energy loss rate arising from the atom loss is then $\dot{N}(U + \alpha k_B T)$, $\dot{N}$ being the rate of atoms evaporating from the trap. Additionally, the forced evaporation is lowering the trap potential at a rate $\dot{U}$. This leads to a change in the average potential energy, which is $E/2$ for a harmonic trap, with the rate of the relative change of the trap depth $\dot{U}/U$. The loss rate of the total energy is then given as the sum of the two contributions, given by

$$\dot{E} = \dot{N}(U + \alpha k_B T) + \frac{\dot{U}}{U}\frac{E}{2} \tag{5.3}$$

Through the equipartition theorem the energy of the atoms is also given by $E = 3Nk_BT$. A change in the total energy therefore results in $\dot{E} = 3Nk_B\dot{T} + 3\dot{N}k_BT$. Assuming that η is fixed and equating this result with 5.3, we obtain the following scaling law

$$\frac{N(t)}{N_i} = \frac{T(t)}{T_i} = \left(\frac{U(t)}{U_i}\right)^{3/[2(\eta'-3)]} \tag{5.4}$$

where i denotes the initial condition at t=0 and $\eta' = \eta + \alpha$. Assuming $k_BT \ll U$, from the s-wave scattering Boltzmann equation, $\alpha = (\eta - 5)/(\eta - 4)$ for a harmonic trap potential. For an energy-independent scattering cross section, with a density for a harmonic potential given by $n \propto N\bar{\omega}^3 T^{-3/2}$ and with $\Gamma_{\text{el}} = n\bar{v}\sigma$, then from 5.4 the

elastic collision rate can be found to scale with the trap depth as

$$\frac{\Gamma_{\mathrm{el}}(t)}{\Gamma_{\mathrm{el},i}} = \left(\frac{U(t)}{U_i}\right)^{\eta'/[2(\eta'-3)]} \tag{5.5}$$

The assumption of having η as a constant parameter, works as a requirement that gives the trap depth an explicit time dependence. From the s-wave Bolzmann equation [26], to lowest order in $\exp(-\eta)$, one finds

$$\dot{N} = -2(\eta - 4)\exp(-\eta)\Gamma_{\mathrm{el}}N \tag{5.6}$$

By differentiating 5.4 and writing $\Gamma_{\mathrm{el}}/\Gamma_{\mathrm{el},i}$ in terms of U/U_i, we get the time dependent expression for the trap depth

$$\frac{U(t)}{\hat{U}_i} = \left(1 + \frac{t}{\tau}\right)^{-2(\eta'-3)/\eta'} \tag{5.7}$$

where the time constant τ is given by

$$\frac{1}{\tau} = \frac{2}{3}\eta'(\eta - 4)\exp(-\eta)\Gamma_{\mathrm{el},i} \tag{5.8}$$

It is important to notice that the expression has been derived without taking background collisions or inelastic collisions into account.

5.2.2 Quantum Optimal Control

Advances in laser technology and flexible pulse shaping capabilities has opened a new area of experiments with a high control over the quantum phenomenon in question. Experimental control systems are getting even more sophisticated with the ability to steer and manipulate these complex quantum systems[27]. The gain of this controllability is present in the diversity of fields of chemistry, biology and physics [28].
To exploit the full potential of these complex experimental systems, a control theory has been developed, which in general is referred to as Optimal Control Theory (OCT) and in specific for quantum mechanical problems as Quantum Optimal Control Theory (QOCT). In an experimental context, QOCT aims to achieve the best possible results in an experiment of environment with fluctuating conditions, by steering the system towards the desired goal, and has been realised in various closed loop control experiments. A description of QOCT is given in the following.

The full Hamiltonian of a system can be described as an uncontrollable drift Hamiltonian H_0 and a control Hamilton H_c which depend on the *control field* $\mathbf{u}(t)$, $t \in [0, T]$

$$H = H_0 + H_c(\mathbf{u}(t)) \tag{5.9}$$

The control field is a term incorporating all physical manipulation available in a given experiment, which could incorporate both a laser pulse and a magnetic pulse. The objective of QOCT is to find a control field $\mathbf{u}(t)$ that steers a particular quantum system from an initial state $|\psi(0)\rangle$ to some target state $|\psi(T)\rangle$, thereby maximizing the expectation value $\langle\psi(T)|\hat{O}|\psi(T)\rangle$ for a given observable $\hat{O}$. The time evolution of the state can be described by the time-dependent Schrödinger equation

$$i\hbar\frac{\partial}{\partial t}|\psi(t)\rangle = [H_0 + H_c(\mathbf{u}(t))]|\psi(t)\rangle \tag{5.10}$$

The expectation value for a given operator $\hat{O}$ is associated with the success of the control, and is used to assign a figure of merit to a given control field $\mathbf{u}(t)$. The *control landscape* of the QOCT problem, is given by the functional

$$J(\mathbf{u}(t)) = \langle\psi(T)|\hat{O}|\psi(T)\rangle \tag{5.11}$$

which describes the figure of merit as a function of the control parameters.
The control field $\mathbf{u}(t)$ can be realized in various ways by performing a parametrization with parameters $\mathbf{c}$, which maps the control field from a low dimension control space into a high dimension space. This could be the expansion of the control field into a functional basis f_i, with coefficients c_i

$$\mathbf{u}(t) = \sum_i c_i f_i(t) \tag{5.12}$$

were the c_i forms the parameters $\mathbf{c}$. In choosing another parametrization the control landscape change, and are thereby defined by $\{\mathbf{c}, J(\mathbf{u}(t))\}$. It must be emphasized that the quantum optical control theory does not describe the classical optimization problem of evaporative cooling covered in this chapter. The outline of this theory aims at giving a conceptual understanding of an optimization methodology.

5.2.3 Control landscape topology

Usually a OCT problem consist of ten to hundreds of control parameters, making the control landscape amazingly vast. Despite of this huge control space, it has been possible in a large amount of problems to find solutions with a high figure of merit with surprising ease [29]. Aiming at finding an explanation of this, Rabitz proved in [29], that in a fully

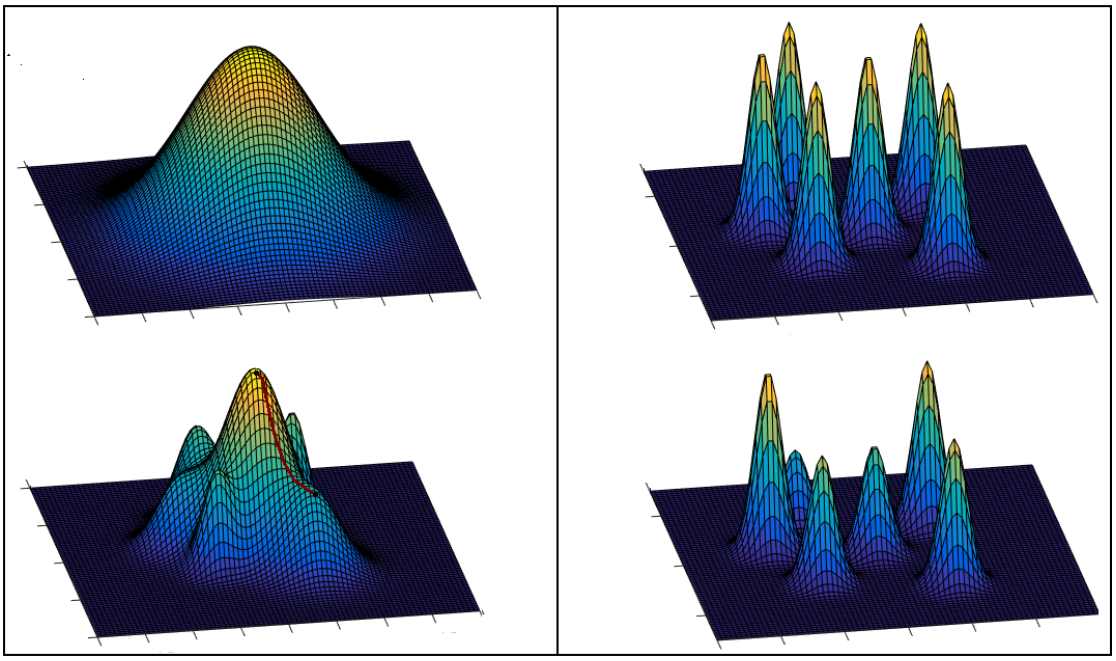

Figure 5.1: Illustrations that gives two visual proposals of the change in the control landscape, when it is no longer fully controllable or constraints on the controls are placed. Top images represents the fully controllable landscapes with no constraint imposed. The bottom images represents the distorted landscapes. The red path on the bottom image to the left represent a bridge between two points.

controllable quantum system with no constrains on the control, all local optima in the landscape are also global optima. When parts of the system are uncontrollable or when a constraint is introduced on a control, the landscape changes and this general statement breaks. Intuitively, one would expect the landscape to change gradually with the loss of control and thereby keeping some of its original structure, which could explain the relatively ease in finding solutions with a high figure of merit in a constraint optimization landscape. In figure 5.1, two proposals of initial full controllable landscapes transition to a constrained one are illustrated. These should be seen as representations of arbitrary high dimensional landscapes. In the fully controllable case all local maxima are also global maxima, whereas when constraints are placed, the landscapes get distorted, though keeping some of its original structures. In this new distorted landscape, non-global optima can appear letting a local search algorithm converge premature, therefore sometimes called *traps*. The degree of change from the original landscape, is related to the difficulty of reaching a high optima by performing local search in the landscape. Thereby it can be of interest to map the structure of a control landscape, to get knowledge of the degree of distortion. This can give an indication of the limitation of the performance of local search algorithms in the landscape in question. As an indicator of this, the term *bridge* is introduced as being a connection from one point in the control

landscape to some other point, where a monotonously increasing path of the figure of merit exists. An example of a bridge is shown in figure 5.1.

5.2.4 Visualization by dimensionality reduction

When dealing with a problem described in a high-dimensional space the human mind fails to comprehend the situation. Not only can we not visualize spatial objects in more than three dimensions, but our human intuition breaks as well. As an illustrative example, most of the volume of a high-dimensional sphere is in a thin slice of the surface and not in the bulk. When going to a high-dimensional space, many problems arises which together are formulated as "the curse of dimensionality" [30]. The problems comes because that the number of states of the space grows exponentially with the number of dimensions.

Dimensionality reduction

In order to interpret or get an intuition about the high-dimensional data various dimension reduction techniques exist. They aim at making a mapping from the high-dimensional space to a low-dimensional space, with a reduction down to arbitrary few dimensions. This mapping come at the price of information, and therefore the measure of success is by preserving as much of the significant structure of the high-dimensional data as possible in the low-dimensional representation. The different techniques vary in the type of structure they preserve. Typically they are separated as whether they preserve local or non-local structure. Non-local techniques includes Principal Component Analysis (PCA) [**?**] and classical Multidimensional scaling (MDS) [39], which are linear techniques that focus on keeping dissimilar pair of points far apart from each other. There exist a large number of techniques for preserving the local structure, where the most prominent according to [31] is the t-Distributed Stochastic Neighbour Embedding (t-SNE). In the following the PCA and the t-SNE techniques will be described more thoroughly.

Principal Component Analysis PCA is a statistical method that can be used to reduce the dimensionality of a dataset while preserving as much of the variance of the dataset as possible. This is done by making an orthogonal transformation of the dataset into a new set of variables, called the principal components. The new base vectors are ordered by the amount of variance covered by the vectors, where the first is in the direction of the largest variance and the last in the direction of the least variance. The

last variables can therefore be neglected without much lose of information. An example of the reduction from two dimensions to one is shown in figure 5.2.

Given a dataset with n dimensions and p observations $\mathbf{X} = (\mathbf{x}_1, \mathbf{x}_2, .., \mathbf{x}_p)$ where $\mathbf{x}_i = (x_1, x_2, .., x_n)$, the k'th Principal Component $\mathbf{z}_k$ is found by a linear transformation

$$\mathbf{z}_k \equiv \mathbf{a}_k^T \mathbf{X} = a_{1k}\mathbf{x}_1 + a_{2k}\mathbf{x}_2 + ... + a_{pk}\mathbf{x}_p \tag{5.13}$$

where $\mathbf{a}_k = (a_{1k}, a_{2k}, .., a_{pk})$ is chosen so that the variance of $\mathbf{z}_k$ is maximum. Let $\mathbf{S}$ be the covariance matrix for the data $\mathbf{X}$. It can be shown that if the $\mathbf{a}_k$ vectors are assumed to be normalized, then $\mathbf{a}_k$ is the k'th eigenvector of $\mathbf{S}$

$$\mathbf{S}\mathbf{a}_k = \lambda_k \mathbf{a}_k \tag{5.14}$$

making the problem of finding the PC's to finding eigenvectors of the covariance matrix $\mathbf{S}$. The size of the eigenvalues λ_k determines the amount of variance for the k'th PC and by calculating these, the most important PC's can be distinguished, and a measurement for the information loss can be established.

t-student Stochastic Neighbor Embedding The algorithm t-SNE is focuses on preserving the local structure of the data when making a dimensionality reduction. Instead of using a distance measure like the Euclidean distance, the algorithm uses conditional probability to represent similarities between two data points. The similarity

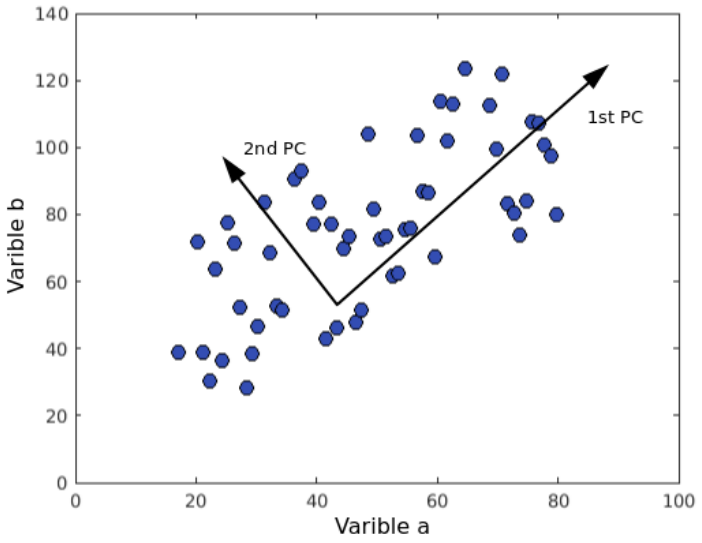

Figure 5.2: Plot of a data sample. The two added axis indicates the first and second principal component. The size of the arrows gives an estimate of the variance.

of the data point x_j to data point x_i is the conditional probability, p_{ij} that x_i would pick x_j as its neighbour, if neighbours were picked in proportion to their probability density under a Gaussian centred at x_i. Described formally as

$$p_{ij} = \frac{\exp(-\|x_i - x_j\|^2/2\sigma_i^2)}{\Sigma_{k\neq l}\exp(-\|x_k - x_l\|^2/2\sigma_i^2)} \tag{5.15}$$

were σ_i is the variance of the Gaussian that is centred on data point x_i. The choice of the value of σ_i is dependant on the data density in the region of the i'th point, and is found by a binary search [31]. For the low-dimension pairs y_i and y_j the conditional probability is defined by a t-student distribution

$$q_{ij} = \frac{(1 + \|y_i - y_j\|^2)^{-1}}{\Sigma_{k\neq l}(1 + \|y_k - y_l\|^2)^{-1}}. \tag{5.16}$$

If the map points y_i and y_j correctly models the similarity between the high dimensional data points x_i and x_j, then the conditional probabilities p_{ij} and q_{ij} will be equal. Therefore the aim of the t-SNE algorithm becomes to find that model in low dimension that minimize the mismatch between p_{ij} and q_{ij}. This is being realized by using a gradient descent method on a defined cost function, called the Kullback-Leibler divergence [32]. The fact that t-SNE uses probability distributions, means that t-SNE is stochastic algorithm, giving different result for each execution.

Evaluating a reduced dimensionality representation In order to quantify the success in the mapping from the high dimensional space to the reduced representation, the concept called *trustworthiness* is introduced [33]. It describes how similar the set of the k closest neighbours in the reduced dimensional space is in relation to the same set in the original space.

Consider the data sample j. Let $r(i, j)$ be the rank of the ordering, according to the distance in the original space between the i'th data sample in relation to the j'th data sample. Ordered in such a way that if j is the n'th closets point with respect to i, then the rank $r(i, j)$ is equal to n. Let $U_k(i)$ be the set of those data samples, that are in the neighbourhood of size k of the sample i in the reduced space, but not in the original space. The measurement of the trustworthiness of a dimensionality reduction is given by

$$M(k) = 1 - \frac{2}{Nk(2N - 3k - 1)} \sum_{i=1}^{N} \sum_{j\in U_k(i)} (r(i, j) - k) \tag{5.17}$$

where N is the number of data samples. The M value can be in the interval $[0, 1]$, describing how well the order of the k nearest point has been preserved. Good values are usually > 0.85 [34].

5.3 Single atom transfer problem

This section aims at giving an historical introduction to our groups journey of understanding the topology of various control landscapes. The work and analysis presented in this section has been performed by Morten Andreasen and is described throughout in [35].

The problem of translating a single atom from one location to another can be realized experimentally with an optical tweezer. This operation is necessary for entangling atoms in a optical lattice, which can form the basics of qubits. When moving an atom the effects of decoherence require this operation to be realized fast. The *quantum speed limit* is a term describing the shortest possible duration were a perfect transfer of the atom exist. To push this limit the optimization algorithm Krotov [36] has been applied on a numerical description of the problem. The variables to control is the position and the amplitude of the optical tweezer, both as a function of time, which utilities the control field. The Krotov algorithm is a local seeking optimizer and because of the huge parameter space, the initial guesses, called seeds, for the algorithm becomes of great importance. In order to generate good seeds a gamification of the problem was created by *ScienceAtHome*[5], seeking the help of the human intuition for solving the problem.

[5]ScienceAtHome is a game developing team connected to our group, working with involving the public in research. www.scienceathome.org

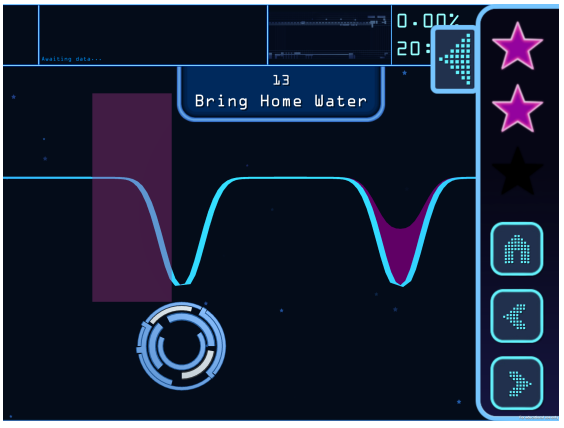

Figure 5.3: Screen shot showing the gameplay of the Bring Home Water game. The deformed curve to the left is representing the tweezer potential and is controlled by the mouse. The deformed curve to the right is representing the potential confining the atom. The purple rectangle to the left is representing the target state. From www.scienceathome.org

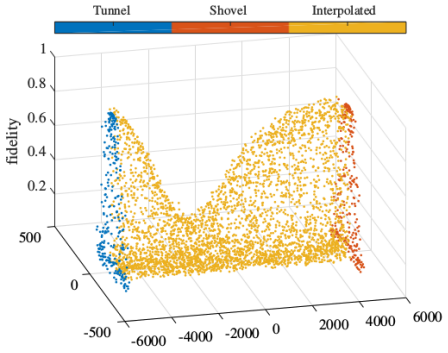

(a) Two dimensional representation of the two strategies with interpolated solution in between. Adapted from [19].

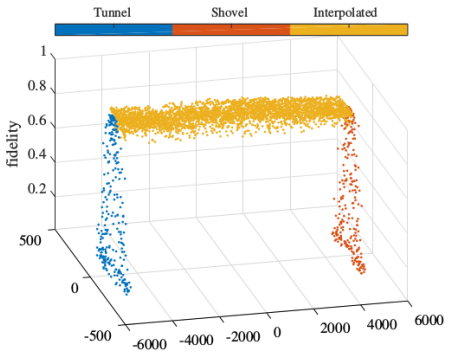

(b) Two dimensional representation of the two strategies with interpolated and optimized solutions in between. Adapted from [19].

An image from the game is shown in figure 5.3. In this game, called Bring Home Water (BHW) the task for the player is to control the optical tweezer with the mouse and "collect" the wavefunction describing the atom, for afterwards to return it to the starting position. The overlap between the target state and the movable atom state gives the fidelity of the solution and defines the score of the game.

The success of the gamification became apparent when some player solutions turned out to be better than the ones made by the optimization algorithm. Letting the Krotov algorithm using these solution as seeds, even better solution were found [23]. A clustering analysis of the good solutions obtained from the game, showed that the players in these cases followed two distinct strategies for solving this problem [23]. These are interpreted as a "tunnelling-strategy", where the quantum tunnelling phenomenon is responsible of transferring the atom to the moveable tweezer potential, and a "shovelling-strategy" where the atom quickly is collected and the excitations brought down by a matching quick movement in the opposite direction.
To investigate new solutions an interpolation was performed between the two strategies. This is visualized with a 2D representation made with the t-SNE algorithm in 5.4(a). It is apparent that the interpolated solution is less good and a lot of the solutions gets a fidelity of zero. By performing the Krotov optimization, using the interpolated results as seeds, high fidelity solutions appears as a bridge. A visualization is given in figure 5.4(b). This tells us that this subset of the control landscape is very spiky, but has a high density of local optima. Furthermore it inspires us to define the term *superlandscape*, which is a landscape formed by the local optimas. An optimization algorithm searching in this superlandscape has been implemented in this group and is described in [19].

5.4 Control landscape of the creation of BEC atoms

This section describes our first approach in optimization of the creation of a BEC and the search in the control space to get knowledge about the topology of the control landscape. In order to get an impression of the distortion of the constrained control landscape, we are interested in finding bridges between known BEC creation strategies.
This creation of BEC atoms takes place in the cube chamber, where a cloud of laser cooled atoms has been transferred by two magnetic coils on a rail. In the Cube chamber the atoms are further cooled down with microwave evaporation. After this pre-cooling, the atoms are loaded from the magnetic quadrupole field to a trap potential consisting of a combination of the magnetic field and two light fields. The last part of the cooling process takes place after the loading as evaporative cooling by lowering the trap potential. This and the next section consist of an thoroughly analysis about the optimization of both the loading process and the evaporative cooling process. Furthermore a study of different kinds of optimizations methods is presented. In this section the landscape analysis is made starting out from already known good solutions. In subsection 5.4.2 the search for new novel solution is performed by an local optimization algorithm. In section 5.5 a game has been developed giving people with limited knowledge about the problem an opportunity to optimize the evaporative cooling process.
During all of the mentioned methods a drift in the amount of yielded BEC atoms has been present in the experimental system. This has been detected by a benchmark measuring of a specific parameter configuration, which over time has yielded different amount of

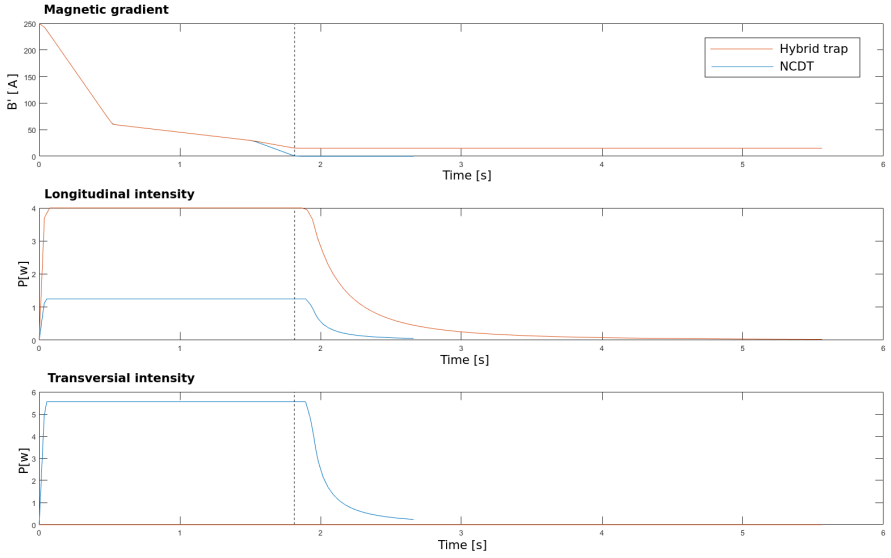

Figure 5.4: Ramps for the control fields of the gradient of the magnetic field, the longitudinal beams light intensity and the transversal beams light intensity, from the top. Shown for both the Hybrid trap (red) and the NCDT (blue). The punctuated line separates the loading and the evaporation part.

BEC atoms. We are not completely aware of the reason for this drift, but it has some relation to the drift in the amount of atoms transferred to the cube chamber. The drift implies some uncertainties when comparing the BEC atom yield from different solutions. We are using as a starting point the two configurations *Crossed Dipole Trap* (CDT) [37] and the *hybrid trap* [38], which are described in section 2.3. Inspired from these trap configurations others are formed. This includes the *Wide Crossed Dipol Trap* (WCDT) which is a version of CDT were the transversal dipole beam is able to move in the axial direction and thereby make a deformation of the crossing volume between the two dipole beams. Due to this the CDT will from now on be called the *Narrow Crossed Dipole Trap* (NCDT). Furthermore a version of the Hybrid trap that also is wider is introduced, called the *wide hybrid* trap. These four configurations are all different in their ramp shapes and is denoted as different *strategies*. The ramp sets for the hybrid trap and the CDT, can be seen in figure 5.4. The first part, before the punctuated lines, is the process of loading the cloud from the magnetic field too the hybrid trap or to the CDT. This loading process is predefined, with the exception of the value of the last ramp point which, due to continuity, is equal to the first point in the evaporation ramp.

5.4.1 Exploring the control landscape

Starting out with the four different strategies, the NCDT, the WCDT, the hybrid trap and wide hybrid trap, we are interested in two objectives:

1. Optimizing locally around the strategies to find the optima.
2. Understanding the control landscape in terms of bridges between strategies.

As mention earlier the specific control landscape depends on the parameters chosen to represent the control problem. In the landscape search in this section the following parameters have been chosen:

- $P_{i,t}$ and $P_{i,l}$, the initial value of the power for respectively the transverse beam and the longitudinal beam.
- $P_{f,t}$ and $P_{f,l}$, the end value of the power for respectively the transverse beam and the longitudinal beam. The ratio between the initial and final value for the two beams are typically set equal to give the same duration of the ramps.
- τ_t, τ_l and β_t, β_l, parameters describing the intensity ramp for respectively the transversal and longitudinal ramps. The expression for the ramp profile using these parameters are given as 5.18.

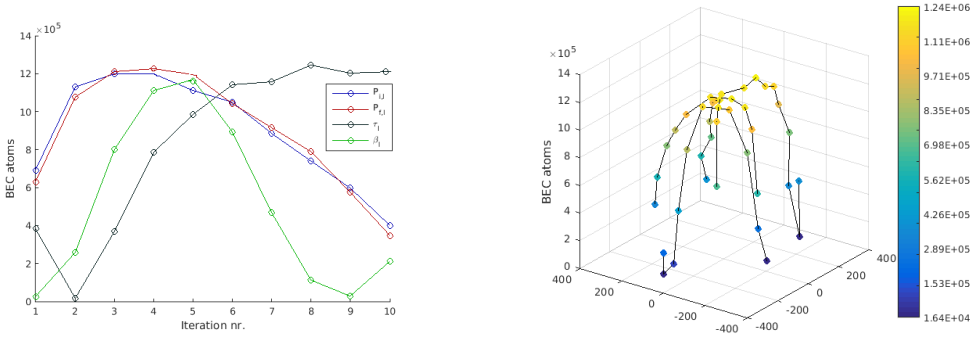

(a) (b)

Figure 5.5: a) Line-scans of four different parameters of the hybrid trap configuration. The parameters being the initial intensity $P_{i,l}$, the final intensity $P_{f,l}$, τ and β for the longitudinal beam (blue, red, black, green). They are all part of the expression in 5.18. b) Same line-scans plotted as a 2D representation. The interpretation of this is that the scans together form a "mountain".

- I_{QP}, the current for the quadrupole magnetic field during the evaporation process.
- I_{CC}, the current for the compensation coil.
- x_{stage}, the position of the translation stage which can change the focus of the longitudinal beam and thereby the crossover volume of the crossed dipole beams.

Both the intensity of the transverse beam and of the longitudinal beam are parametrized through

$$P(t) = P_i\Big(1 + \frac{t}{\tau}\Big)^{-\beta} \tag{5.18}$$

where P_i is the initial power of the beam, τ is a time constant and β determines the lowering rate and $t \in [0, t_f]$. The end value is defined as $P_f = P(t_f)$. The expression is inspired by 5.7. It forms a ramp with flexibility in relation to the decreasing rate, making it possible to tailoring it to the dynamics of the system. For instance when the atoms get colder, their collision rate decrease and therefore the cloud needs longer time to thermalize. This demand can be realized by lowering the decrease rate of the potential for longer time. With this parametrization, we get a control space of 11 dimensions, which is the control landscape that will be investigated in this section.

In order to map out the landscape for we used 1D, 2D and 3D scans. The 1D scans also called line-scans were made by varying one parameter or varying a combination of parameter linearly and holding the other parameters constant. For each of the four strategies multiple line-scans was performed, varying different parameters. In figure 5.5(a) four line-scans are displayed, mapping out the local structure of hybrid trap strategy, by varying the value of the parameters $P_{l,i}$ (blue), $P_{l,f}$ (red), τ_l (black) and β_l (green). To visualize the control landscape and get an overview of the compilation of

scans, a dimensionality reduction algorithm has been applied on the data. By applying the algorithm t-SNE, see section 5.2.4, the line-scans together form a *mountain* in the landscape indicating that a local optima has been reached, is shown in 5.5(*b*). A dimensionality reduction landscape though do not explain the true landscape, but it can maybe give some intuition about it.

Through a number of line-scans and 2D scans we searched for bridges between the four strategies. Only a bridge between the NCDT and the WCDT was found, which can be seen in the figure 5.6. This bridge were also indeed expected, because the difference in the strategy was mainly the size of the crossover volume of the two dipole beams. A search for other bridges was tried out, but couldn't be found. This can be because we haven't scan trough the right parameters, or that it is non-existing in the available control space.

Low dimensionality representation of the scans

Aiming to give an overview and an idea of the control landscape for this given parametrization, a collection of scans are being illustrated in a 2D representation in figure 5.7 and figure 5.8. In this representation each point correspond to a specific configuration of the parameters defined in the 11 dimensional space, and thereby as a specific evaporation sequence performed by the experiment. The axis represent some arbitrary dimensions where only the relative placement of the points is sensible. As intuitively expected four separated mountains, each representing a specific strategy for making a BEC, appears in

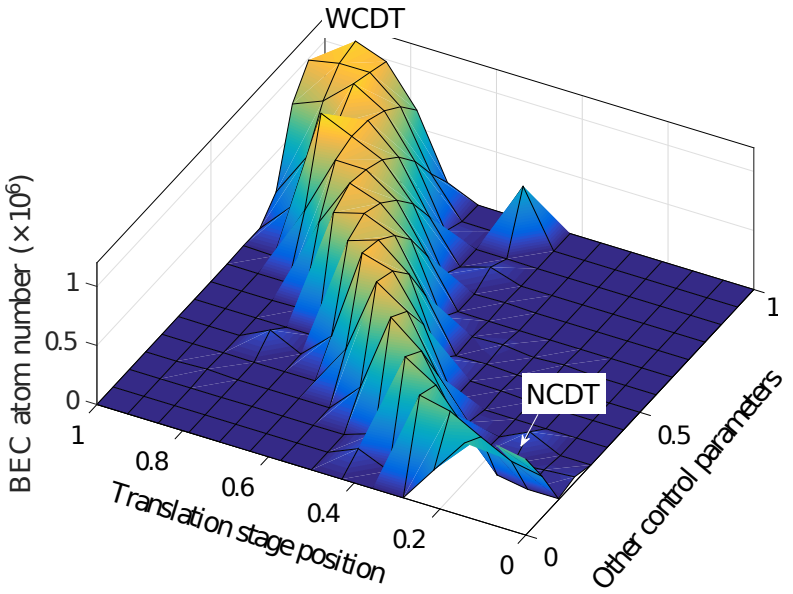

Figure 5.6: a) 2D scan of parameters interpolated between the NCDT trap and the WCDT trap. A bridge is clearly formed.

the landscape. Each of these consist of a number of line-scans, with different parameters as variables. Between these mountains paths are plotted to unite the mountains, these haves been made with 1D scans and 2D scans. It can be seen that a bridge connects the NCDT and the WCDT. In the case of the other paths the BEC atom yield is not increasing monotonously, therefore not forming bridges. A point was created trying to steer the line-scan in a different direction for making a bridge, which are called a mutant-point.

To make the low dimensionality representation, the algorithm tSNE has been used on all the data except the 1D connecting paths, which has been added to the landscape afterwards point by point by a modified MDS algorithm [39]. This version is able to add a new point to an existing landscape by finding the place of this point in the low dimensional map with the lowest corresponding error. The t-SNE and the MDS algorithm uses a predefined set of seeds which is made from a guess about how the landscape should look according to our intuition. The seed can be seen in figure 5.9(a) where the blue color denotes the seed for the t-SNE algorithm and the red color the seeds for the MDS algorithm.

The low dimensional landscape is not a perfect map of the high dimension data, and that raises the question how good a representation the low dimension landscape map is. To give some quantitatively answer the concept of trustworthiness, which gives a measure for the preservation of all points neighbour relations, is being used on the dataset. A

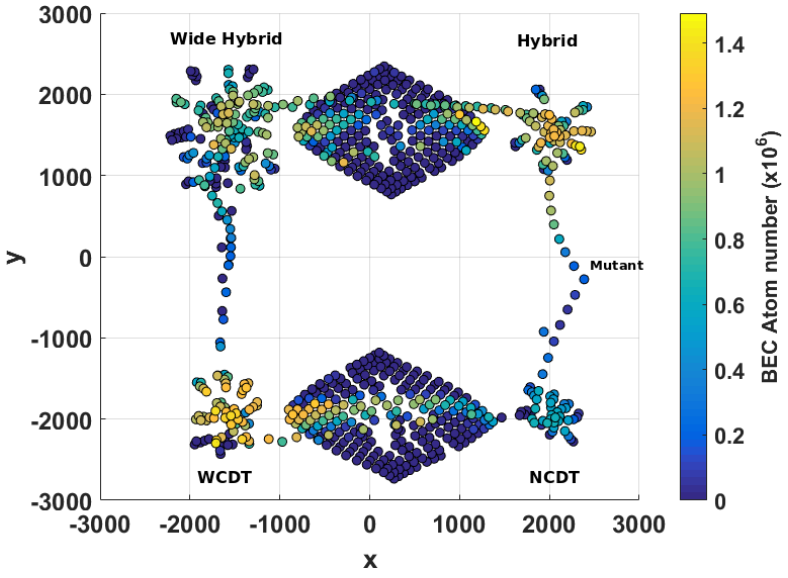

Figure 5.7: Topview of the 2D representation of the control landscape for BEC creation with evaporative cooling. Each point correspond to a specific parameter settings for the BEC creation. The NCDT, WCDT, Hybrid Wide and the Hybrid are BEC creation strategies. The color scale indicates the a number of BEC atom yield for a given point.

more detailed explanation of the trustworthiness measure is given in 5.2.4. In figure 5.9(*b*) the trustworthiness of the dimension reduction of the control landscape is plotted as a function of numbers of neighbours, which for a given point corresponds to how many neighbours has been taking into account for a given trustworthiness score. The trustworthiness is generally high for the representation. It should be mentioned that the trustworthiness measure says nothing about the preservation of the distance between the points, only about the relative positioning between the points.

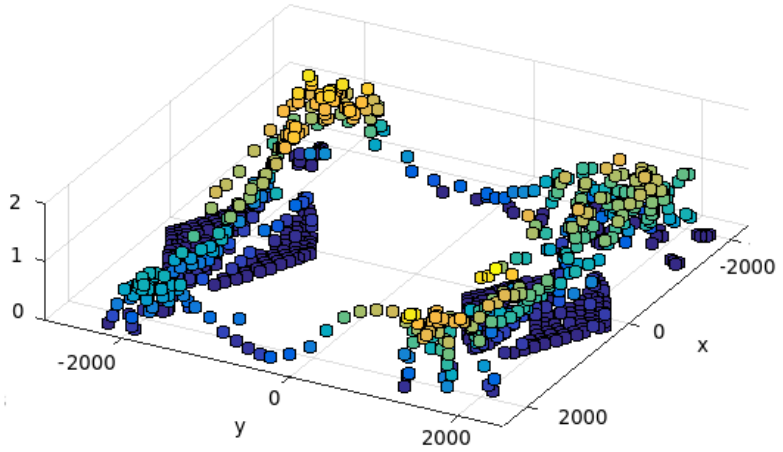

Figure 5.8: Side view of the 2D representation of the control landscape for BEC creation with evaporative cooling. Same data as in 5.7. Each point correspond to a control setting for the BEC creation.

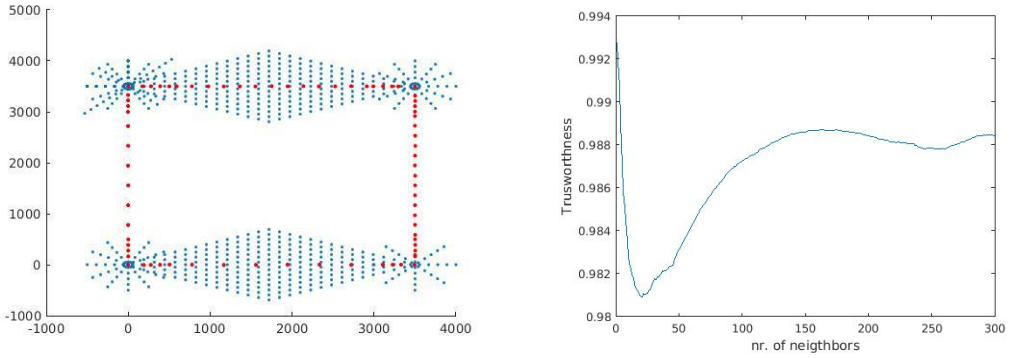

(a) (b)

Figure 5.9: a) Seeds used for dimensionality reduction of the control landscape. The blue dots indicate the seeds for the t-SNE algorithm whereas the red dots indicate the seeds for the MDS algorithm. b) Plot that shows the trustworthiness of the 2D representation of the control landscape, plotted as a function of the number of neighbours taking into account for each point.

5.4.2 Global optimization algorithm

Another way to deal with optimal control problems is to use optimization algorithms. A large diversity of algorithms exist, and which one to use on a given problem is not trivial. That is because the underlying control landscape they are used on, determines their efficiency, and is usually unknown. The optimization algorithms can be separated into two groups being local or global optimizers. The local optimizers can only find the local optimum in the given control space and are usually dependant on the seed given. Examples of these are the Nelder Mead simplex method [40], the gradient ascend method, and the Krotov algorithm [36] or the *Chopped RAndom Basis* (CRAB) algorithm [41, 42]. Local optimizers have the problem of being trapped in a the local optima, thereby converging premature. Global optimizers has the ability to escape from these local traps and go on a further search in the landscape for a higher optima. Examples for global optimizers are genetic algorithms [43, 44].
Through a collaboration with a PhD student from the university of Ulm, a remote controlled closed looped optimization of the creation of BEC atoms by evaporation cooling was performed [6]. This was with an upgraded version of the CRAB algorithm called *dressed-CRAB* (dCRAB) [45]. In this section the process and the outcome of this collaborative optimization experiment is analysis and discussed.

dCRAB optimization algorithm

Suppose you have an optimal control problem, where the system is dependent on the control field $\mathbf{u}(t)$. Solving this problem to find the optimal figure of merit is in many cases very difficult if the whole control space is to be considered due to lack of time in searching in this usually huge space. The CRAB algorithm deals with this problem by only considering a subset of the control space, defined in a randomized basis set. The CRAB algorithm makes an optimization by starting from an initial guess for the control field $\mathbf{u}^0(t)$ and then tries to find the best correction yielding the highest figure of merit. The control field consist of N_{cp} control pulses where for every j'th pulse a correction function is needed

$$u_j(t) = u_j^0(t) f_j(t) \tag{5.19}$$

[6] Thanks to Jonathan Zoller for his help.

where $f_j(t)$ is some function that reshapes the form of $u_j^0(t)$. The functions $f_j(t)$ are expanded in a some basis

$$f_j(t) = \sum_{k=1}^{N_f} c_j^k \hat{f}_j^k(t) \tag{5.20}$$

with coefficients c_j, and basis functions $\hat{f}_j$. Important for the performance of the algorithm is to choose a truncated base consisting of a finite number N_f of basis functions, and let these be somehow randomized. The randomization breaks the orthogonality of the function space, but improves the convergence of the algorithm [42]. The algorithm implemented in our case uses a Fourier basis which gives the following correction to the control field

$$f_j(t) = \frac{1}{\mathcal{N}}\big[1 + \sum_{n=1}^{N_f}(A_n \sin(\omega_n t) + B_n)\cos(\omega_n t)\big] \tag{5.21}$$

were $\omega_k = 2\pi k(1 + r_k)/T$ are Fourier harmonics with a random number $r_k \in [0, 1]$, T is the total time evolution and $\mathcal{N}$ is a normalization constant. The control problem has now been reformulated as an optimization of the figure of merit $\mathcal{F}$ by a control pulse defined by the set of parameters $\{A_k, B_k\}$

$$\mathcal{F} = \mathcal{F}^{CRAB}(\{A_k, B_k\}), \tag{5.22}$$

consisting of $2N_f$ variables. Finding the optimum in this new defined control landscape can be handled by different numerical local or global search methods. In our case a local optimization algorithm is used.

By using this new defined subset of the control space, the algorithm may converge to a local optimum that only exist because of the constraints of the basis choice, a so called *false trap*. To escape from this trapped location the dCRAB version is introduced. When a convergence is reached, the dCRAB algorithm uses the CRAB-optimized control field functions as the new starting guesses for a new CRAB optimization with a *new* random basis and new coefficients. For the i'th super iteration

$$u_j^i(t) = u_j^{i-1}(t) f_j^i \tag{5.23}$$

the control field gets *dressed* with a new correction function, through searching in a new subspace of the full control space available by the control system.

Remote optimal control

Beside being a way to optimize the system by a state of the art algorithm, this optimization experiment gave us the opportunity to test our new remote controlled experimental system. An more detailed explanation of the remote control system ALICE is given in section 3.1. A connection has been established over the internet between the control computers in the laboratory containing the experiment at Aarhus university, and the computer running the dCRAB algorithm at the university of Ulm. Firstly the dCRAB algorithm from an initial seed determined a new set of pulses defining the control field. In specific these are a time dependant ramp for the magnetic field gradient, the longitudinal beam intensity and for the transverse beam intensity. The optimization computer could send the ramps to the ALICE-control system where they are included in a predefined sequence for the whole experiment of the evaporative cooling. An experimental sequence executes of producing a BEC, which then are being detected by absorption imaging and analysed to find the number of BEC atoms present in cloud. The result are being send back to the computer in Ulm where a new iteration of the dCRAB algorithm takes place.

Results for the dCRAB optimization

In this section the results of the dCRAB optimization will be presented and analysed in relation to better understand the topology of the control landscape. During the experiment the ramp for the magnetic field was controlled trough the $I_{\mathrm{QP,evap}}$ value only. The translation stage x_{stage} was on a locked position forming a hybrid trap, being that configuration giving the highest yield so far, and the compensation coil I_{cc} was at a constant value as well. The longitudinal and transversal ramps was fully controllable within the physical bounds of the hardware and could be defined with a custom function defined by the user. In this case this function was the control field decided by the dCRAB algorithm. In trying to find new higher optima we wanted to try out the algorithm starting from two points around the hybrid trap. In figure 5.10(a) and 5.10(b) are two plots showing the results of the optimization from these initial starting points. The blue dots each show the number of BEC atoms, N_{BEC}, for a single sequence evaluation, the red line shows the best BEC value obtained so far at the current time, and the dotted line shows the best BEC value before the optimization given by the hybrid trap configuration. The inset is a line-scan from the hybrid trap to the NCDT made by scanning the parameter $I_{\mathrm{QP,evap}}$. The optimization run in figure 5.10(a) and 5.10(b) started with an initial guess given respectively by the configuration defining the points 0.4 and 0.2 in the inlet. Both of the optimization runs resulted in finding a new better optimum, with the best one yielding $2.3 \cdot 10^6$ BEC atoms. In figure 5.11 are

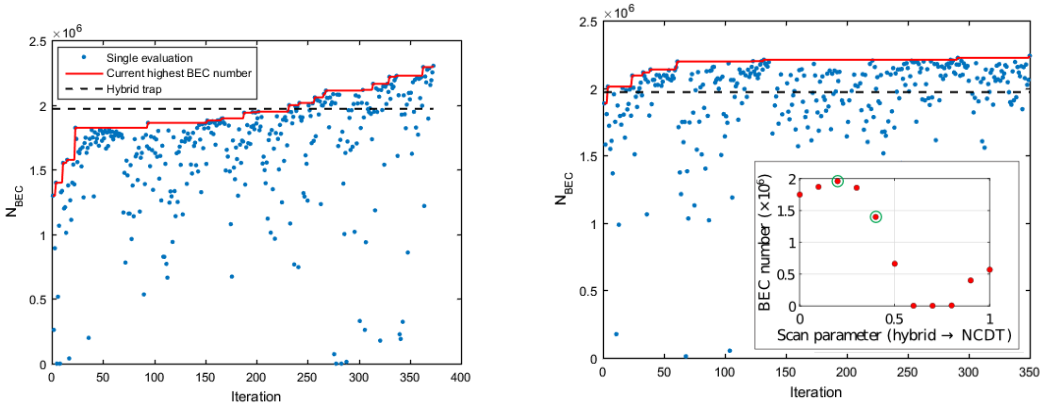

(a) (b)

Figure 5.10: Results from the optimization done by the dCRAB algorithm. The blue points are the BEC atoms result from single sequence evaluations, the red line is indicating points with increasing yield and the punctuated line is showing the value of the benchmark hybrid trap. The inlet shows a line-scan from the hybrid trap to the NCDT. The starting points for the algorithm in a) and b) are the points at 0.4 and 0.2 from the inlet, respectively.

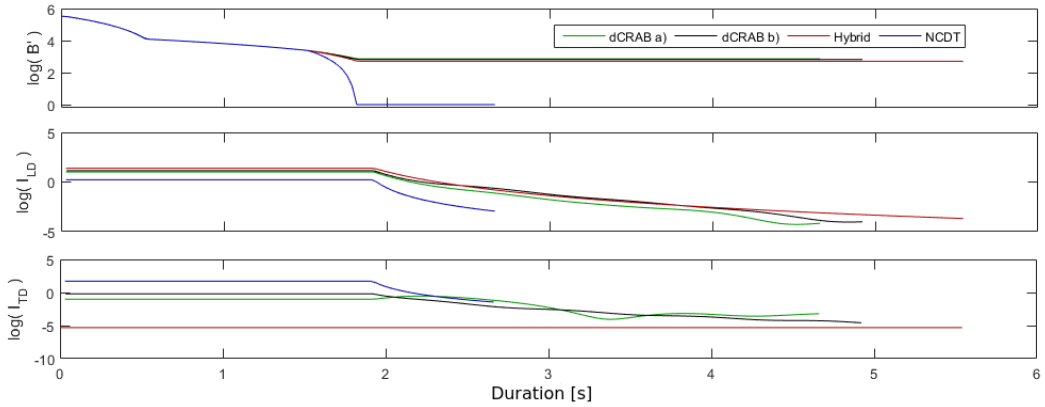

Figure 5.11: The ramp sets for the four different configurations of the dCRAB optimum in 5.10(*a*) and 5.10(*b*), hybrid trap and the NCDT. From the top, the figures shows the logarithm of the ramps for the strength of the magnetic gradient and the intensity of the longitudinal and the transversal beam.

the ramps for the new obtained optima from the two dCRAB runs, compared with the ramps for the hybrid trap and the NCDT. The new found optima are close to each other compared with the hybrid trap and the NCDT. They resembles the hybrid trap, but with the transverse field included and a lower intensity for the longitudinal field in the evaporation process.

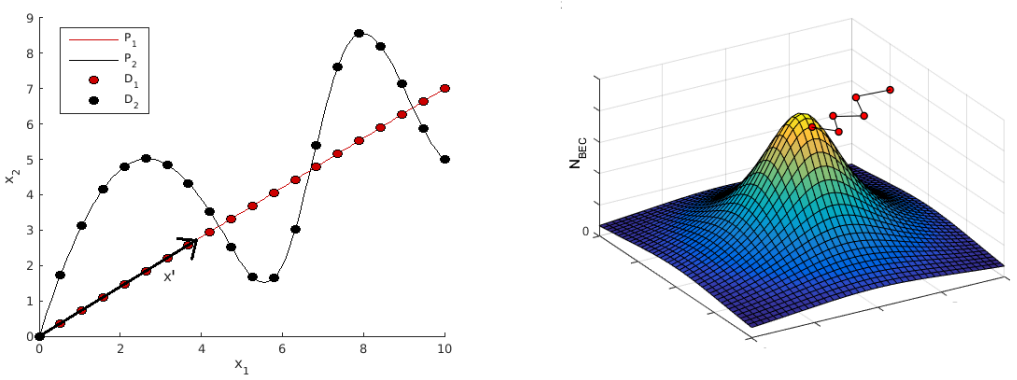

(a) (b)

Figure 5.12: a) Graph indicating the difference of a control space and a fully reduced control space. x_1, x_2 is the basis vectors of the control space and x' is the base vector of the fully reduced control space. D_1 and D_2 are two different datasets, and P_1, P_2 is the paths formed by the two data sets, respectively. b) Illustration showing the hyperpath made by the dCRAB algorithm, making it possible to escape the hybrid mountain forming a local false trap.

Analysing the topology of the control landscape

The dCRAB algorithm should be able to reach the same optima as a multidimensional gradient ascent method thereby avoiding false traps, according to [42]. A reason for using the dCRAB instead is the inefficiency and the time consuming of the other when searching in a high dimensional space. Both of the methods creates a search path that can extend trough the full dimensionality of the control space defined by the controls available to steer and the constraints on these controls. In the following I will refer to a given path in relation to the dimensions of the *fully reduced* control space it propagates in. A fully reduced control space I define as the space spanned by the smallest set of basis vectors possible to describe a given dataset. As an example of this, consider the following two datasets D_1, D_2 forming the paths p_1, p_2, in the control space $\{x_1, x_2\}$, showed in figure 5.12(a). The fully reduced control space for the dataset D_1 is a linear combination $\{x' = ax_1 + bx_2\}$ where for D_2 it is $\{x_1, x_2\}$, thereby p_1 is a 1D-path whereas p_2 is a 2D-path. The reason for this distinction is to emphasis the difference between exploring the control landscape by using scans, as was done in section 5.4, and by applying the dCRAB algorithm. The scans can be linear combination of different controls and therefore make a trail trough a control space of more than three dimensions, but only trough a fully reduced control space given by the scan dimensions. The highest scan dimension in our former analysis was 3 dimensions, though only creating a 3D-path in the fully reduced control space. Because the dCRAB algorithm can change its basis, the path created will could extend in more than a 3 dimensional fully reduced control

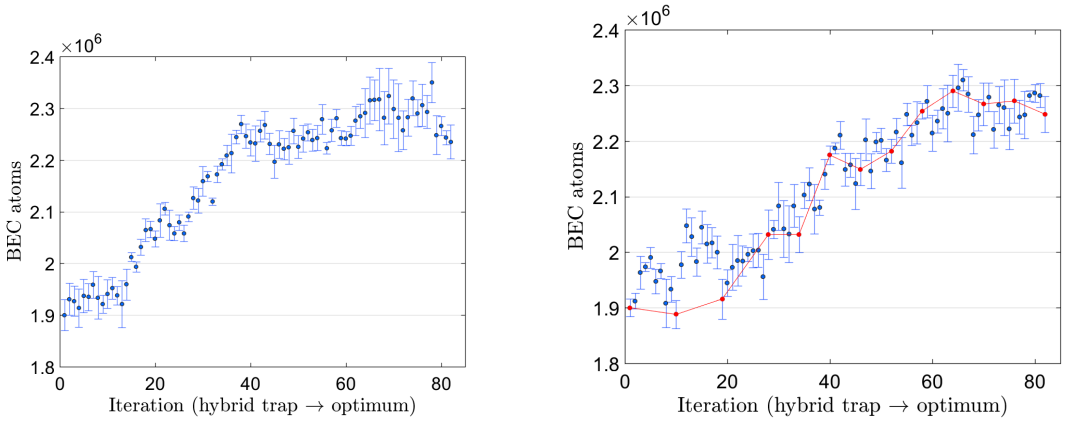

Figure 5.13: a) Results for a direct interpolation between the hybrid trap and the dCRAB-optima. b) Results for an interpolation between the points of the hybrid trap and the optimization steps in 5.10(b). The red points indicates the points used to the interpolation.

space, and form a *hyperpath*. This is defined as a path propagation in more than 3 dimensions in a fully reduced control space.
It is interesting to notice that the mountain made by line-scans 5.5(b) indicating a local optimum, was apparently a false trap made by the constraints of the sub control space formed by the line-scan parameters. The dCRAB algorithm was able to make a hyperpath and exploring the full available control space, and thereby travel a path to a higher optima not found before. In figure 5.12(b) is an illustration of the hybrid mountain and the hyperpath taken by the dCRAB algorithm, escaping the false trap. The figure is not based on real data, but is included for illustrative reasons.

Finding a new optimum with the dCRAB algorithm, we are interested in whether there is a bridge between the hybrid trap and the new found optima, from now on referred to as the dCRAB-optima. The dCRAB have found a path with only increasing points in its multidimensional climbing, formed by the increasing yield points, but these points are few and to state it as a bridge a better resolution of points is necessary. Therefore a linear interpolation was made between the ramps defining the increasing yield points, referred to as steps. The result for these ramps can be seen in figure 5.13(b), referred as the multi-step path. Furthermore we made a linear interpolation between just the ramps of the hybrid trap and of the ramps of the dCRAB-optima. The results is shown in figure 5.13(a) referred as direct path.

Within the errorbars of the points, none of the two results from the interpolated ramps completely form a bridge, due to the fact that neither increases exactly monotonously. Though the direct path almost increases monotonously and therefore almost forms a

bridge, whereas the multi-step path is way more rugged. Looking at the red line in the multi-step figure, the steps do not monotonous increase as they did in the dCRAB run. This monotonous increase of the steps was an assumption for making a bridge, and can explain the failure of our attempt to find one. The change in the yield of the steps can be because of drifts in the system, or because of the dCRAB path was distorted by noise, making a path of only seemingly increasing yield points.
That the direct path almost made a bridge is interesting, suggesting that a non-hyperbridge exists connecting the hybrid and the dCRAB-optimum. To get an idea about how the two paths extends in the control space, the t-SNE algorithm has been applied to get a 2D representation of the paths, shown in figure 5.14(a) and 5.14(b). The 2D reduction has been made without any user defined seeds, thereby starting with random points defined by the algorithm. The dots in the figure marks the steps of the multi step path, including the red, black and green dots, that marks the hybrid trap point, the dCRAB starting point, and the dCRAB-optimum point, respectively. The figures indicate that the two paths start at the same place at the hybrid trap, separate in two distinct paths, and unite again at the dCRAB-optimum point. In the multi-step path there is a detour from step two to step four which maybe could be noise driven, making the dCRAB algorithm get on a wrong track, but later to recover on the path towards the optimum. This can maybe explain the large bump emerging in figure 5.13(b) between step two and three. It is important to keep in mind to be careful about making conclusions based on a dimensionality reduced dataset. These can be misleading and wrong due to the inevitable information loss which happens by the mapping to a lesser dimension span. Therefore to back up the landscape analysis made here, a distance measure will be introduced in the next section.

Distance analysis of the landscape

In the following, a distance measure is being defined to give a simple measure of the difference between two applied control fields. In this case the control field consists of the magnetic field gradient pulse, the longitudinal field pulse and the transversal field pulse. Letting each ramp be discretized, in equally sized time bins, into $N = 200$ parameters. The distance between pulse set i and j is defined by a weighted Manhattan distance given by

$$d_{i,j} = \sum_k \alpha_k \Big(\frac{1}{N} \sum_{l=1}^{N} |u^i_{l,k} - u^j_{l,k}| \Big) + \beta |T_i - T_j| \tag{5.24}$$

where $k = 1, 2, 3$ correspond to the rescaled magnetic gradient pulse, the longitudinal pulse and the transversal pulse weighted with α_k, with $u^i_{l,k}$ being the k't pulse for the

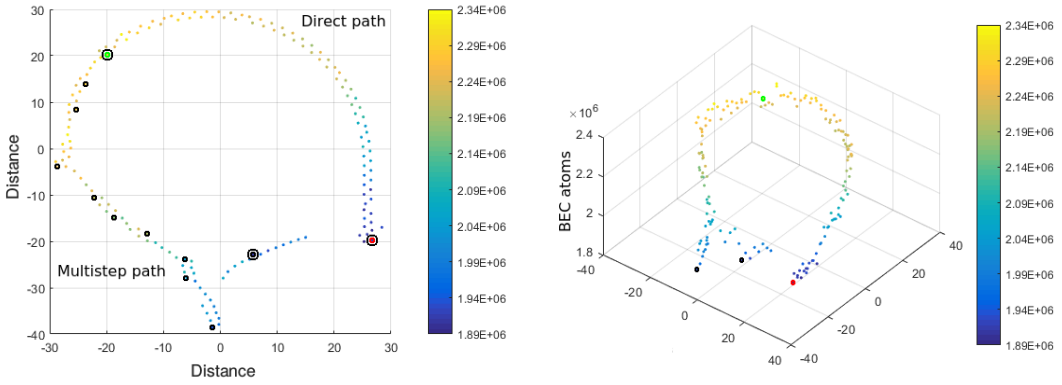

(a) (b)

Figure 5.14: The path of the direct interpolation and of the multistep interpolation presented with a two dimensionality representation made by the t-SNE algorithm. a) The paths seen from above. The multistep path is propagating to the left along the way of the optimum steps which are indicated with black circles, starting from the red point (hybrid trap), going to a point with two black circles (dCRAB start) and ends at the green point (dCRAB optimum). The direct path is propagating to the right towards the dCRAB optimum point. b) The same 2D representation viewed from the side.

i'th pulse set. The first term of the expression only takes the shape of the curve into consideration, so to include duration difference of two pulse sets the term $\beta|T_i - T_j|$ is

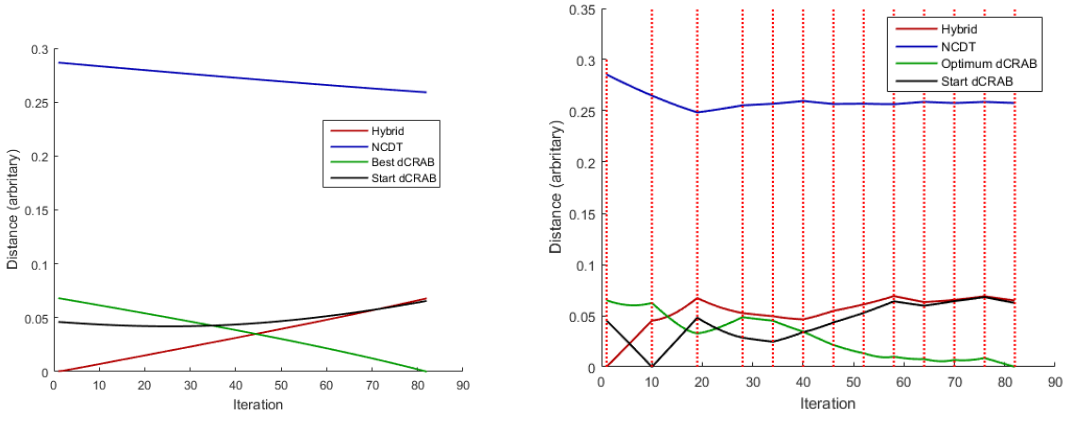

(a) (b)

Figure 5.15: Distance between the ramps of each iteration and the ramps of four reference points, being the hybrid trap (red), the NCDT (blue), dCRAB-optima (green) and the starting point in the dCRAB optimization (black) showed in 5.10(b). The distance is defined in 5.24. a) Distances given for the direct interpolation 5.14(a). b) distance given for the multi step interpolation 5.14(b). The red punctuated lines indicates the location of the steps.

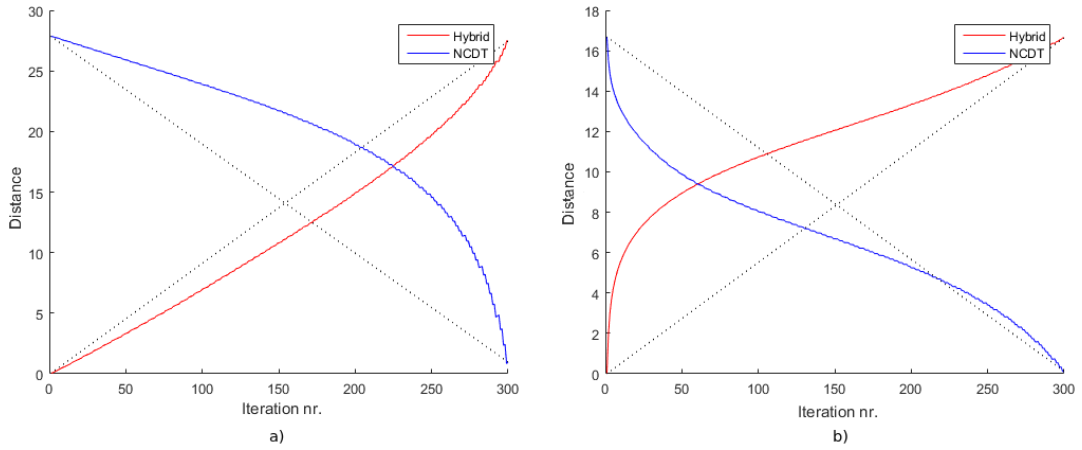

Figure 5.16: Tests of different versions of the normalization by comparing the distance to the hybrid trap and the NCDT. Both with no time dependence ($\beta = 0$). a) Normalizing in relation to the minimum and maximum value of each of the parameters. b) Normalizing by taking the logarithm of the ramps first.

included. T_i being the duration time of the i'th pulse set and β is a weight factor. Furthermore the pulses are normalized. The choice of normalization is not entirely trivial. If for example the transverse field pulse is normalized in relation to the minimum and maximum value of the intensity for the whole pulse, the evaporation part of the pulse would matter very little because of its low values of intensity in relation to the loading part. Two normalizations choices could be used to include the variations of the whole ramp. By taking the logarithm of the ramps and then normalize, or by normalizing in relation to the minimum and maximum value of each of the parameter alone, instead of the ones obtained from the whole pulse. In order to find out which one to use, a test was made to see which one described the path of the linear interpolation between the hybrid trap and the NCDT best. An linear interpolation of 300 steps between the hybrid trap and the NCDT was performed, and the distance to these two trap configurations was measure for each step by different versions of the normalization. The results are shown in figure 5.16. By comparing them with the punctuated lines, which represent a perfect distance measure for a comparison with the hybrid trap and the NCDT, the normalization in relation to each parameter was chosen.

To get a better understanding of the paths of the direct path and multi-step path, a measurement of the distance between the points on the paths and a few selected reference points has been performed. The reference points correspond to the ramps for the hybrid trap, the NCDT, the starting point and the dCRAB-optimum. In the figure for the direct interpolation 5.15(a) the distance changes linearly between the hybrid trap and

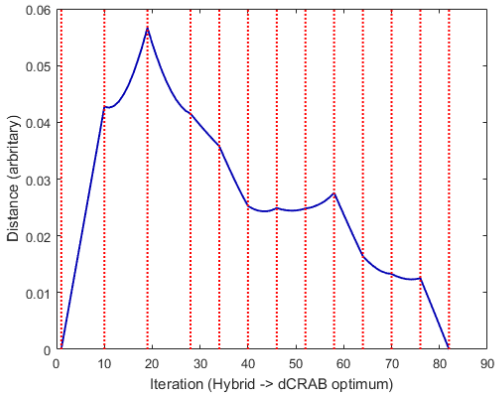

Figure 5.17: Distance between each point in the multistep path and the direct path. Red punctuated lines indicate the optimization step points.

the dCRAB-optimum as expected, which can be used as a benchmark for the correctness of the distance measure in this case. It is as well moving linearly towards the NCDT and linearly away from the hybrid trap and ends in a good distance away from both of them. The multi-step interpolation in 5.15(b) indicates a fast linear change in distance in regard to the NCDT and the hybrid trap until iteration 20 where both are fluctuating around the ending distance. Still after this the distance from the optimum changes a lot indicating that a kind of different path than the direct path is taken towards the optimum, propagating in some other dimension. To empathize this difference of the paths a comparison between the distance of each iteration of the two paths are shown in figure 5.17. It gives the same impression as figure 5.14(a), that the interpolation results follows two completely distinct paths from the hybrid trap to the optimum.

5.5 Optimization with gamification

In this section a gamification of the process of evaporative cooling will be presented. Due to the fact that people are able to solve complex problems, we want to investigate whether people, with limited knowledge of the physics behind the problem, are able to find new strategies in the evaporative cooling control landscape. This by letting people searching the control landscape, using the resource of *crowd sourcing* by a gamification of the problem. In the first part of this section the remote system will be used, letting two persons with different knowledge of the process of evaporative cooling, search the control landscape trying to optimize the cooling process. In the next part the gamification of the problem with be introduced and the result from it presented and analysed.

5.5.1 Optimization with the intuition of a physicist

With the remote control system, we opened up the experiment for two physicist, an intern student in our group and a postdoc from the university of Nothingham, whom had worked in our group earlier [7]. Both of them had knowledge about evaporative cooling of cold atoms, and had some insight into our usual strategies of creating BEC atoms. The access to the experiment was through a ALICE-client interface where the user was able to define a function controlling the magnetic gradient and the two laser beam intensities. They where both given the same initial solution as in 5.10(a), with the dipol beam ramps defined by the function given sby equation 5.18. Both of them kept this function and only changed the values of the parameters defining the ramps. Furthermore they were able to control the loading process. They both used about half a day on optimizing the yield and both obtained good results.
In figure 5.18 and 5.19, the progress of the optimization are shown for the students and the postdocs attempts, respectively. In the lower plot the trail of BEC atoms evaluation is shown. The upper panel show the distance defined in 5.24 with respect to some reference points being the hybrid trap, the NCDT, the dCRAB-optima and the starting point of the optimization. The highest number of BEC atoms achieved for the two participants was $2.2 \cdot 10^6$ and $2.4 \cdot 10^6$ for the postdoc and the student, respectively, thereby setting a new record for the amount of BEC atoms produced in our experiment.

The path taken by the student shows a good example of the shift between exploiting and exploring the landscape. In the largest part of the trail up to about 300 iterations, not much progress is appearing. Mostly the search is exploiting local without much success. A couple of times some exploration is performed, visible as the larger distance

[7] Thanks to Lærke Lyhne and Mark Bason for their help.

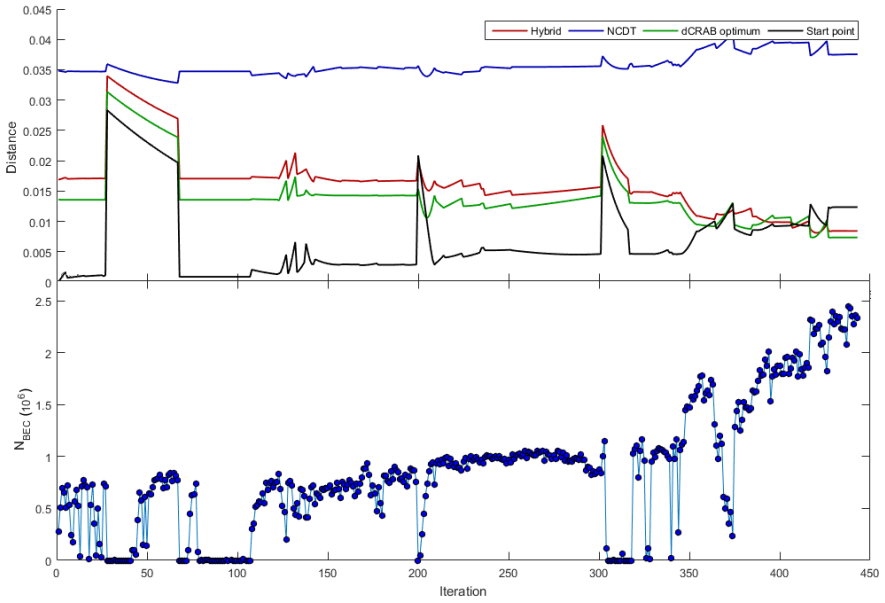

Figure 5.18: The figures in the lower plot show the obtained number of BEC atoms for a given evaluation indicated with blue dots. In the upper panel the distance between the ramps of each iteration and the ramps of four reference points, being the hybrid trap (red), the NCDT (blue), the dCRAB-optimum (green) and the starting point of the optimization path under question (black), respectively. Graphs for the students optimization.

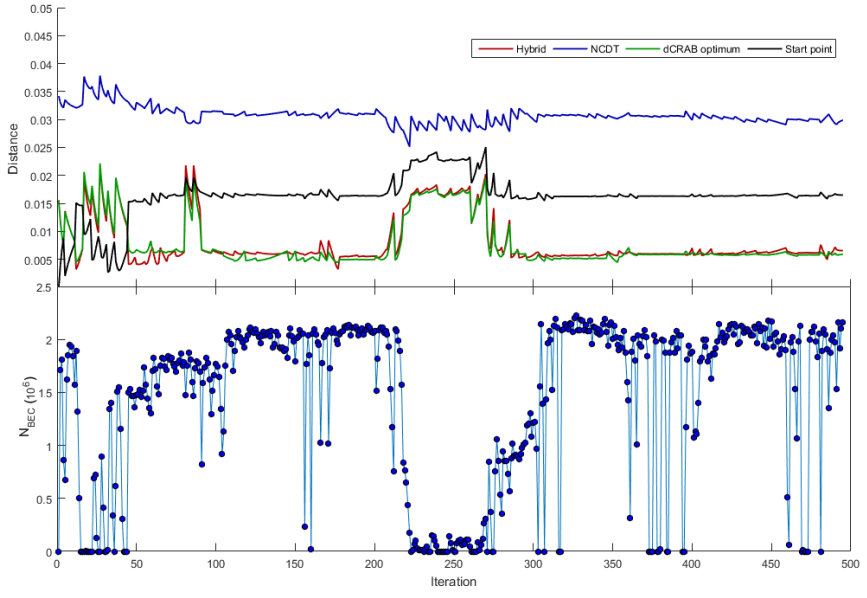

Figure 5.19: Same as in 5.18, but with graphs for the postdocs optimization.

with respect to the start point, again with a only small gain in the BEC atom number. At about 340 a sudden change happens when a new strategy is introduced apparently leading towards the hybrid trap and away from the NCDT resulting in a great improvement of the BEC atom number yield.
In the case of the postdoc, already from the beginning, a strategy being near the hybrid trap is being pursued, making a high yield appear almost from the start. Apart from some exploration in the beginning, the same strategy of local search seem to be kept for almost the whole run. An exception occur at around iteration 225 where a new part of the control space is being investigated without success.

5.5.2 Crowdsourced optimization

Different initiatives have been started to incorporate people form outside the world of academia to help out in various science related problems, this without a requirement for the participants of a detailed knowledge of the problem. A platform used to engage people are computer games, by a translation of the scientific problem into a game through *gamification*. Example of such gamifications is *Foldit*, which is an online game about folding the structures of selected proteins as well as possible [46]. The astronomy project *Galaxy zoo* invites people to classify galaxies [47], and the game *Eyewire* challenges players to map neurons in a 3D model of a retina [48].
The BHW-gamification, described in section 5.3, showed how people were able to find new solutions which in some cases are better than the ones found by a computer algorithm [23]. Inspired by this, a gamification for the problem of optimizing the evaporative cooling of atoms was created.

The ALICE-game

The ALICE-game is the name of the computer game created as a gamification of the problem of optimizing the evaporative cooling process. The main objective of the game is for the players to find a configuration of three coloured curves which correspond to the highest score. These curves defines the ramps for the magnitude of the magnetic field gradient, as well as the intensity of the transverse and longitudinal beams, highlighted with the colors yellow, red and blue, respectively. The game interface can be seen in figure 5.20(*b*). The score is directly proportional to the number of BEC atoms obtained by realizing the evaporative sequence with the given ramps. The ramps defined by the players both describe the loading and the evaporation part of the experimental sequence. The game is played by multiple players at the same time in a collaborative way, where the goal is to reach the highest score. The cooperation consists of a shared visual panel,

where old solutions can be revived, copied and manipulated. Thereby the players can exploit each others successful configurations. The score for a configuration made by a player can't be given instantly, because it has to be evaluated in the real experiment which takes about 30 s pr. evaluation.
For each game session the players start with five initial sets of curves, which corresponds to either a zero score or a low score. These have been varied for each run to guide the players optimization towards different parts of the control landscape. The representation of the curves in the game had to be made so that the players manipulations make sense with regard to the physical problem. A little change by the player should optimally result in a little change in the physical realization of the evaporation. This request was met by letting the players work with the curves of the logarithm of the magnetic field gradient and the logarithm of the laser intensities instead of a linear representation. To match the values of the curves in the game with the physical constraints of the experiential equipment, the curves were normalized with the following values defining the minimum and maximum values: $1\,\mathrm{mW} < I_{\mathrm{TDT}} < 5\,\mathrm{W}$, $1\,\mathrm{mW} < I_{\mathrm{LDT}} < 9\,\mathrm{W}$, $1\,\mathrm{A} < I_{\mathrm{B}'} < 250\,\mathrm{A}$. The lower bound is introduced because of the logarithmic scale, and has been chosen at values small enough that no effect on the trap is expected at these values and below. Two different versions of the game have been realized. A round based version and a so called Swarm version.

Round based version In this version five persons play together in a game session consisting of 10 rounds. Each round starts by a time constrain on one minute where the players each can find their own ramp configuration to submit for evaluation. It is followed by a waiting time of around 3 minutes where the solutions of the players are evaluated in the experiment. After this, the score board is updated with the new results from the solutions, and a new round begins. The persons attending this version of the game had to sign up beforehand, organized in timeslots reserving about an hour of there time for the game, so we could be certain to form groups of five that stayed for the whole session. In total we had 142 participants for this game version, with the highest yield being $1.8 \cdot 10^6$ BEC atoms. The analysis of this version is not covered in this thesis due to lack of time.

Swarm version In this version there is no limit to the participants. To handle multiple participants playing at the same time a queue system was created, were the requests is attended in the order that they arrived, a so called *first-come, first-served* policy, described in 3.3. Submission of an solution is possible at all time, but to prevent people from filling the queue to quickly a time penalty has been added for a personal submission. The overall waiting time could be long and reached 70 minutes at its peak.

(a) (b)

Figure 5.20: a) Screen shot from the ALICE game tutorial describing the experiment behind the game. b) The game interface of the ALICE game. The coloured curves represent the time dependent power of the magnetic gradient, and the time dependent intensity of the longitudinal and transversal beams.

When the change in yield in a session had stagnated for a longer period of time, the game was restarted. By having an open game where all can join at any time, it is possible for experienced players to force the game in the same direction by submitting an earlier high yield solution. To prevent this the duration of the evaporation ramps have been varied between 1.75 and 8 seconds for different sessions, thereby not being a free parameter for the players. In the following the data received from the ALICE swarm version will be analysed.

5.5.3 Results and analysis of the Swarm version data

In total 704 users played the swarm version of the game, submitting 9852 solutions, which have been evaluated in the experiment. The game was open for almost a week, 24 hours a day, divided in 18 sessions of different ramp duration. In the histogram in figure 5.21, the distribution of the BEC atom yield from the solutions is depicted. The players succeeded in having 72.0% of the solution with a yield above zero and 28% above $2 \cdot 10^6$ BEC atoms. The solution with the highest yield obtained was $2.8 \cdot 10^6$ BEC atoms, setting a new record for our experimental system.

For each session, the ramp set corresponding to the 21 best result are used to find a mean and a standard deviation of the BEC atom numbers which are shown in 5.22. This plot indicates that the players have been able to optimize the evaporation sequence in each session to yield a fairly high BEC atom number, even when the duration time was forced to a low time period, with the extreme being 1.75 s. A high change in the yield is present at about 3 s duration time, seeming to set the limit for obtaining yields above $2 \cdot 10^6$ BEC atoms.

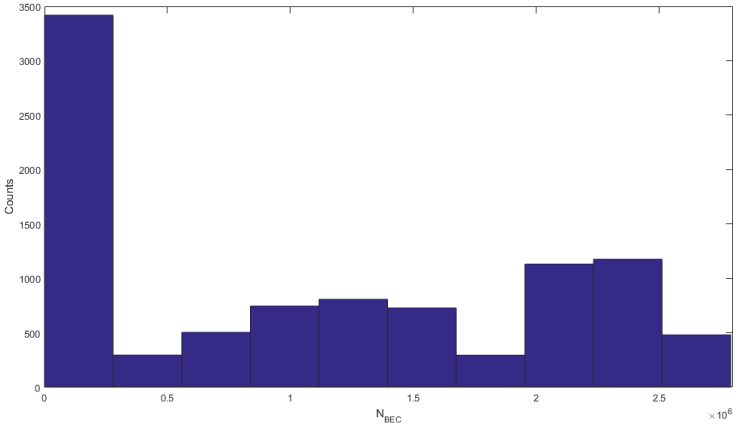

Figure 5.21: Histogram showing the distribution of the yield in BEC atoms number for the swarm game, divided into 10 bins.

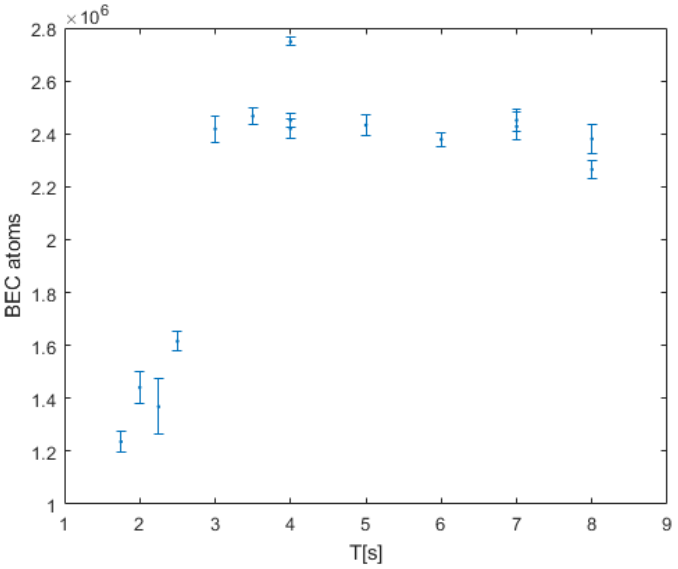

Figure 5.22: Best BEC atom yield for each session, plotted in relation to duration.

Duration scan of ramps

In figure 5.23 the shapes of the ramp set for the Swarm optima strategy, the dCRAB optimal strategy and the short duration strategy (1.75 s) have been scanned by duration. The black rings indicate the original ramps sets defining the shape used for the scans. The swarm optima and dCRAB optima curve increases until about 4 s and 5 s. For long durations the atom yield decrease slowly. The short duration curve behaves quite differently, by starting the increase at 1 s having a maximum around 2 s, followed by a drastic decrease until the yield stagnates at about 4 s. This observation indicate two points:

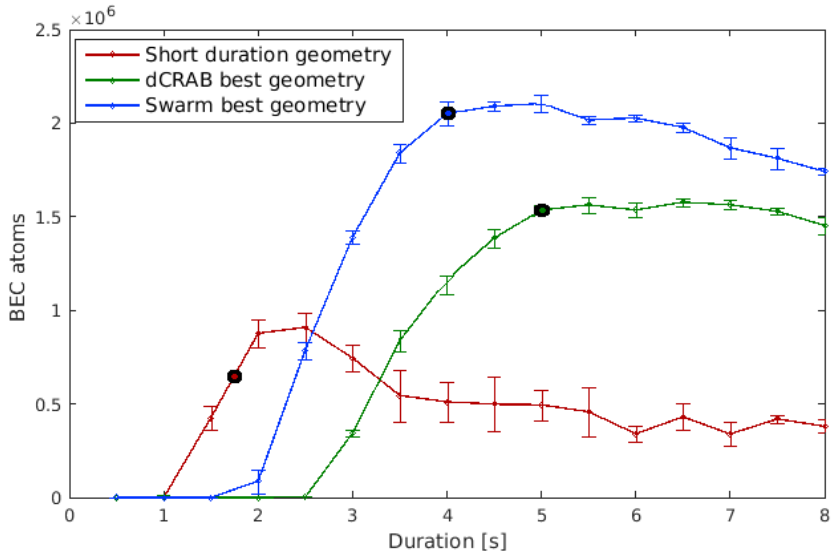

Figure 5.23: Scan over duration for the shape of the ramp sets from short-duration, dCRAB-optima and Swarm-optima. The black rings indicates the duration time defining the given shape.

1. The geometry optimized for low durations and the geometry optimized for large durations is fundamentally different.

2. The game players are able to adapt to an arbitrary given condition, and find optimized solution within the bounds of its constraints.

Searching for novel strategies

During the Swarm game, the players were able to archive a great amount of solutions with high BEC atom numbers. It would be of interest to find out if the players had used different strategies to obtain these results, and if so, which form these solutions have. Taking only solutions with a greater yield than two million BEC atoms into account, we are interested in groupings of solutions with similarities into clusters. Several of different kinds of algorithms has been proposed in the literature to be able to group big data sets into clusters. Examples of clustering algorithms are K-means [49] and OPTICS [50]. The one used in this case is created in this group and called *modest algorithm for distance sorting* (MADS) [35]. It works by sorting a *distance map*, made over all the solutions in question, by grouping the solutions closest in distance together. A distance map is a n x n matrix, where n is the number of solutions to consider, where the (i, j) element in the matrix is given by $d(i, j)$, with the distance measure defined in equation 5.24. Furthermore the normalization used in this case is carried out by taking the logarithm of the ramps before normalizing which is discussed in section 5.4.2. The distance map for

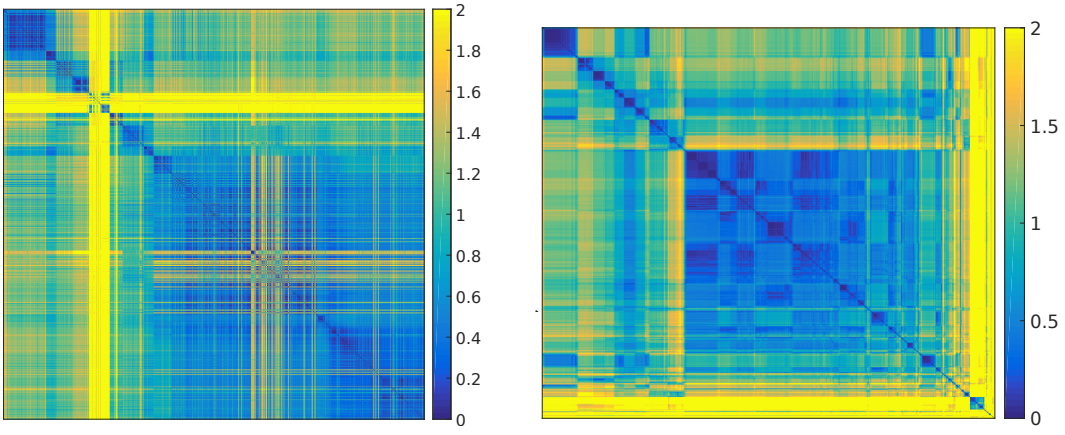

(a) Raw distance map (b) Sorted distance map

Figure 5.24: a) Distance map for the solutions with a yield of more than 2 million BEC atoms. Each axis indicates the solution number. b) Sorted distance map. Both maps are color coded by the amount of distance between two solutions.

the solutions with a yield of more than 2 million BEC atoms is shown in figure 5.24(a). The sorting algorithm works by iterating trough the n rows. For the i'th row it sorts the i+1,..,n values in the row, from smallest to largest distance value. Then both the columns and the rows are interchanged to match the new sorted order. When the algorithm has iterated trough the n rows the distance map is sorted, which is shown in 5.24(b).

From the map it can be seen that several separated clusters are present in the dataset, indicating that the players have found different strategies that yields good solutions. Four seemingly interesting cluster has been chosen, indicated by different colors, 5.25. They have been chosen with the aim to select for diverse and large clusters for further analysis of the strategies defining them.

The ramp sets that compose each cluster are shown in figure 5.26. The shaded bars are the standard deviation of the ramps for each cluster and the main solid line is the mean. The shaded bars indicate the diversity of the ramp sets for a given cluster, and the mean represent the strategy corresponding to the cluster. In figure 5.27 the same ramp sets are plotted in a logarithmic scale to highlight the difference of the ramps in the last part of the sequence. All the ramp sets have a unique features, thereby defining four different strategies. It is notable that the cluster number 4 is including the solution yielding the best result of Swarm session. The duration of the ramps for each of the clusters was $T_1 = 8s$, $T_2 = 8s$, $T_3 = 3.5s, 4s$, $T_4 = 7s, 8s$, the subscript being the cluster number.

From the plots it can be seen that the four strategies are all some variation of hybrid strategies using both the magnetic field gradient and the two dipole beams for the

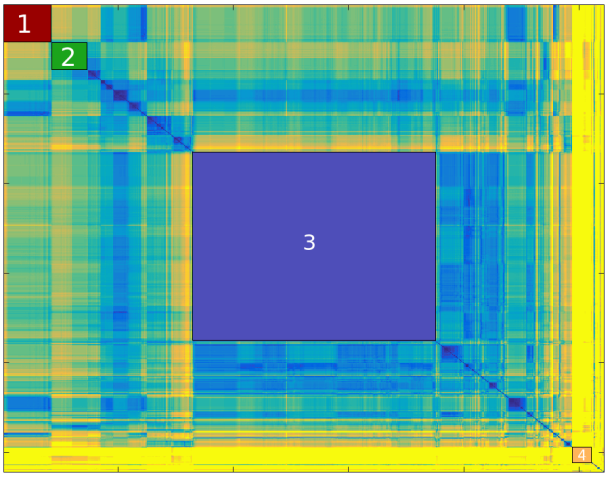

Figure 5.25: Same as 5.24(*b*) with the four chosen clusters indicated by different coloured areas.

evaporation sequence, but still are different from our hybrid trap strategy defined earlier. In the loading phase of the dipole intensity ramps, strategy 1 and 2, seem have the same shape. The magnetic field gradient for these two are however different both in the loading and in the evaporation part. Looking at the dipole beam intensities for the loading of cluster 3 and 4, a strong deviation from the constant ramps of the other strategies is present. This different in the intensity of the dipole beams leads to different trap frequencies in the transversal and longitudinal directions, giving an more elongated trap for the cloud to be loaded into. For strategy 3 it seems that the transversal beam is almost shut off in the loading phase, compensated by a stronger longitudinal beam intensity, but have about the same magnitude as the others in the evaporation part.

Analysis of the ramp sets To get a better understanding of the difference of the four obtained strategies, the trap depth $\hat{U}$ and the trap volume has been calculated for the mean of the four ramps. The trap depth is measured in units of temperature, determined by the kinetic energy $k_B T$ an atom at the bottom of the trap needs to escape the potential barrier. At a given instance in the evaporation, the value of the magnetic gradient power and the intensity of the two dipole beams have been used to calculate the total potential

$$U_{\text{tot}} = U_{\text{B}} + U_{\text{TDT}} + U_{\text{LDT}} + U_{\text{grav}} \tag{5.25}$$

were U_{B} is the potential energy for the magnetic field described in equation 2.12, U_{TDT}, U_{LDT} are the potential energy for the transversal and longitudinal dipole fields, respectively, given by equation 2.9, and $U_{\text{grav}}(z) = mgz$ is the gravitational potential, with g

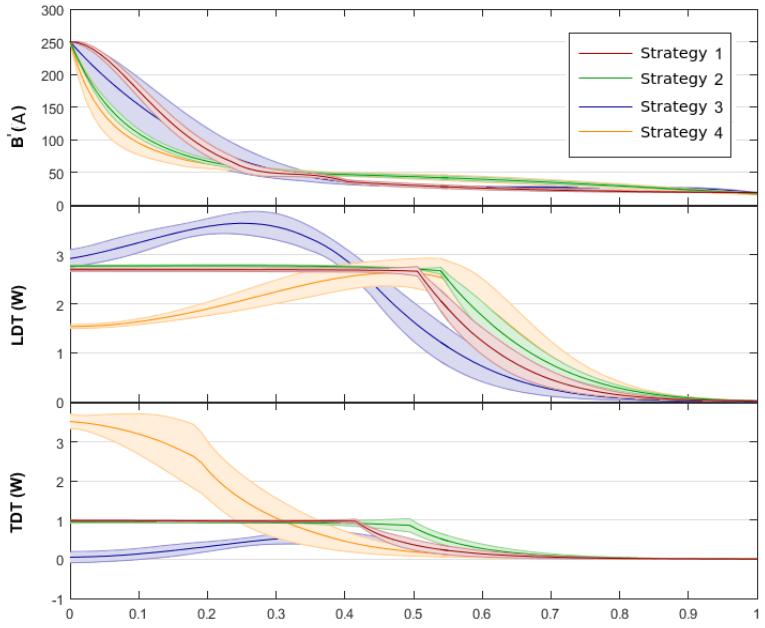

Figure 5.26: The ramps of the four chosen clusters. With the solid line indicating the mean and the shaded area the standard deviation, of the ramps set for a given cluster.

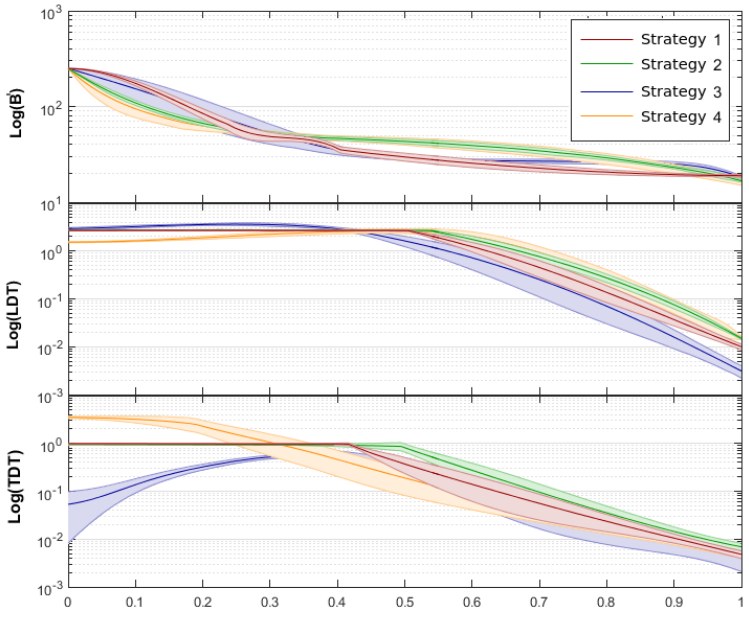

Figure 5.27: The same ramps as in figure 5.26, but on a logarithmic scale.

being the gravitational acceleration. The calculated potential for each spatial dimension is shown in figure 5.28. The trap depth is then the minimum of the potential depth from the three potential of each spatial direction. The 3D surface that is defined through the points in space with the same potential ϵ is called the *equipotential*. The volume spanned by this equipotential surface with $\epsilon = \hat{U}$ defines the trap volume. It is illustrated in figure 5.29.
In figure 5.31(a) and 5.31(b), respectively, the evolution of the trap depth and the trap volume for these four strategies are shown as logarithmic plots. The suddenly change in decrease rate, visible in both plots at around 0.5 and 0.8 at the normalized time axis, are due to a change from a total potential defining the loading part to a total potential defining the evaporation part. The sudden change happens when the magnetic field gradient is to weak to levitate the atom cloud. Before this moment, the trap depth is entirely defined by the strength of the magnetic field gradient, and is being a too large barrier for efficient evaporation to occur. In figure 5.30 are two potential that shows the loading potential and the evaporation potential. Due to the way the trap volume calculated it is only meaningful for the evaporation part.

The plots of the trap depth indicate that the four strategies in the control space defined by the controls of the three pulses, are reduced to only two strategies in the *physical space*, which is the space defined by the possible curves for the trap depth and the trap volume. They are parameters with a direct physical interpretation. These however don't explain all characteristics of the trap in relation to the evaporation process, for instance not the shape of the trap, which can be quantified by the trap frequencies. The two physical strategies seem to differ a lot in terms of loading time and evaporation time. In the first physical strategy, composed of the strategies 1 and 3, the evaporation part starts after about 0.5 T, where T is the duration time of the total sequence. For the second physical strategy composed of the strategies 2 and 4, the evaporation starts at

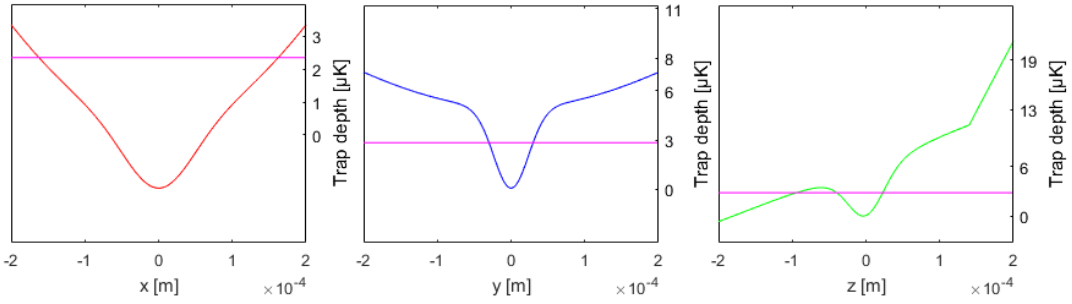

Figure 5.28: Example of the calculated total potential, plotted in all three spatial dimensions. The purple line is defined by the value of $\epsilon = \hat{U}$, and its crossing with the potential defines the equipotential.

about 0.8 T, having only a fifth of the total duration time for the evaporation process. The size of the trap depth is in the beginning different for the two strategies, being $\hat{U}_{1,i} = (95 \pm 12)\mu\,\mathrm{K}$ and $\hat{U}_{2,i} = (18.5 \pm 1.5)\mu\,\mathrm{K}$, but in the end they reach the same size of $\hat{U}_f = (3.2 \pm 0.2)\mu\,\mathrm{K}$. The trap volume is almost the same in both the beginning and in the end of the evaporation part for both strategies though.

Analysing the evaporation ramps

One of the motivations for gamifying the problem of evaporative cooling, was to reformulate the problem into another context in the hope of achieving new solutions, that

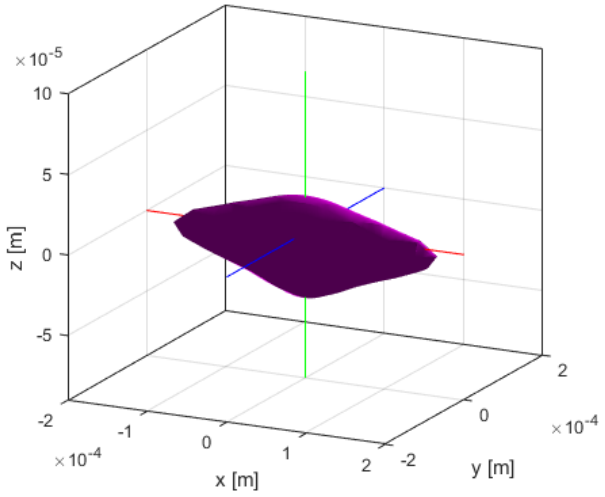

Figure 5.29: The equipotential surface for a specific value of ϵ.

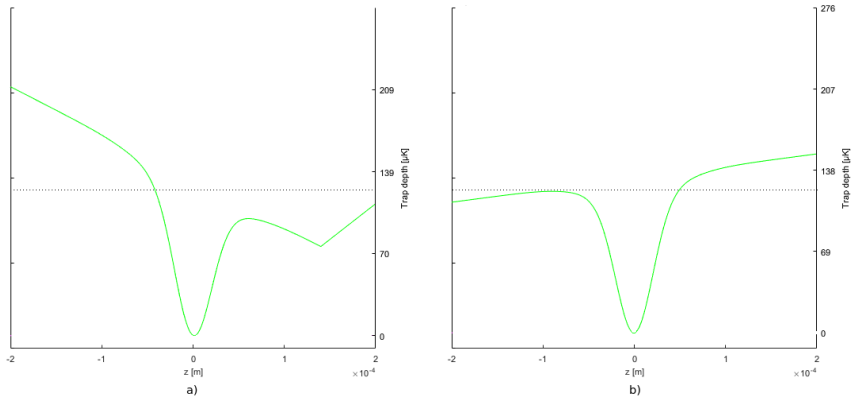

Figure 5.30: Illustration the difference of a loading potential and a evaporation potential. a) The loading potential where magnetic field potential is larger than the gravitational. b) The evaporation process where the energetic atoms can escape the trap.

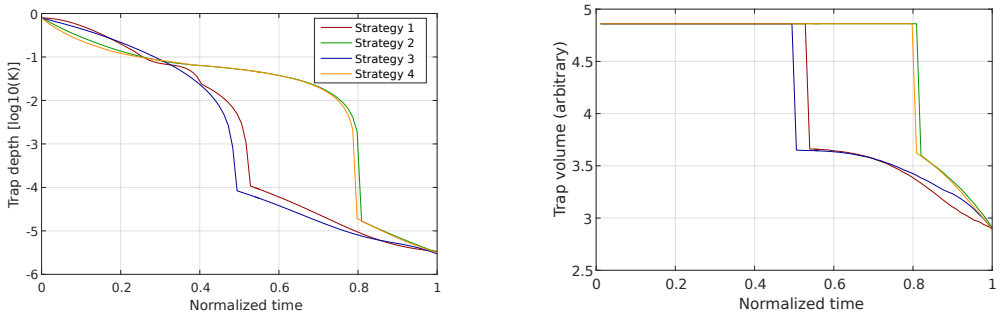

(a) Trap depth

(b) Trap volume

Figure 5.31: a) The trap depth of the four strategies on a logarithmic scale. b) Trap volume of the four strategies on a logarithmic scale. The trap volume is only calculated for the evaporation part, but the time scale starts with the beginning of the loading.

would not have been considered in the frame of a physical understanding of the problem. To give some indication for whether the players were able to find such solutions, the evaporation ramps from the four clusters found will be compared with the expression in 5.7. The expression is used to fit the data of the trap depth in the evaporation part of figure 5.31(a). Because of the tendency of the fitting function to be dependent on the initial value to find the best fit, a scan of the guess variables η and $\Gamma_{\mathrm{el},i}$ was performed with a constant initial trap depth guess. For the strategies 2 and 4 the best fits gave $\mathrm{R}^2 = 0.99$ for both cases, thereby describing the model well. The fitting parameters was $\eta = 10 \pm 13$ and $\Gamma_{i,\mathrm{els}} = 610 \pm 5400 s^{-1}$. These high bounds of the fit is properly due to inter-correlation between the fit parameters. Therefore to give a better estimate of the truncation parameter η, the elastic collision rate γ_i was fixed to the value 610 a new fit only with η as a variable was performed giving $\eta = 10 \pm 0.3$ for both cases, which is a typical value used value in optical traps [25]. The fits for the four strategies that had the lowest R^2 are plotted in figure 5.32 with the data for the trap depth ramps. The start of the of the evaporation process is sat to $t = 0$. For strategies 2 and 4 the fitted curves match very well the data points.

For the strategies 1 and 3 the fitted curves are displaced from the data points, with $\mathrm{R}^2 = 0.95$ and $\mathrm{R}^2 = 0.96$, respectively. In each case the best fitting model only roughly describes the data. The deviation of this strategy from the expression could be because the strategy is changing η during the evaporation, or because of an optimizing in relation to background loses and inelastic collisions.

Pointing out that the best solution of our experiment is included in the strategy nr. 3, the players has been able to find a new strategy yielding a new record in BEC atoms, that we could not find by using the physical model of equation 5.7. This indicates that the players, by searching in another part of the control space, are able to find strategies

that we would not have found by using our physical understanding of the problem.

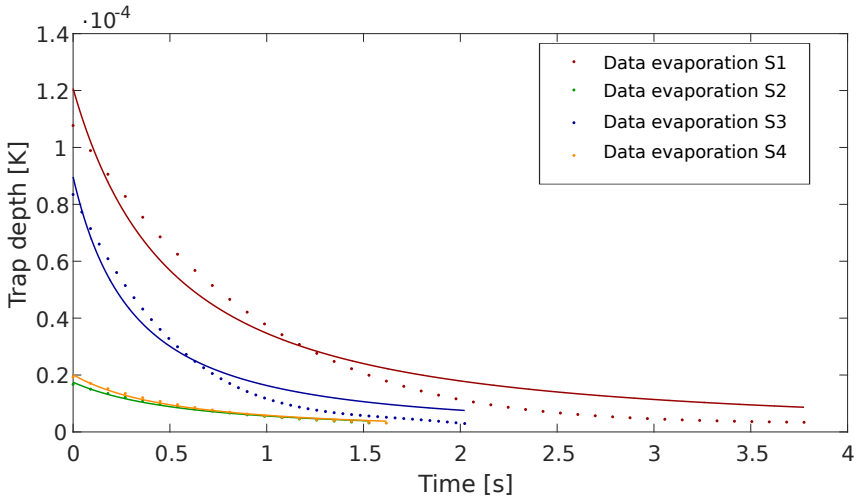

Figure 5.32: The trap depth in the evaporation part, for the four strategies. The solid lines are fit to the data from the expression 5.7.

Chapter 6

Conclusion and Outlook

Conclusion

In this thesis the first experiments done in the HiRes group with a remote control system are presented. A description of the control system is given and a suggestion for a variation in the design which will realize a stronger closed loop experimental system. A module for creating an arbitrary potential with an AOD has been incorporated in the control system. Thereby exploit the properties of the control system to make an automated experiment. The AOD module was used to create a movable tweezer with a dimple beam to investigate the fast transport of a thermal cloud and of a BEC. The center-of-mass oscillation of the cloud at the end of the movement was measured in relation to the duration of the movement. The data was compared with a theoretical 1D classical model given in [21]. The experimental data for the BEC-movement was fitted to an expression from the model.

The measured center-of-mass oscillation frequency of the experiment and fitted value for the frequency agreed within the bounds of one sigma. The other fit parameter was a scaling factor, which was determined to be $a = 0.50 \pm 0.08$, showing an inconsistency between the experimental data an the model. The model assumes that the trap potential can be described by a harmonic oscillator. A partially explanation of the inconsistency could be a failure for large oscillation amplitudes of this assumption.
The major part of this thesis was an analysis of the complex control landscape describing the process of evaporative cooling for the creation of BEC atoms. Furthermore it was an investigation of the methodology of this problem. The landscape was investigated using three different methods. The first was a manual scan of parameters to map out the control landscape, with special interest in the area around known strategies from the literature. The second was by using a an optimization algorithm called dCRAB, to

search in the control landscape. A PhD student from the University of Ulm implemented the algorithm, and remotely controlled our experiment with it. The algorithm obtained a yield of $2.2 \cdot 10^6$ BEC atoms.
The third was an alternative approach for optimization, realizing a gamification of the problem, enabling the transformation of a physical problem into an easily understandable game problem. A motivation for this setup was to exploit the power of the human intuition for finding new solution strategies.
The game run for about two weeks and produced around 12000 solutions that were subsequently tried out. It found several good strategies yielding over $2 \cdot 10^6$ BEC atoms, and obtained the highest yield ever reached in our experimental setup at $2.76 \cdot 10^6$ BEC atoms. The results obtained indicated that the players were adapting well to new experimental conditions. A cluster analysis resulted in four distinct strategies, for which ramp sets were interpreted. Two of the strategies couldn't be explained by the evaporation model given in [25], showing that the players could reach new areas of the control space, not available by our first method.

Outlook

The remote capabilities of our control system is at present time in its starting phase. As a next step it is important to integrate all parts of the closed loop control system with a strong connectivity and implement error handling. This can be a solution to realize a less flawed and more automated system, which is vital for the next steps in relation to the remote control opportunities.
The idea of an *open laboratory* is being pursued, where a GUI has been developed for people outside our group, aiming for involving people in *citizen science*. An image of this GUI is shown in figure 6.1. The idea is to separate the experiment in building blocks which people can play around with, and make their own experiment.
The experiment is also in the process of being upgraded, adding equipment to the science chamber with the aim to image atoms in a 3D optical lattice, with single site resolution. A DMD is planned to manipulate with the atoms in the lattice, making it possible to realize two qubit quantum logic gates, the building block of a quantum computer. In relation to this, the possibility of gamifying parts of the experiment, can be used to optimize the system. This for example by making a coupling between the Bring Home Water computer game, already developed in this group, and the movement of a single atom from site to site. One option would be to realize player solutions from the game Quantum Moves, developed in the group, where people have solved the challenging problem of single atom transport. This knowledge can be used to optimally move single atoms between sites of a lattice, fast and maintaining them in the lowest energy state.

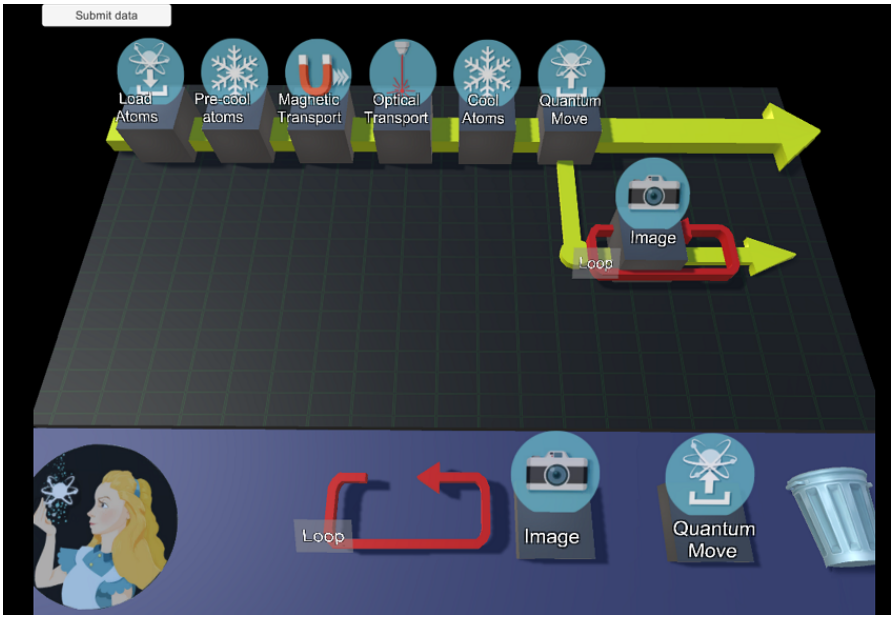

Figure 6.1: Screen-shot of the Graphical User interface for the possible new version of the ALICE experiment control accessible to everyone.

Bibliography

[1] S. N. Bose. Plancks gesetz und lichtquantenhypothese. *Z. phys, 26(3):178*, 1924.

[2] K.B.Davis, M.O. Mewes, M.R. Andrews, N.J. Vandruten, D.S. Durfee, and W. Ketterle. Bose-einstein condensation in a gas of sodium atoms. *Physical review letters, 75(22):3969–3973*, 1995.

[3] D. Z. Anderson B. T. Seaman, M. Krämer and M. J. Holland. Atomtronics: Ultracold-atom analogs of electronic devices. *Physical Review A, 75(2):1–12*, 2007.

[4] D. Z. Anderson R. A. Pepino, J. Cooper and M. J. Holland. Atomtronic circuits of diodes and transistors. *Physical Review Letters, 103(14):1–4*, 2009.

[5] J. I. Cirac and P. Zoller. Quantum computations with cold trapped ions. phys. *Rev. Lett., 74:4091–4094*, 1995.

[6] K. M. C. W., S. K. and J. F. Sherson. Quantum computation architecture using optical tweezers. *Phys. Rev. A 84:032322*, 2011.

[7] R. C. Müller. A new experiment to prope and manipulate quantum systems. *PhD Thesis*, 2015.

[8] C. J. Pethick and H. Smith. Bose-einstein condensation in dilute gases. *Cambridge University Press, Cambridge*, 2002.

[9] Yurii B. Ovchinnikov R. Grimm, M. Weidemüller. Optical dipole traps for neutral atoms. *Advances in Atomic, Molecular and Optical Physics Vol. 42, 95-170*, 2000.

[10] M. Trupke J. Schmiedmayer T. Schumm W.Rohringer, D. Fischer. Stochastic optimization of bose-einstein condensation using a genetic algorithm. *Vienna Center for Quantum Science and Technology, Atominstitut*, 2011.

[11] M. Kubasik. Towards spin squeezing in cold atomic ensembles. *PhD thesis, Univeristat Politècnica de Catalunya*, 2009.

[12] W. Ketterle A. Keshet. A distributed gui-based computer control system for atomic physics experiments. *Review of Scientific Instruments 84*, 2013.

[13] H. B. Christensen. Flexible, reliable software: Using patterns and agile development. *CRC Press*, 2010.

[14] A. R. Thorsen. A modular control system for cold atom experiments. *Master's thesis, Aarhus University*, 2015.

[15] C. MacCormick K. Henderson, C. Ryu and M. G. Boshier. Experimental demonstration of painting arbitrary and dynamic potentials for bose-einstein condensates. *New Journal of Physics vol 11*, 2009.

[16] V. Lienhard T. Lahaye A. Browaeys D. Barredo, S. de Léséleuc. An atom-by-atom assembler of defect-free arbitrary two-dimensional atomic arrays. *Science Vol. 354, Issue 6315, pp. 1021-1023*, 2016.

[17] J. Meineke T. Esslinger B. Zimmermann, T. Müller and H. Moritz. High-resolution imaging of ultracold fermions in microscopically tailored optical potentials. *New Journal of Physics 13*, 2011.

[18] B. E. A. Saleh and M.C. Teich. Fundamentals of photonics, chapter 19. *Wiley*, 2007.

[19] R. Heck. A toolbox for optimized and stable experiments with ultracold quantum gases. *PhD Thesis, Aarhus University*, 2016.

[20] M. K. Mønster. Intensity stabilization of an optical tweezer for manipulation of ultracold atoms. *Master thesis*, 2014.

[21] G. Reinaudi David Guery-Odelin A. Couvert, T. Kawalec. Optimal transport of ultracold atoms in the non-adiabatic regime. *Europhys. Lett. 83*, 2008.

[22] D. Guéry-Odelin and J. G. Muga. Transport in a harmonic trap: Shortcuts to adiabaticity and robust protocols. *Phys. Rev. A 90, 063425*, 2014.

[23] M. Munch P. Haikka J. H. Jensen T. Planke M. G. Andreasen M. Gajdacz K. Mølmer A. Lieberoth J. J. W. H. Sørensen, M. K. Pedersen and J. F. Sherson. Exploring the quantum speed limit with computer games. *Nature, 532(7598):210–213*, 2016.

[24] R. J. Niffenegger A. J. Olson and Y. P. Chen. Optimizing the efficiency of evaporative cooling in optical dipole traps. *Phys. Rev. A 87, 053613*, 2013s.

[25] S. R. Granade K. M. O'Hara, M. E. Gehm and J. E. Thomas. Scaling laws for evaporative cooling in time-dependent optical traps. *Phys. Rev. A 64, 051403(R)*, 2001.

[26] M. W. Reynolds O.J Luiten and J.T.M. Walraven. Kinetic theory of the evaporative cooling of a trapped gas. *Phys. Rev. A 53, 381*, 1996.

[27] J. Schmiedmayer S. Hild C. Gross M. Cheneau I. Bloch T. Pichler A. Negretti T. Calarco S. Montangero S. van Frank, M. Bonneau. Optimal control of complex atomic quantum systems. *Scientific Reports 6, 34187*, 2016.

[28] T. Ho K. Moore Tibbetts H. Rabitz, R. Wu and X. Feng. Fundamental principles of control landscapes with applications to quantum mechanics, chemistry and evolution. *Recent Advances in the Theory and Application of Fitness Landscapes, chapter 2*, 2014.

[29] M. M. Hsieh H. A. Rabitz. and C. M. Rosenthal. Quantum optimally controlled transition landscapes. *Science vol 303*, 2004.

[30] R. E. Bellman. Adaptive control processes: A guided tour. *Princeton University Press*, 1961.

[31] Geoffrey Hinton L. van der Maaten. Visualizing data using t-sne. *Journal of Machine Learning Research 1, 1-48*, 2008.

[32] S. Kullback and R. A. Leibler. On information and sufficiency. *Ann. Math. Statist., 22(1):79–86*, 1951.

[33] J. Venna and S. Kaski. Local multidimensional scaling with controlled tradeoff between trustworthiness and continuity. *In Proceedings of 5th Workshop on Self-Organizing Maps, pages 695–702. Citeseer*, 2005.

[34] L. Maaten. Learning a parametric embedding by preserving local structure. *In International Conference on Artificial Intelligence and Statistics, pages 384–391*, 2009.

[35] M. G. Andreasen. Characterizing strategies in quantum optimization landscapes. *Master thesis, Aarhus University*, 2015.

[36] S. E. Sklarz and David J. Tannor. Loading a bose-einstein condensate onto an optical lattice: An application of optimal control theory to the nonlinear schrödinger equation. *Phys. Rev. A, 66:053619*, 2002.

[37] T. Wenger T. Kinoshita and D. S. Weiss. All-optical bose-einstein condensation using a compressible crossed dipole trap. *Phys. Rev. A 71, 01160eR*, 2005.

[38] R. L. Compton I. B. Spielman Y.J. Lin, A. R. Perry and J. V. Porto. Rapid production of 87rb bose-einstein condensates in a combined magnetic and optical potential. *Phys. Rev. A 79, 063631*, 2009.

[39] W. S. Torgerson. Multidimensional scaling: I. theory and method. *Psychometrika, Volume 17, Issue 4, pp 401–419*, 1952.

[40] J. A. Nelder and R. Mead. A simplex method for function minimization. *The Computer Journal, 7(4):308–313*, 1965.

[41] S. Montangero T. Calerco. Optimal control techniqeu for many-body quantum dynamics. *Phys. Rev. 106, 190501*, 2011.

[42] T. Calarco T. Caneva and S. Montangero. Chopped random-basis quantum optimization. *Phys. Rev. A 84, 022326*, 2011.

[43] D. E. Goldberg. Genetic algorithms in search, optimization, and machine learning. *Kluwer Academic Publishers, Boston*, 1989.

[44] M. Trupke T. Schumm W. Rohringer, D. Fischer and J. Schmiedmayer. Stochastic optimization of bose-einstein condensation using a genetic algorithm. *Stoch. Optim. - Seeing Optim. Uncertain, 1*, 2011.

[45] T. Calarco N. Rach, M. M. Müller and S. Montangero. Dressing the chopped-random-basis optimization: A bandwidth-limited access to the trap-free landscape. *Phys. Rev. A 92, 062343*, 2015.

[46] A. Treuille J. Barbero J. Lee M. Beenen A. Leaver-Fay D. Baker Z. Popović S. Cooper, F. Khatib and F. players. Predicting protein structures with a multiplayer online game. *Nature, 466(7307):756–760*, 2010.

[47] A. Slosar K. Land S. Bamford D. Thomas M. J. Raddick R. C. Nichol A. Szalay D. Andreescu P. Murray C. J. Lintott, K. Schawinski and J. Vandenberg. Galaxy zoo: morphologies derived from visual inspection of galaxies from the sloan digital sky survey. *Royal Astronomical Society, 389(3):1179–1189*, 2008.

[48] A. Zlateski K. Lee M. Richardson S. C. Turaga M. Purcaro M. Balkam A. Robinson B. F. Behabadi M. Cam-pos W. Denk J. S. Kim, M. J. Greene and H. S. Seung. Space–time wiring specificity supports direction selectivity in the retina. *Nature, 509(7500):331–336*, 2014.

[49] J. B MacQueen. Some methods for classification and analysis of multivariate observations. *Proceedings of 5th Berkeley Symposium on Mathematical Statistics and Probability. 1. University of California Press. pp. 281–297*, 1967.

[50] H. peter Kriegel M. Ankerst, M. M. Breunig and J. Sander. Optics: Ordering points to identify the clustering structure. *ACM Press. pages 49–60.*, 1999.